Angiogenesis in Graft-versus-Host Disease

Inaugural-Dissertation
to obtain the academic degree
Doctor rerum naturalium (Dr. rer. nat.)

submitted to the Department of Biology, Chemistry and Pharmacy
of Freie Universität Berlin

by

Sarah Mertlitz

2020

The present thesis was prepared from April 2015 until February 2020 at the Medical Department of Hematology, Oncology and Tumor Immunology, Charité University Medicine under the supervision of Prof. Dr. Olaf Penack.

First Reviewer:	Prof. Dr. Olaf Penack
Second Reviewer:	Prof. Dr. Rupert Mutzel
Date of defense:	12.06.2020

Für meine Familie

The acknowledgement is not included in the online version for data protection reasons.

The acknowledgement is not included in the online version for data protection reasons.

Table of contents

Abstract

For a variety of hematopoietic diseases, allogeneic hematopoietic stem cell transplantation (allo-HSCT) is the only curative treatment option. Due to numerous improvements in the treatment procedure and the constant expansion of indications, the number of transplanted patients has increased rapidly during the last decades. Despite many achievements, the mortality rate after allo-HSCT is still high. The main and most severe complication after allo-HSCT is the graft-versus-host disease (GVHD) and up to 30% of allo-HSCT recipients die due to GVHD or GVHD-related side effects. GVHD is characterized by a systemic inflammatory reaction that is mainly mediated by alloreactive T cells. Alloreactive T cells cause severe tissue damage in main GVHD target organs colon, liver and skin via different cytotoxic mechanisms. All current treatment options aim at the suppression of T cell function, however, the inhibition of immune responses results in an increased risk for infections and tumor relapse. Therefore, there is a clear medical need in defining alternative targets for the development of therapies that act without hampering immune functions.

Recent work by us and others, identified an important role of the endothelium in the development of acute GVHD (aGVHD). However, the inhibition of vascular endothelial growth factor receptor 1 (VEGFR1) and VEGFR2, key mediators of angiogenesis, led to impaired hematopoietic engraftment, which is essential for a beneficial transplantation outcome. This thesis discusses two new approaches for the treatment of aGVHD after allo-HSCT. The first part of this work deals with an aspect that has not been studied in the context of aGVHD before, namely lymphangiogenesis. It is well known that lymph vessels carry out important immunologic functions and that lymphangiogenesis is involved in inflammation, cancer and graft rejection. However, the influence of lymphangiogenesis on inflammation can be beneficial or harmful and seems to depend on various factors such as the inflammatory trigger and the site of inflammation.

Evaluation of murine and human tissue samples showed a significant increase in lymph vessel density during aGVHD, confirming the clinical relevance of lymphangiogenesis in aGVHD. The inhibition of VEGFR3, a main regulator of lymphangiogenesis, revealed that reduced lymphangiogenesis attenuates clinical and histopathological features of aGVHD, without affecting malignant lymphoma growth.

In the second part of the thesis an alternative pathway of hemangiogenesis is investigated. Besides the prominent vascular endothelial growth factor (VEGF)/VEGFR signaling, an alternative pathway involved in angiogenesis is the transforming growth factor-beta (TGF-β) pathway. Depending on downstream signaling, the TGF-β pathway can initiate or inhibit

angiogenesis. A study by Greenwood et al. identified the glycoprotein leucine-rich alpha-2-glycoprotein 1 (Lrg1) as regulator of the angiogenic switch in TGF-β signaling. Elevated serum levels of Lrg1 in samples from patients with inflammatory diseases further confirmed the assumption that Lrg1 is expressed under pathological rather than physiological conditions. The correlation between Lrg1-regulated TGF-β signaling and angiogenesis during aGVHD has not been investigated so far. We show that Lrg1 expression is increased in target organs during aGVHD and that the genetic loss of Lrg1 attenuates aGVHD. Using the additional inflammation models of experimental colitis and paw edema, we could also show that Lrg1 contributes to angiogenesis, altered vessel structure and increased inflammation in these disease models.

With this work, we were able to confirm the crucial role of the lymphatic and blood vascular system during aGVHD. We identified two novel factors that provide potential therapeutic targets to reduce aGVHD without interfering with anti-tumor immunity and immune reconstitution.

Zusammenfassung

Für eine Reihe von hämatopoetischen Erkrankungen ist die allogene hämatopoetische Stammzelltransplantation (allo-HSZT) die einzige kurative Behandlungsoption. Aufgrund zahlreicher Verbesserungen des Behandlungsverfahrens und der ständigen Erweiterung von Indikationen, ist die Zahl der transplantierten Patienten in den letzten Jahrzehnten rapide gestiegen. Trotz vieler Erfolge ist die Sterblichkeitsrate nach einer allo-HSZT jedoch immer noch hoch. Die wichtigste und schwerwiegendste Komplikation nach einer allo-HSZT ist die Graft-versus-Host Reaktion (GVHR). Bis zu 30% der allo-HSZT-Empfänger sterben an GVHR oder GVHR-bedingten Nebenwirkungen. GVHR ist durch eine systemische Entzündungsreaktion gekennzeichnet, die von alloreaktiven T-Zellen vermittelt wird. Alloreaktive T-Zellen verursachen über verschiedene zytotoxische Mechanismen schwere Gewebeschäden in den wichtigsten GVHR-Zielorganen Darm, Leber und Haut. Alle derzeitigen Behandlungsmöglichkeiten zielen auf eine Unterdrückung der T-Zell-Funktion ab, die Hemmung der Immunantwort führt jedoch zu einem erhöhten Risiko von Infektionen und Tumorrezidiven. Daher besteht ein klarer medizinischer Bedarf, alternative Ziele für die Entwicklung von Therapien zu definieren, die ohne Beeinträchtigung der Immunfunktionen wirken.

Aktuelle Arbeiten von uns und Anderen haben die wichtige Rolle des Endothels bei der Entwicklung der akuten GVHR (aGVHR) identifiziert. Die Hemmung von VEGFR1 (engl. vascular endothelial growth factor receptor 1) und VEGFR2, Schlüsselmediatoren der Angiogenese, führte allerdings zur Beeinträchtigung des Anwachsens von Stammzellen, was für ein günstiges Transplantationsergebnis unerlässlich ist.

In dieser Arbeit werden zwei neue Ansätze zur Behandlung von aGVHR nach allo-HSZT diskutiert. Der erste Teil dieser Arbeit befasst sich mit einem Aspekt, der bisher noch nicht im Zusammenhang mit aGVHR untersucht wurde, nämlich der Lymphangiogenese. Es ist bekannt, dass Lymphgefäße wichtige immunologische Funktionen erfüllen und dass die Lymphangiogenese bei entzündlichen Erkrankungen, Tumoren und Transplantatabstoßung involviert ist. Lymphangiogenese kann sich jedoch positiv oder negativ auf eine Entzündung auswirken, dies scheint von verschiedenen Faktoren wie dem Entzündungsauslöser und dem Ort der Entzündung abhängig zu sein.

Die Auswertung von murinen und humanen Gewebeproben zeigte eine deutliche Zunahme der Lymphgefäßdichte während aGVHR, was die klinische Relevanz der Lymphangiogenese bei aGVHR bestätigt. Die Hemmung von VEGFR3, dem Hauptregulator der Lymphangiogenese, ergab, dass eine Reduzierung der Lymphangiogenese klinische und histopathologische

Merkmale der aGVHR abschwächt, ohne das Wachstum maligner Lymphome zu beeinträchtigen.

Im zweiten Teil der Arbeit wird ein alternativer Weg der Blutgefäßangiogenese untersucht. Neben dem prominenten vascular endothelial growth factor (VEGF)/VEGFR-Signalweg ist ein alternativer Signalweg, der an der Angiogenese beteiligt ist, der TGF-β (engl. transforming growth factor-beta) Signalweg. Abhängig von den nachgeschalteten Signalen kann der TGF-β Signalweg Angiogenese initiieren oder hemmen. Eine von Greenwood et al. durchgeführte Studie identifizierte das Glykoprotein leucine-rich alpha-2-glycoprotein 1 (Lrg1) als Regulator des angiogenen Schaltmechanismus bei der TGF-β Signalübertragung. Erhöhte Serumspiegel von Lrg1 in Proben von Patienten mit entzündlichen Erkrankungen bestätigten die Annahme, dass Lrg1 eher unter pathologischen als unter physiologischen Bedingungen exprimiert wird. Der Zusammenhang zwischen dem Lrg1-regulierten TGF-β Signalweg und der Angiogenese bei aGVHR wurde bisher nicht untersucht. Wir zeigen, dass die Expression von Lrg1 in den Zielorganen während der aGVHR erhöht ist und dass der genetische Verlust von Lrg1 aGVHR abschwächt. Mit Hilfe der zusätzlichen Entzündungsmodelle der experimentellen Colitis und dem Pfotenödem-Modell konnten wir zudem zeigen, dass Lrg1 zu Angiogenese, veränderter Gefäßstruktur und verstärkter Entzündung in diesen Krankheitsmodellen beiträgt.

Mit dieser Arbeit konnten wir die entscheidende Rolle des Lymph- und Blutgefäßsystems bei aGVHR bestätigen. Wir haben zwei neue Faktoren identifiziert, die potentielle therapeutische Ziele zur Verringerung von aGVHR darstellen, ohne dabei die anti-Tumor-Immunität und Immunrekonstitution zu beeinträchtigen.

1 Introduction

1.1 Hematopoietic stem cell transplantation

Hematopoietic stem cell transplantation (HSCT) is the clinical term for the procedure of transferring hematopoietic stem cells (HSCs) from a donor to a recipient in order to replace dysfunctional bone marrow and cure the underlying disease. It has become a standard therapy for multiple congenital or acquired hematopoietic malignancies and often displays the only curative treatment option.[1]

Edward Donnall Thomas was a pioneer in the field of stem cell transplantation. In 1957, Thomas performed the first allogeneic hematopoietic stem cell transplantations (allo-HSCTs) to replace the hematopoietic system of six patients who underwent immune cell ablation previously. Due to limited knowledge about donor-recipient matching at this time, all of those patients died.[2] Nevertheless, further research and his unbroken belief in the effectiveness of allo-HSCT revealed key insights in stem cell transplantation, which were honored with the Nobel Prize in 1990.[2]

During the last 60 years of extensive research in the field of hematopoietic stem cell transplantation, many improvements were made, not only in the transplantation setting itself but also in the treatment of side-effects.

According to the current method, three decisions must be taken before an HSCT is performed, these are:

1) the donor type, 2) the source of hematopoietic stem cells and 3) the conditioning regimen[3-5] (**Figure 1**).

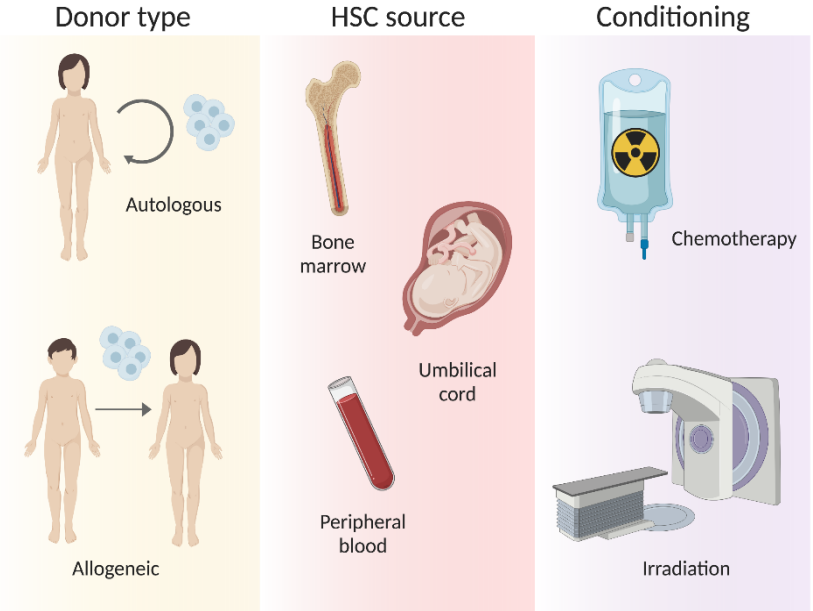

Figure 1. Requirements for HSCT. The three main decisions before performing a HSCT include the donor type, HSC source and the type of conditioning. HSC: hematopoietic stem cell.

1) Autologous HSCT (auto-HSCT) is performed using hematopoietic stem cells from the recipient (=patient) itself while allo-HSCT uses hematopoietic stem cells from another person that is either a sibling, a relative or unrelated to the patient. Syngeneic HSCT (syn-HSCT) is referred to HSCTs that use hematopoietic stem cells from an identical twin.

2) Sources of hematopoietic stem cells are the donor's bone marrow, peripheral blood and the umbilical cord. Currently, approximately 80% of all unrelated donor transplants use peripheral blood as hematopoietic stem cell source.[6] Though it is still controversial if the stem cell source has any impact on the outcome of the transplantation, the use of peripheral blood stem cells (PBSCs) shows faster immune reconstitution and may result in lower risk of relapse, but higher risk of chronic GVHD.[5]

3) Before the transplantation of donor stem cells is performed, recipients need to undergo conditioning treatment. The conditioning regimen before the actual HSCT may consist of chemotherapy, radiation, or a combination of both. The conditioning is needed to eliminate cancer cells, suppress the recipient´s immune system and to create a niche for transplanted donor cells.[3,4]

In general, conditioning regimens can be divided into myeloablative, reduced intensity conditioning and non-myeloablative conditioning. Myeloablative regimen usually consists of a combination of different chemotherapeutic agents or a combination of chemotherapeutics and total body irradiation. Due to its high toxicity, myeloablative conditioning is not suitable for all patients. The development of reduced intensity conditioning and non-myeloablative conditioning regimen allows the treatment of elderly patients or patients with comorbidities.

The choice of the conditioning regimen is dependent on the underlying disease, graft source, disease status and the patient's age and condition.[3,4]

1.2 Indications for allo-HSCT

Due to the ability of hematopoietic stem cells to differentiate in every mature blood cell type, allo-HSCT is the only curative treatment option for a variety of hematologic malignancies and disorders.

The actual survey report from the European Society for Blood and Marrow Transplantation (EBMT) reports of 45,418 HSCTs in Europe in 2017, 17,155 (42%) of them being allogeneic.[7] The most common indications for allogeneic transplantation were myeloid malignancies like acute myeloid leukemia, chronic myeloid leukemia, myelodysplastic syndrome or myeloproliferative neoplasm and lymphoid malignancies including acute lymphatic leukemia,

chronic lymphocytic leukemia, Hodgkin lymphoma, non-Hodgkin lymphoma and plasma cell disorders (**Figure 2**).[6]

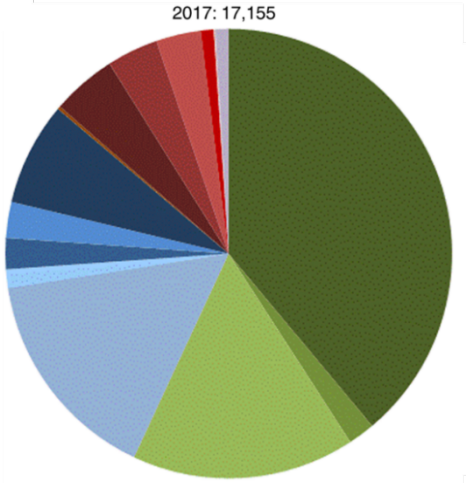

	Proportion of allogeneic HCT (%)
	2017
Acute myeloid leukemia	38.9
Chronic myeloid leukemia	2.0
Myeloproliferative disorders	16.1
Acute lymphatic leukemia	15.6
Chronic lymphocytic leukemia	1.3
Plasma cell disorder	2.2
Hodgkin lymphoma	2.6
Non hodgkin lymphoma	7.4
Other solid tumor	0.2
Bone marrow failure	4.7
Hemoglobinopathies	3.7
Primary immune disorders	3.2
Inherited disorders of metabolism	0.9
Auto immune disorders	0.1
Others	0.9
	100

Figure 2. Indications for allo-HSCT in 2017, according to the actual EBMT survey report (from Passweg et al., 2019[6]).

1.3 Limitations of allo-HSCT

Complications after allo-HSCT may occur due to high-dose chemotherapy, are immune-activation-related or develop as consequence of an impaired immune defense. Basically, complications can be divided into infections and non-infectious complications, such as GVHD, sinusoidal obstruction syndrome and transplantation-related thrombotic microangiopathy.[1]

1.3.1 Infections

Patients who undergo allo-HSCT are at high risk to suffer from infections. In general, the risk is higher in the early phase after allo-HSCT but infections may occur at any time after transplantation. Nevertheless, certain types of infections can be classified into approximate time periods after transplantation (**Figure 3**).[8]

The early phase after transplantation (pre-engraftment phase) is characterized by conditioning-induced immunodeficiency, incomplete engraftment and further immune suppression as preventive treatment for GVHD. During the early pre-engraftment phase (2-4 weeks after transplantation), conditioning results in neutropenia and mucosal damage. Bacterial infections mainly occur in this phase whereas viral and fungal infections are less prevalent. However, infections with aspergillus and candida species (fungal) as well as herpes simplex virus are possible.[1,8-13]

The early post-engraftment phase refers to the second and third month after transplantation. Risk factors for serious infections include immunosuppressive therapy and the onset of acute

GVHD (aGVHD). During this phase, viral and fungal infections are predominant. Cytomegalovirus infection or reactivation as well as infections with Pneumocystis jirovec and aspergillus species are among the most frequent.[8,13]

During the late phase (more than 3 months after transplantation), infections with encapsulated bacteria like streptococcus pneumoniae and haemophilus influenzae may occur. Further, the risk for Epstein-Barr virus and varicella-zoster virus infection or reactivation is increased. In addition, chronic GVHD prevents immune reconstitution and promotes further infections due to prolonged immunosuppression.[1,9-13]

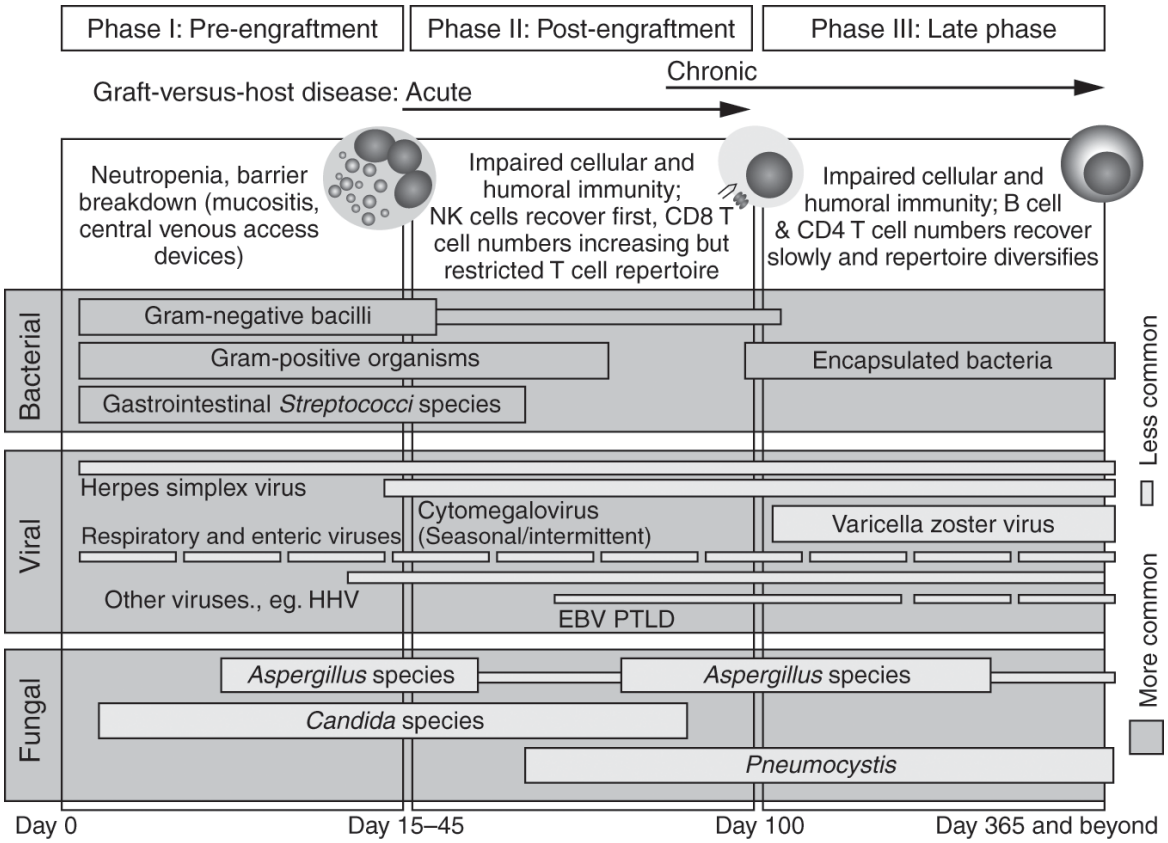

Figure 3. Occurrence of infections after allo-HSCT. HHV: human herpesvirus, EBV: Epstein-Barr virus, PTLD: post-transplant lymphoproliferative disease (from Mackall et al., 2009[8]).

1.3.2 Noninfectious complications

Besides infections, there is a broad range of noninfectious diseases that may develop after allo-HSCT and can be divided into two groups: early noninfectious complications (within 3 months post allo-HSCT) and late noninfectious complications (later than 3 months post allo-HSCT).

Early complications usually occur due to conditioning-related tissue damage and include hepatic sinusoidal obstruction syndrome (veno-occlusive disease of the liver), engraftment failure,

transplant-related thrombotic microangiopathy, capillary leak syndrome, idiopathic pneumonia syndrome and diffuse alveolar hemorrhage.[14-16]

At the onset of late complications, the recovery of immune cells is complete but humoral immunity is still weak. The most common and serious late complication of allo-HSCT is chronic GVHD. Chronic GVHD may develop directly from aGVHD (progressive onset chronic GVHD), after a disease-free interval (quiescent chronic GVHD) or without previous aGVHD (de novo chronic GVHD).[15,17]

1.4 Graft-versus-Host Disease

As mentioned before, GVHD is the side effect that is responsible for most deaths after allo-HSCT. The next chapters provide a more detailed explanation of clinical manifestations, molecular mechanisms and therapeutic targets of GVHD, with a particular focus on aGVHD.

1.4.1 Onset of GVHD

As shown above in **Figure 3**, the occurrence of complications following allo-HSCT can be associated with reconstitution of immune cell subsets.

The pre-engraftment phase (phase I) is characterized by neutropenia and mucosal barrier loss due to previous conditioning regimen, allowing a high risk for infections. During phase II, patients show an impaired cellular and humoral immune response. Neutrophils and natural killer cells proliferate and return to normal levels. The reconstitution of T cells extends over phases II and III. $CD8^+$ T cell number increases by expansion and de novo synthesis in the thymus during phase II, while recovery of $CD4^+$ T cells, together with B cells, occurs during phase III (**Table 1**). Phase II is accompanied by fungal and viral infections and the onset of aGVHD. Phase III is related to high reactivation rates of latent virus infections[18] and the occurrence of chronic GVHD.[8,19,20]

Immune cells	Duration after allogeneic HSCT
Neutrophils >0.5 × 10^9/L	~14 days for PBSC, ~21 days for BM, and ~30 days for CB
NK cells	30–100 days
T cells	100 days
CD19+ B cells	1–2 years

Table 1. Immune reconstitution after allo-HSCT. NK cells: natural killer cells, PBSC: peripheral blood stem cells, BM: bone marrow, CB: cord blood (from Ogonek et al., 2016[12]).

aGVHD is the most serious side effect after allo-HSCT. Severe cases, grade III and grade IV aGVHD, show a bad prognosis with about 30% and 5% long-term survival rate, respectively.[21,22] In addition, the complications mentioned above occur, but are mostly related to aGVHD, e.g. patients usually die of infections when treated with immunosuppressive drugs for aGVHD. The pathomechanism of aGVHD is based on allogeneic donor T cells attacking endogenous cells of the allo-HSCT recipient (described in detail under **1.4.4**).

1.4.2 Clinical manifestation of GVHD

GVHD can be divided into two different forms, acute and chronic GVHD. Patients can develop one of them or an overlap syndrome with characteristics of both, acute and chronic GVHD. The classical distinction between acute and chronic GVHD is based on the time of onset of symptoms. The appearance of symptoms within the first 100 days after transplantation was defined as acute form, later onset as chronic form. Due to the increased use of reduced intensity conditioning or the infusion of donor lymphocytes, the classical division into acute and chronic GVHD has changed. Nowadays, distinction is made based on clinical symptoms rather than on precise time points.[23] The National Institute of Health (NIH) has refined the classification of acute and chronic GVHD according to **Table 2**.[24]

Category	Time of Symptoms after HTC or DLI	Presence of Acute GVHD Features	Presence of Chronic GVHD Features
Acute GVHD			
Classic acute GVHD	≤100d	Yes	No
Persistent, recurrent, or late-onset GVHD	>100d	Yes	No
Chronic GVHD			
Classic chronic GVHD	No time limit	No	Yes
Overlap syndrome	No time limit	Yes	Yes

Table 2 Categories of acute and chronic GVHD. DLI: donor lymphocyte infusion (from Strong Rodrigues et al., 2018[24]).

In the following sections, we focus on aGVHD. Main target organs of aGVHD are the skin, gastrointestinal tract, and the liver. Skin aGVHD often occurs as the first sign of aGVHD and is expressed by maculopapular skin rash and blistering. Usually, skin aGVHD starts to form on the face, ears, palms and soles. In more pronounced stages skin rash can spread to the whole body surface.[21,24]

Early signs of the involvement of the gastrointestinal tract include loss of appetite, early satiety and weight loss. With more severe affection patients suffer from abdominal cramps, diarrhea, severe nausea, vomiting and gastrointestinal bleeding.[21,25]

Clinical signs of hepatic aGVHD are jaundice of skin or eyes and rising bilirubin concentration. Elevated levels of aspartate transaminase and alanine transaminase further indicate liver injury.[21,25,26]

Table 3 displays classification of aGVHD grades based on organ involvement and severity of symptoms.

Extent of organ involvement			
Stage	**Skin**	**Liver**	**Gut**
1	Rash on <25% of skin	Bilirubin 2–3 mg/dl	Diarrhea >500 ml/day or persistent nausea
2	Rash on 25–50% of skin	Bilirubin 3–6 mg/dl	Diarrhea >1000 ml/day
3	Rash on >50% of skin	Bilirubin 6–15 mg/dl	Diarrhea >1500 ml/day
4	Generalized erythroderma with bullous formation	Bilirubin >15 mg/dl	Severe abdominal pain with or without ileus
Grade			
I	Stage 1–2	None	None
II	Stage 3	Stage 1	Stage 1
III	Stage 1–3	Stage 2–3	Stage 2–4
IV	Stage 4	Stage 4	–

Table 3. Staging and grading of aGVHD (from Strong Rodrigues et al., 2018[24]).

While patients with grade III and grade IV aGVHD show poor long-term survival rates, 30% and under 5%, survival rates increase to over 80% for patients with grade I-II aGVHD.[21] A mild form of aGVHD is even desirable due to the graft-versus-tumor (GVT) effect. Allogeneic T cells from the donor attack not only healthy recipient cells, but also remaining malignant tumor cells of the recipient. Therefore, mild forms of aGVHD reduce the occurrence of relapse and could be an advantage over syngeneic or T cell depleted transplantations.[27]

1.4.3 Risk factors for the development of aGVHD

Numerous factors are supposed to influence the development of aGVHD. The most important risk factor is human leukocyte antigen (HLA) mismatching. The term HLA complex refers to the human major histocompatibility complex (MHC), one of the most gene-dense and polymorphic regions of human DNA, located on the short arm of chromosome 6.[21] Genes encoded by the MHC complex are classified into three groups: MHC class I, MHC class II and MHC class III (**Figure 4**).[28,29] HLAs play an important role in immune activation processes and a match of HLAs between allo-HSCT donor and recipient is crucial to prevent graft rejection. HLA typing is done for the five loci HLA-A, HLA-B, HLA-C (class I), HLA-DRB1 and HLA-DQB1. The gold standard for an allo-HSCT is a 10/10 match, meaning allele compatibility in all five loci.[29-32]

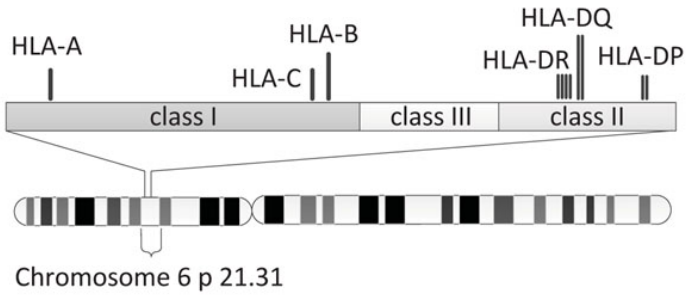

Figure 4. Major histocompatibility complex (MHC). The MHC is located on chromosome 6 in humans and encodes for a number of human leukocytes antigens (HLAs) (from Xie et al., 2010[29]).

MHC class I consists of the genes HLA-A, HLA-B and HLA-C that translate proteins that are found on the surface of all nucleated cells and are responsible for antigen presentation of intracellular antigens. MHC class I proteins present peptides to $CD8^+$ T cells and induce cell-mediated cytotoxicity upon the recognition of a foreign peptide.[21,33]

MHC class II proteins include HLA-DPA1, HLA-DPB1, HLA-DQA1, HLA-DQB1, HLA-DRA1, and HLA-DRB1. In contrast to MHC class I proteins, these proteins are almost exclusively present on the surface of certain immune cells. MHC class II proteins present extracellular peptides to $CD4^+$ T cells that activate B-cells or macrophages to destroy foreign structures.[21,29]

The importance of donor and recipient APCs on the development of aGVHD depends on the type of antigen presentation (via MHC I or MHC II). Since MHC I presentation mainly includes endogenous peptides, recipient APCs may be more important in CD8-mediated aGVHD. In contrast, MHC II molecules present endogenous as well as exogenous peptides, assuming an important role of donor and recipient APCs on CD4-mediated aGVHD.[33]

Unlike MHC class I and class II proteins, MHC class III proteins are not involved in antigen presentation. MHC class III genes encode for proteins of the complement system and tumor necrosis factor (TNF) family genes.[34]

During allogeneic tumor experiments in the 1940s, the analog complex in mice on chromosome 17 was identified and designated as histocompatibility locus 2, H-2 for short.[35] The H-2 complex is also divided into three regions that encode for class I, class II and class III molecules. As in human, class I (H-2K, H-2D, H2-L) and class II (IA-αβ, IE- αβ) function in antigen presentation.[36]

Despite good HLA-matching up to 50% of allo-HSCT recipients develop grade II-IV aGVHD.[37] This is explained by differences in 'minor' histocompatibility antigens (miHAs) outside the HLA loci. miHAs are peptides derived from polymorphic genes. Bound to MHC receptors, miHAs can be recognized by donor T cells. (**Figure 5**).[33] Differences between donor and recipient minor antigens are limited to one or multiple base pairs and occur despite HLA matching through single-nucleotide polymorphisms (SNPs), base pair insertions or deletions or

copy number variations.[38] The importance of miHA matching is supported by the finding that a 1% increase in genome-wide mismatching results in a 20% increase of severe aGVHD.[39] However, besides triggering aGVHD, miHAs can also cause the beneficial GVT effect, if the mismatch is also present in malignant cells.[40]

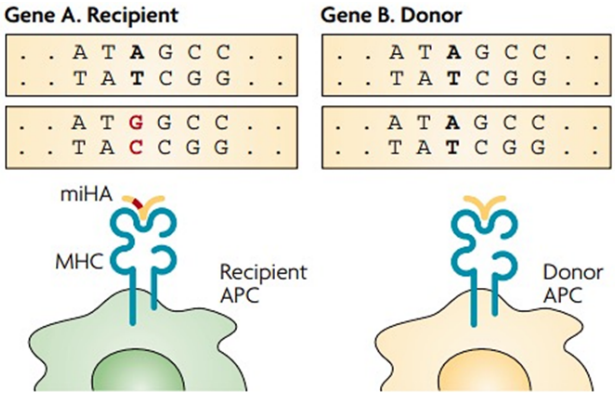

Figure 5. miHA differences between donor and recipient. APC: antigen presenting cell, MHC: major histocompatibility complex, miHA: minor histocompatibility antigen (from Shlomchik, 2007[33]).

Some miHAs are known, including antigens on the Y chromosome. The gene SMCY differs from the SMCX gene homologue on the X chromosome in more than 200 residues, generating male-specific H-Y antigens. Due to these X-Y chromosome differences, the risk for aGVHD is increased in transplantations of HSCs from a female donor to a male recipient. Other known miHAs include the human HA-1 and HA-2 allelic pairs that differ only in single amino acids.[33] Another risk factor for aGVHD is the age of donor and recipient that may influence the transplantation outcome. A higher age of either the donor or the recipient correlates with increased occurrence of aGVHD. Further, higher doses of conditioning regimen probably induce higher degrees of tissue damage that results in exacerbated inflammation due to alloreactive T cells. This was proven by the use of non-myeloablative conditioning that showed less cases of aGVHD development in different studies.[21,41]

1.4.4 Pathomechanisms of aGVHD

The immunopathology of aGVHD relays on the alloreactivity of donor T cells. Despite donor-recipient matching, donor and recipient cells differ slightly in the expression of surface miHAs. The recognition of these antigens as 'nonself' and the subsequent attack by immune cells is fundamental for the development of aGVHD.[39]

The initiation and progression of aGVHD can be divided into three phases (**Figure 6**)[22,40,42]:

I) tissue damage and activation of host antigen presenting cells (APCs)

II) donor T cell activation

III) cellular and inflammatory effector phase

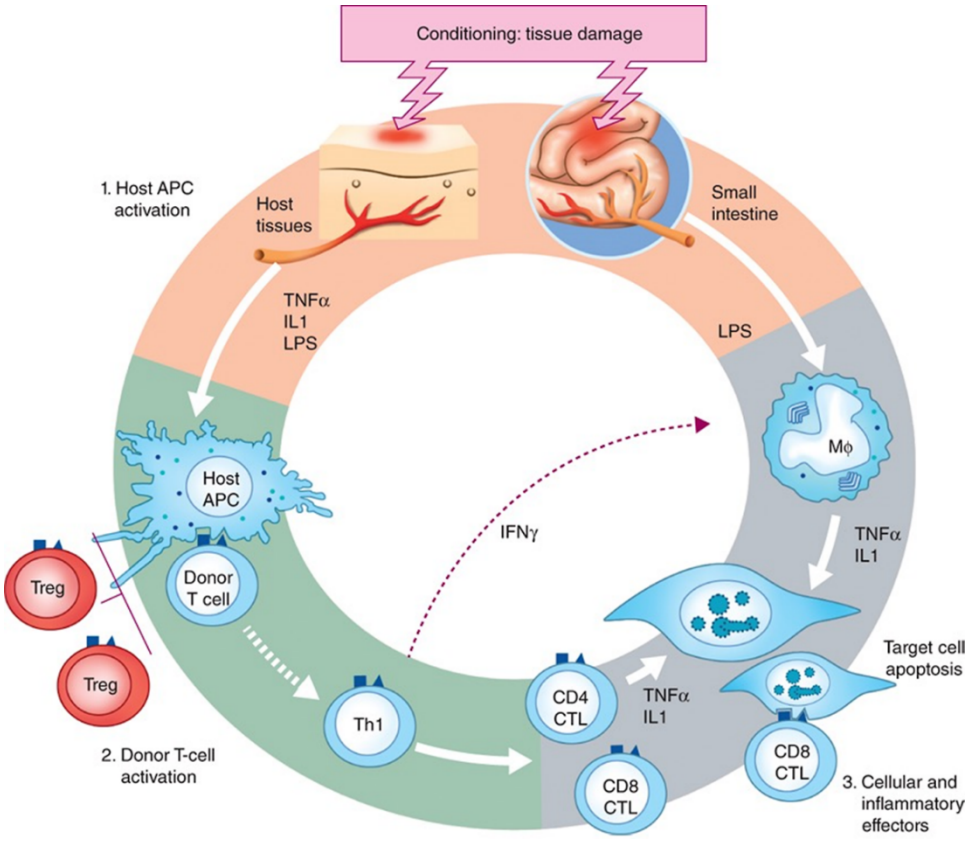

Figure 6. Pathomechanisms of aGVHD. IL1: interleukin 1, IFN γ: interferon gamma, LPS: lipopolysaccharide, Treg: regulatory T cell, Th1: T-helper cell type 1, CTL: cytotoxic T lymphocyte, APC: antigen presenting cell (from Ferrara et al., 2009[22]).

Phase I: Tissue damage and activation of host APCs

The onset of the first phase lies prior to the actual allo-HSCT and is characterized by tissue damage due to the conditioning regimen. As described in chapter **1.1**, the conditioning is needed to destroy cancer cells, prevent transplant rejection and to create room for donor stem cells. However, conditioning causes extensive damage of host tissue that is accompanied by the release of damage-associated molecular patterns (DAMPs) including uric acid (UA), adenosine triphosphate (ATP), high-mobility group box 1 (HMGB-1) and interleukin-33 (IL-33). DAMPs activate their according receptors (NLRP3, P2X7, P2Y2) and trigger the release of proinflammatory cytokines (TNF-α, IL-6, IL-1)[39,42,43] and chemokines (C-C motif ligand 2-5 (CCL2-5), CXC-motif ligand 9-11 (CXCL9-11)).[40] In addition, the conditioning-induced damage of the gut epithelium leads to loosening of tight junctions between epithelial cells and

the release of pathogen-associated molecular patterns (PAMPs). PAMPs, like the cell-wall component lipopolysaccharide (LPS), are derived from bacteria and further triggers the production of TNF-α and IL-1.[40] The extensive release of cytokines and chemokines, DAMPs and PAMPs drives host APCs to enhance the expression of adhesion molecules, costimulatory molecules and MHC antigens.[40] Further, activated immune cells cause local tissue damage by the release of reactive oxygen species (ROS) (**Figure 7**).[44] During the first phase of aGVHD pathology, the intensity of the conditioning and degree of tissue damage correlate with the risk of aGVHD.[40,42,43,45]

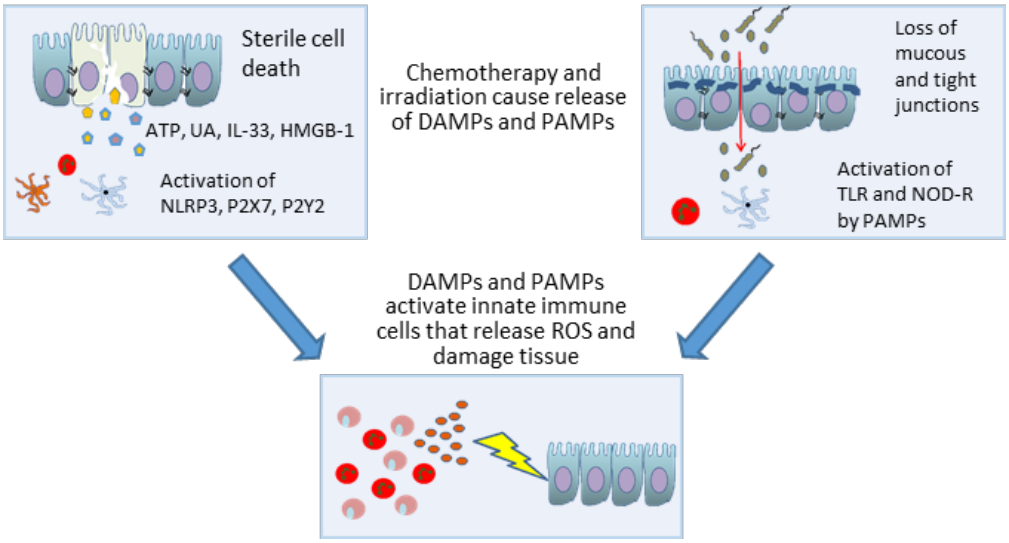

Figure 7. Early events in the pathogenesis of aGVHD. DAMPs: danger-associated molecular patterns, PAMPs: pathogen-associated molecular patterns, ATP: adenosine triphosphate, UA: uric acid, IL-33: interleukin 33, HMGB-1: high-mobility group box 1 protein, NLRP3: nucleotide-binding domain leucine-rich repeats family protein 3, P2X7: P2X purinoceptor 7, P2Y2: P2Y2 purinoceptor 2, TLR: toll-like receptor, NOD-R: nucleotide-binding oligomerization domain-like receptor, ROS: reactive oxygen species (adapted from Zeiser, 2019[44]).

Phase II: Donor T cell activation

The main purposes of the second phase are the activation, differentiation and migration of donor T cells.[40]

After allo-HSCT, APCs from the host (that survived conditioning) and from the recipient are present in the recipients' bone marrow, this condition is referred to as chimeric. The infused donor T cells are able to recognize foreign antigens presented either by host or donor APCs. The activation of donor T cells subsequently leads to the enhanced expression of MHC molecules, increasing the antigen presentation ability of APCs. Further, activated T cells differentiate to T helper cells and cytotoxic T cells. T helper cells are classified as Th1

(interferon-gamma (IFN-γ), IL-2 and TNF-α), Th2 (IL-4, IL-5, IL-10 and IL-13) and Th17 (IL-17A, IL-17F, IL-21 and IL-22) cells, based on their cytokine expression profile.[40,46] Th1 cytokines are strongly involved in the development of aGVHD e.g. via the induction of APC activation by TNF-α.[40]

However, the response of the TCR depends on the costimulatory signal[47] which is needed to lower TCR activation threshold, amplify and sustain cytokine production, inhibit apoptosis and to support T effector metabolism.[39] Various costimulatory interactions are known, whereas B7-CD28 and B7-CTLA-4 are among the most important. Central molecules of the B7 family are CD80 (B7-1) and CD86 (B7-2). The binding of CD80/CD86 to the CD28 co-receptor on T cells promotes T cell activation and survival, while binding to the cytotoxic T lymphocyte antigen 4 (CTLA-4) transmits an inhibitory signal.[39,47]

The stimulation of T cells results in the activation of multiple pathways for the production of inflammatory cytokines, representing the third signal of T cell activation. IL-2 and IFN-γ are among the most important cytokines. IL-2 is known to further activate T cells but also induces natural killer cell responses and stimulates macrophages for the release of TNF- α, all together driving inflammation and tissue damage.[7]

Phase III: Effector phase

The third phase is the cellular and inflammatory effector phase. The main cellular effectors of this phase are cytotoxic T cells and natural killer cells that mediate through three cytolytic pathways: the perforin/granzyme B pathway, Fas receptor (Fas)/Fas ligand (FasL) signaling and direct cytokine-mediated injury.[47] Target organ damage in the liver seems to be mediated mainly via Fas/FasL interaction, while the perforin/granzyme-mediated tissue injury is predominant in the gastrointestinal tract. Fas and FasL are both members of the TNF family, Fas is expressed on aGVHD target tissue cells, while FasL is expressed on activated T cells, macrophages and neutrophils. Interaction between Fas and FasL leads to Fas-mediated cell apoptosis and thus tissue damage. Perforin, together with granzymes, is stored in cytolytic granules of cytotoxic T cells and natural killer cells. The presence of calcium triggers the formation of membrane channels composed of perforin polymers in the membrane of target cells. These channels allow the infiltration of granzymes that activate caspase cascades to induce target cell apoptosis.[40,45,47]

Besides cellular effectors also inflammatory effectors contribute to target organ damage during the third phase of aGVHD pathology. LPS and other pathogenic factors that diffuse through the damaged mucosa promotes the secretion of TNF-α, that can further activate APCs, trigger the production of chemokines for effector cell recruitment to target organs and directly induce

cell apoptosis.[40,45] Further, the increased expression of IL-1 on mononucleated cells was shown to be important in target organ damage during the effector phase.[40,47]

1.4.5 Prevention and current treatment of aGVHD

Currently, there is no optimal prevention strategy for aGVHD. Even if aGVHD can be prevented for the most part, it is at the expense of other serious complications. The prophylaxis procedure aims to suppress immunoreactions of donor T cells, either by using pharmacologic agents or by T cell depletion of the graft. Pharmacological regimen includes the combination of a calcineurin-inhibitor, clyclosporin A or Tacrolimus in combination with methotrexate (MTX) or mycophenolate mofetil (MMF).[48-51]

Cyclosporin A and Tacrolimus act by blocking the calcium-dependent nuclear factor of activated T cells (NFAT) pathway which prevents the production of the proinflammatory cytokine IL-2.[48] MTX inhibits the dihydrofolate reductase and thus prevents thymidylate and purine synthesis. Subsequently, T cell response, proliferation and the expression of adhesion molecules are suppressed.[52] Severe side effects of MTX are hampered hematopoietic recovery and the incidence of mucositis.[48,53] The alternative drug MMF appears to cause less toxicity. MMF impairs proliferation of activated lymphocytes by the intracellular inhibition of purine synthesis.[53] Nevertheless, it is not clear whether the incidence of aGVHD is the same in MTX- and MMF-treated patients[48], as some studies found a higher prevalence for aGVHD grade III-IV in patients treated with MMF in combination with a calcineurin inhbitor.[51]

Considering the fact that aGVHD is T cell mediated, another approach of aGVHD prophylaxis is T cell depletion of the hematopoietic graft. T cell depletion can be done with *ex vivo* or *in vivo* methods. *Ex vivo* methods include negative selection with soybean lectin agglutination and sheep erythrocyte resetting or the use of T cell specific antibodies like CD2, CD3, CD5 that are conjugated to immunomagnetic beads. Another *ex vivo* approach is the positive selection of $CD34^+$ T cells, which is the predominant *ex vivo* method of T cell depletion in clinical use. In contrast, treatment with antithymocyte globulin (ATG) or Alemtuzumab (anti-CD52) allows *in vivo* depletion of T cells.[54,55]

ATG causes T cell depletion via complement-dependent lysis and activation-associated apoptosis. ATG was also shown to exhibit other immunomodulating effects, including the induction of B cell apoptosis, the modulation of cell surface molecules, the influence of maturation and migration of dendritic cells and the induction of regulatory T cells (Tregs) and natural killer-T cells.[56] Though ATG was shown to reduce the incidence of aGVHD, the overall

survival benefit is limited because of the increased risk of Epstein-Barr virus-induced posttransplant lymphoproliferative disease, other serious infections and tumor relapse. So far it is not fully understood which circumstances lead to beneficial or harmful effects of ATG.[57]

The humanized monoclonal antibody against the B and T cell surface marker CD52, Alemtuzumab, functions via antibody-dependent cell-mediated lysis to deplete B and T cells from the recipients' bone marrow.[48] Though Alemtuzumab was shown to reduce the incidence of aGVHD, its use has declined because of an increased risk of relapse, delayed engraftment and a high risk for infections.[58]

The majority of stem cell transplantation centers start treatment at aGVHD grade II. Treatment consists of systemic immunosuppression by continuing the prophylactic treatment plus treatment with glucocorticoids, mainly methylprednisolone or prednisolone. Glucocorticoids reduce aGVHD by their anti-inflammatory and lymphotoxic characteristics.[50,59,60] Despite high responding rates, the mortality rate of patients who do not respond to steroids is up to 80%, which is attributable to poor effectiveness of second-line therapy.[60-62] In contrast to the common corticosteroid use as first-line treatment, therapy for steroid-refractory aGVHD (SR-aGVHD) is individually chosen depending on organ affection. For instance, severe gut involvement is often treated with additional anti-TNF antibodies.[50]

The need for novel treatment options for aGVHD is obvious. Several new approaches are currently being intensively researched, these include[61]:

1) Sirolimus (rapamycin): Sirolimus is an inhibitor of the mammalian target of rapamycin (mTOR) and acts immunosuppressive by blocking T cell signaling. Sirolimus is already used as prophylactic agent and as second-line treatment for SR-aGVHD, its effect during aGVHD is still under investigation.
2) Kinase inhibitors: Inhibitors of the Janus kinase (JAK) family affect proliferation, survival and differentiation. The inhibition of JAK1/2 results in impaired immune signaling function in lymphocytes. The JAK1/2 inhibitor ruxolitinib (Jakafi, Incyte) has currently been approved as treatment for acute and SR-aGVHD by the U.S. Food and Drug Administration.
3) Proteasome inhibitors: Proteasome inhibitors are already approved for the treatment of multiple myelomas. The inhibition of the proteasome shows different immunomodulating effects like the deletion of alloreactive T cells or the inhibition of APCs and IL-6 production.

4) Cytokine modulation: The protease inhibitor alpha-1 antitrypsin (AAT) increases anti-inflammatory functions by the increase of Tregs and IL-10. The addition of IL-22 strengthens the epithelial barrier and thus improves pathogen defense.
5) Monoclonal antibodies: Currently under investigation are Natalizumab, an inhibitor of α4-integrin-containing adhesion molecules; Vedolizumab, an α4β7 integrin inhibitor that prevents the homing of lymphocytes to the gut mucosa, and Brentuximab Vedotin that acts against CD30, which is expressed on activated lymphocytes.
6) Adoptive cell therapy: The transfer of pluripotent mesenchymal stem cells (MSCs) results in impaired B- and T cell activation, inhibition of APCs and natural killer cells and increase of Tregs.
7) Microbiome restauration: Fecal microbiota transplants result in reduced aGVHD by the upregulation of intestinal Tregs and anti-inflammatory cytokines.

As described above, there are several promising new approaches under investigation. However, all of them directly or indirectly target T cell functions. Though it is known that the occurrence of aGVHD is T cell mediated, the inhibition or elimination of T cells bears the risk of serious infections and increased relapse rates.

1.5 Angiogenesis

1.5.1 Inflammation-induced angiogenesis

It is well known that the two processes angiogenesis and inflammation are closely related. Inflammation is induced in order to eliminate the inflammatory stimulus (pathogens, damaged cells, toxic compounds, or irradiation) and start the healing process. The five cardinal signs of inflammation are redness, swelling, heat, pain and loss of function of the affected tissue. Though these symptoms are mostly mediated by immune cells, the endothelium bears the important function of immune cell recruitment to the site of inflammation. Among others, the induction of angiogenesis is mediated by main characteristics of inflamed tissue, hypoxia and immune cell infiltration.[63-65]

Hypoxic conditions cause the inhibition of prolyl hydroxylases and von Hippel-Lindau protein and allow hypoxia-inducible factor (HIF) dimerization and translocation to the nucleus.[65] HIF proteins not only increase the expression of VEGF, but also interact with nuclear factor kappa B (NFkB) pathway factors that are involved in immune responses.[65,66]

Immune cell infiltration is accompanied by the release of proinflammatory cytokines including TNF-α, IL-1, IL-6, IL-8, IL-15, IL-17, IL-18, granulocyte colony-stimulating factor (G-CSF) and oncostatin M that may directly trigger angiogenic processes or act by inducing the production of VEGF. Inflammatory cytokines can further influence the expression of adhesion molecules and matrix metalloproteases (MMPs) and mediate the angiopoietin (ANG)-Tie2-signaling axis.[66]

CXC-motif chemokines that are released by immune cells can act directly on endothelial cells (ECs) or indirectly promote angiogenesis by further attracting immune cells to the site of inflammation. In turn, recruited immune cells release proangiogenic mediators to trigger the vessel sprouting.[65,66]

Several pathways are known that involve the transcription of proinflammatory mediators and the regulation of angiogenesis. Among the best characterized pathways are the NFκB, mitogen activated protein kinase (MAPK), Janus kinase – signal transducer and activator of transcription (JAK-STAT) and phosphoinositide 3-kinase – serine-threonine-protein kinase (PI3K-AKT) signaling pathways (**Figure 8**). The binding of proinflammatory or proangiogenic mediators to transmembrane receptors activates TNF receptor associated factor (TRAF), focal adhesion kinase (FAK) and Src kinase that further trigger downstream signaling.[66]

The translocation of transcription factors finally results in transcription of respective target genes that promote cell growth, survival, migration, proliferation and differentiation, thus inducing angiogenesis.[65,66]

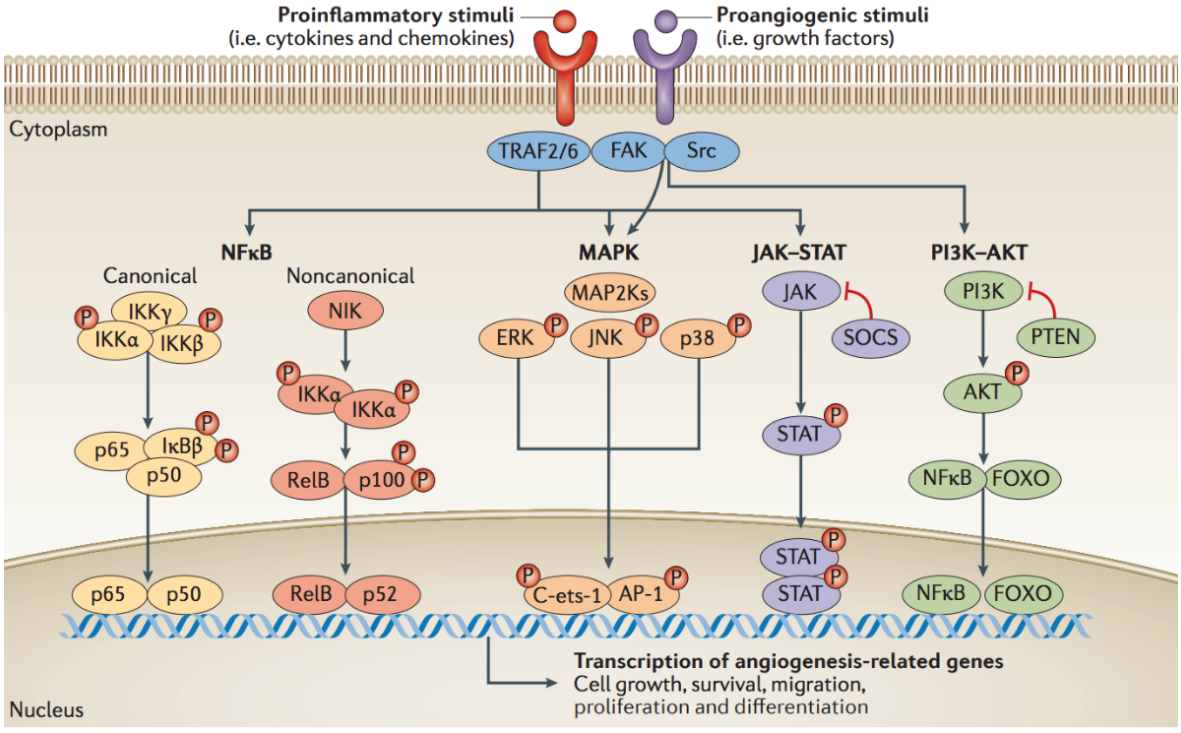

Figure 8. Inflammatory signal transduction pathways involved in angiogenesis. TRAF: TNF receptor associated factor, FAK: focal adhesion kinase, Src: acronym from cellular and sarcoma, NFκB: nuclear factor kappa B, IκB: inhibitor of kappa B, IKK: IκB kinase, NIK: NFκB-inducing kinase, RelB: Rel-like domain-containing protein, MAPK: mitogen activated protein kinase, MAP2K: mitogen-activated protein kinase kinase, ERK: extracellular signal-regulated kinase, JNK: c-Jun N-terminal kinase, C-ets-1: known as transforming protein p54, AP-1: transcriptional activator protein 1, JAK-STAT: Janus kinase – signal transducer and activator of transcription, SOCS: suppressor of cytokine signaling, PI3K-AKT(PKB): phosphoinositide 3-kinase - serine/threonine protein kinase (protein kinase B), PTEN: phosphatase and tensin homologue, FOXO: forkhead box protein O (from Tas et al., 2016[64]).

1.5.2 Blood and lymph vessel development

In general, the formation of vessels can be divided into the three processes, vasculogenesis, angiogenesis and lymphangiogenesis, the latter partly belonging to angiogenesis (**Figure 9**). During embryogenesis, blood vessels are formed via vasculogenesis. Endothelial progenitor cells (EPCs) or angioblasts that derived from mesodermal cells in the early embryo, aggregate to form blood islands. The further fusion of blood islands leads to the formation of a primitive vascular network, the honeycomb-shaped primary capillary plexus. Remodeling of primary capillary plexi (arteriovenous differentiation) gives rise to a network of arteries and veins. The dorsal aorta and the cardinal vein are formed by the aggregation of angioblasts without previous plexus formation.[67]

In contrast to the vessel formation via embryonic vasculogenesis, angiogenesis is referred to the process of sprouting from existing vessels and requires the division and migration of differentiated ECs.[67]

Lymphangiogenesis combines both processes. Whereas the formation of the first lymphatics requires the sprouting of single cells from embryonic veins and the formation of lymphatic sacs, the further increase of the lymphatic network occurs via sprouting angiogenesis (see chapter **1.5.8**).[67,68]

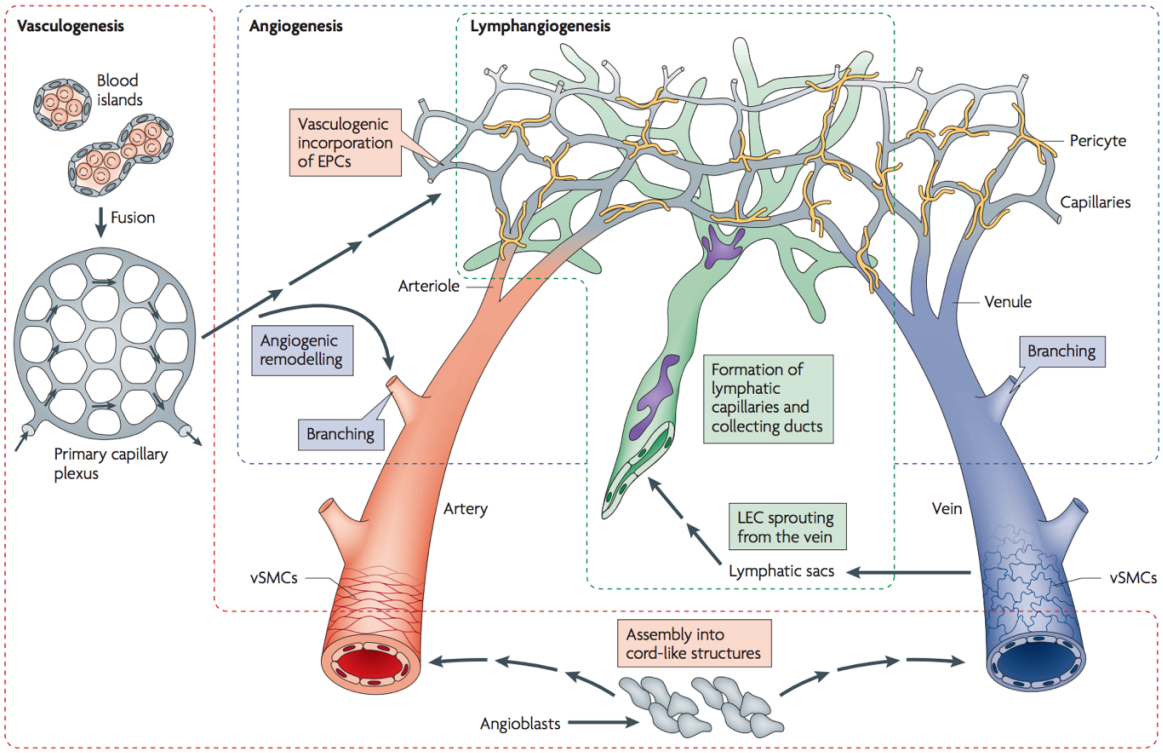

Figure 9. Origin of the blood and lymphatic vasculature. EPCs: endothelial progenitor cells, vSMCs: vascular smooth muscle cells (from Adams and Alitalo, 2007[67]).

In adulthood, angiogenesis is the predominant process for the formation of new vessels in healthy processes like wound healing but also in pathologic conditions like inflammation or cancer.

In the late 1970s, Asprunk and Folkman were the first who described the different steps of sprouting angiogenesis, that are: 1) the degradation of the basement membrane, 2) the migration of ECs into the connective tissue 3) the formation of a solid cord of ECs, 4) lumen formation, 5) the connection of newly formed tubular sprouts (anastomosis) and simultaneously the synthesis of a new basement membrane and the recruitment of pericytes.[69]

1.5.3 Molecular mechanisms of angiogenesis

Molecular mechanisms behind the formation of new vessels via angiogenesis consist of a complex interplay between angiogenic factors and activated pathways. The different steps of vessel formation require strictly regulated processes like the selection of a guiding tip-cell, stalk cell proliferation, fusion of adjacent sprouts and maturation of the newly formed vessel,[70] that are discussed below.

Under healthy conditions, the endothelium remains in a quiescent state and EC proliferation is inhibited due to their connection to pericytes that release VEGF and ANG1 to promote cell survival and suppress proliferation. Hypoxic, inflamed and tumor tissue are able to release

angiogenic stimuli, including members of the VEGF family, ANG2, fibroblast growth factor (FGF) and chemokines, that start the cascade of angiogenic remodeling. The angiogenic stimuli trigger the degradation of the basement membrane by MMPs to enable endothelial migration. ANG2 induces the detachment of pericytes from ECs, which in parallel loosen their adherens junctions and increase vascular permeability.[70]

During the next step, three types of endothelial cells are differentiated in the sprouting vessel. One single cell is dedicated as guiding cell for the nascent vessel, the tip cell. Tip cells are highly polarized, form filopodia, expose a high migratory potential but do not proliferate. Cells behind the tip cell are so-called stalk cells that ensure elongation of the newly formed sprout. In contrast to tip cells, stalk cells show high proliferation potential but do not migrate. Phalanx cells are located next to stalk cells and compose the quiescent, non-proliferating vessel.[71,72]

The decision for tip cells and stalk cells is highly regulated by VEGF and Notch signaling pathways. Endothelial cells that are exposed to the highest concentration of VEGF become tip cells and the subsequent activation of VEGFR2 induces the expression of Notch ligand delta-like 4 (Dll4). Dll4 activates Notch in neighboring cells which in turn results in reduced expression of VEGFR2 and VEGFR3, while VEGFR1 is upregulated (**Figure 10**).[71,72]

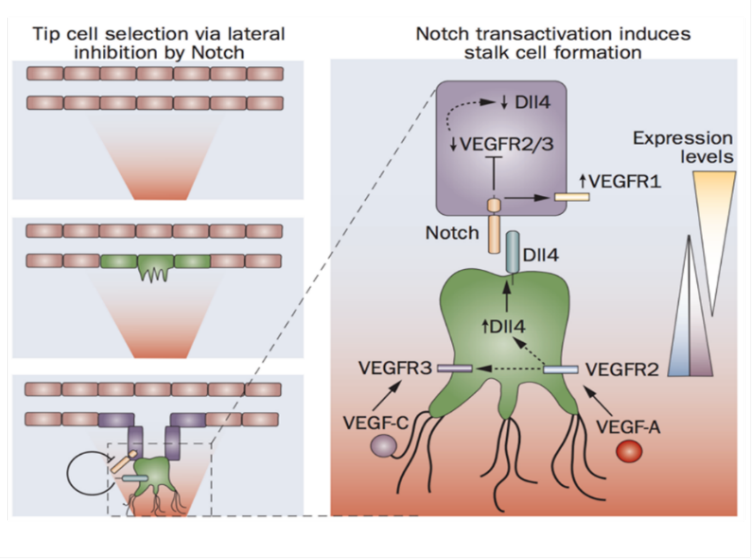

Figure 10. Notch-mediated tip cell selection. DII4: delta-like 4, VEGFR: vascular endothelial growth factor receptor, VEGF: vascular endothelial growth factor (from Carmeliet et al., 2009[71]).

Tip cells are guided by signals like semaphorins and ephrins and adhere to the extracellular matrix to migrate. Stalk cells start to proliferate in response to the stimulation by Notch, Notch-regulated ankyrin repeat protein (NRARP), wingless/integrated proteins (WNTs), placental growth factor (PlGF) and FGFs.[71] After the elongation phase, the process of lumen formation starts with the polarization of ECs to generate an apical (luminal) site that is characterized by negatively charged glycoproteins (CD34, podocalyxin) to emit a repellent signal for neighboring cells.[69] The generation of a circulating blood flow requires the connection of two adjacent sprouts. By the contact of tip cells from two nascent sprouts, the interaction of filopodia triggers

the formation of vascular endothelial cadherin (VE-cadherin) junctions between tip cells and inhibits further migration. Additionally, macrophages accumulate and facilitate tip cell fusion.[69,71] The subsequent blood flow that comes along with oxygen and nutrients, results in a downregulation of VEGF and the return to a quiescent state of endothelial cells.[71]

Stabilization of newly formed vessels is mediated by the attachment of mural cells (pericytes or smooth muscle cells (SMCs)). ECs release platelet-derived growth factor B (PDGFB), ANG1, transforming growth factor-beta (TGF-β), ephrin-B2 and Notch to attract pericytes and vascular smooth muscle cells (vSMCs). The reconstruction of the basement membrane is subsequently promoted by tissue inhibitors of metalloproteinases (TIMPs) and plasminogen activator inhibitor-1.[69,70] **Figure 11** displays the basic steps occuring in angiognesis.

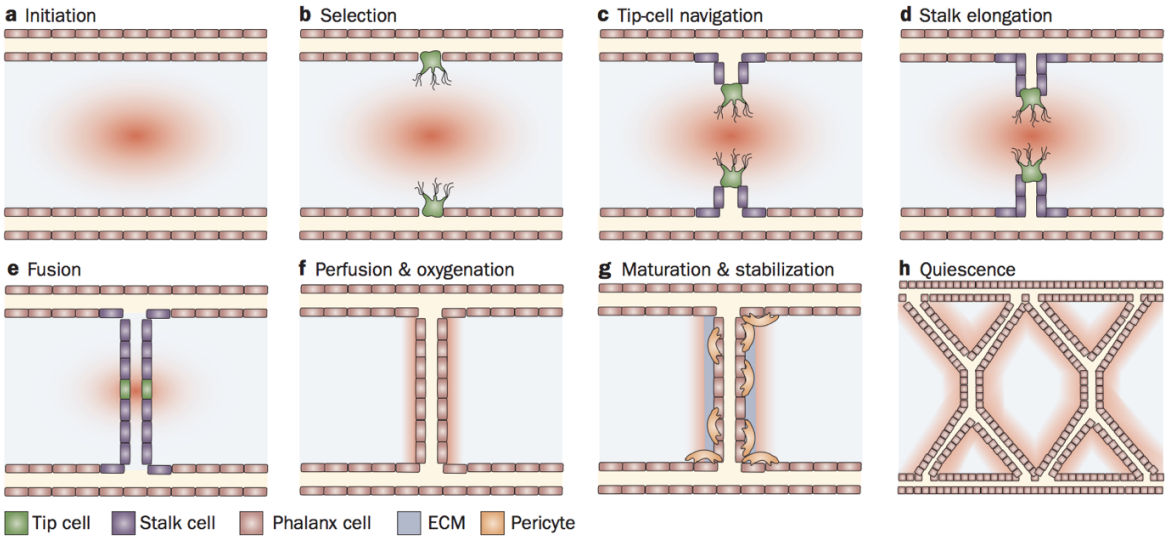

Figure 11. Basic step in the formation of new vessels via angiogenesis. ECM: extracellular matrix (from Carmeliet et al., 2009[71]).

1.5.4 Tgf-β pathway

Despite the outstanding role of VEGF family members in angiogenesis, other factors are involved in the regulation of vessel formation. The TGF-β family consists of numerous evolutionarily conserved pleiotropic cytokines that are divided into activins, bone morphogenic proteins (BMPs) and TGF-β isoforms. TGF-β signaling is crucial during development but also exhibits important functions in adult tissues. This is confirmed by the connection of TGF-β signaling and the occurrence of various diseases like cancer, auto-immune and cardiovascular diseases or fibrosis. The binding of TGF-β ligands to a complex of type II and type I serine/threonine kinase receptors modulates proliferation, migration, differentiation, survival and extracellular matrix synthesis. In mammals, seven type I receptors (activin receptor-like

kinases (ALK1-7)) and five type II (ActRIIA, ActRIIB, BMPRII, TβRII, and AMHRII) receptors are currently known. In most cells, TGF-β signals via Tgf-β receptor type II (TβRII) and ALK5, activins via activin receptor type IIA (ActRIIA) and IIB and ALK4, and BMPs form a complex with BMP type II receptor (BMPRII), ActRIIs and ALK1, 2, 3 and 6.[73,74]

In endothelial cells TGF-β is able to signal either via ALK5 or via ALK1 (**Figure 12**).[73] Upon binding of Tgf-β, TβRII forms a dimer with an ALK receptor. The constitutively active TβRII phosphorylates the type I receptor, which in turn phosphorylates receptor-regulated Smads (small mothers against decapentaplegic). Type I receptors ALK4, ALK5 and ALK7 are able to phosphorylate Smad2 and Smad3, while ALK1, ALK2, ALK3, and ALK6 phosphorylate Smad1, Smad5, and Smad8. The specific activated Smads form a complex with the common mediator Smad4 and translocate to the nucleus to regulate the transcription of their target genes.[73,75] Betaglycan and endoglin serve as co-receptors and are supposed to facilitate TβRII/ALK5 and TβRII/ALK1 signaling. Inhibitory Smads (I-Smads) are able to inhibit the function of Smads by causing the binding of ubiquitin ligases or phosphatases to the activated Smad/receptor complex, thus labeling it for proteasomal degradation or dephosphorylation.[73,75]

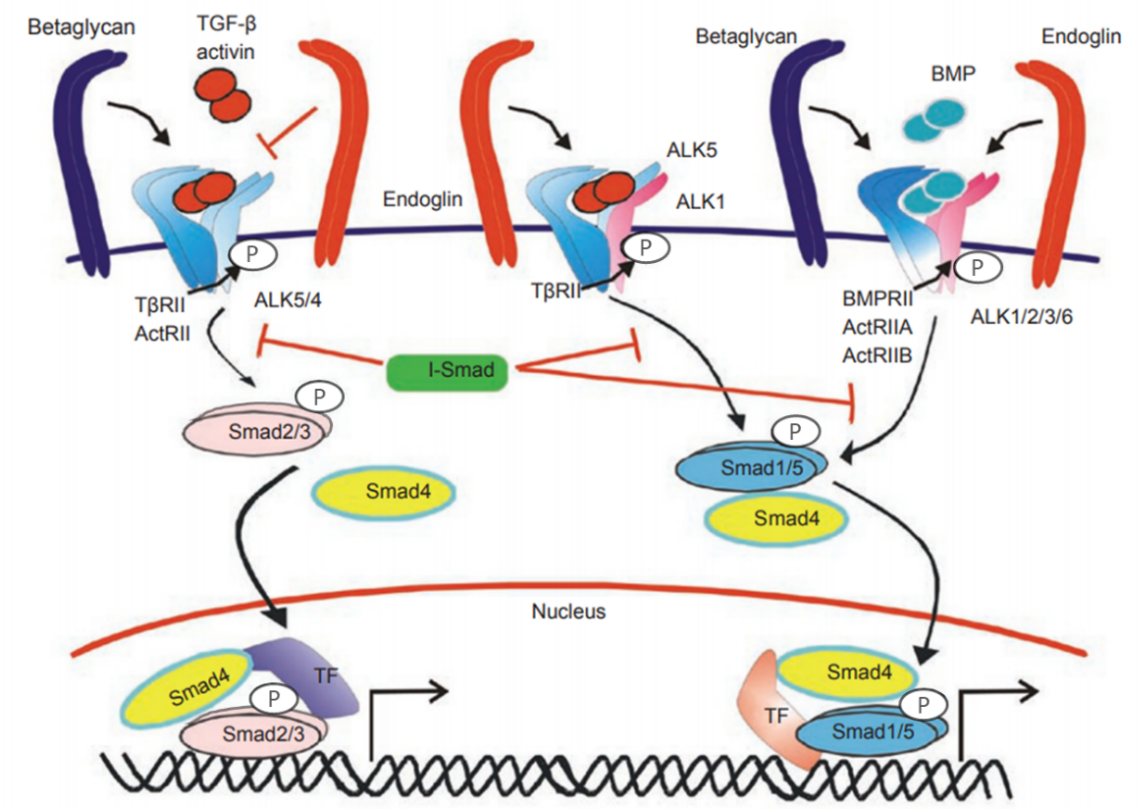

Figure 12. TGF-β signaling in endothelial cells. ALK: activin receptor-like kinases, TGF-β: transforming growth factor beta, TβRII: TGF-β receptor II, Smad: small mothers against decapentaplegic, ENG: endoglin , TF: transcription factor (from Goumans et al., 2009[73]).

1.5.5 Role of TGF-β in endothelial cells

In comparison to other cell types, TGF-β can bind both, ALK5 and ALK1, in endothelial cells. Thus, the receptor-regulated Smads 2, 3, 1, 5, and 8 can be activated by the same ligand. Whereas ALK5 is expressed on most tissues, ALK1 is expressed exclusively on endothelial cells during embryogenesis and angiogenesis. However, depending on the activation of ALK5 or ALK1, TGF-β signaling functions angiostatic or proangiogenic.[73]

The TGF-β/TβRII/ALK5 complex formation and subsequent phosphorylation of Smad2/3 inhibits EC proliferation, tube formation and migration, thus preventing angiogenesis. Mechanisms for the inhibition of angiogenesis include ALK5-induced expression of fibronectin and plasminogen activator inhibitor 1, that prevent endothelial migration. Further, plasminogen activator inhibitor 1 is known to prevent extracellular matrix degradation around the nascent vessel during angiogenesis.[76] Additionally, the TβRII/ALK5 complex results in VE-cadherin accumulation and vessel stabilization and promotes endothelial quiescence.[73]

In contrast, ALK1 activation and phosphorylation of Smad1/5/8 stimulates EC proliferation, tube formation and migration. An important downstream target gene of ALK1 is inhibitor of differentiation or DNA binding (Id-1). ALK1 activation results in an upregulation of Id-1 leading to an increased migratory and tube formation potential of ECs.[73,76]

Besides the assignment of proangiogenic effects to ALK1 and angiostatic effects to ALK5, there are still uncertainties regarding their involvement in angiogenesis. ALK5 seems to be necessary for the recruitment of ALK1 to the TβRII/ALK1 complex and therefore important for functional ALK1 signaling. Further, ALK1 signaling shows inhibitory effects on angiogenesis if it complexes with BMPRII upon the binding of the ligand BMP9.[73]

The regulation of TGF-β signaling in ECs depends on several factors like TGF-β doses, regulatory factors and accessory receptors but the exact mechanisms of TGF-β regulation in ECs are still not fully understood.[73]

1.5.6 Lrg1 as regulator of TGF-β signaling

Leucine-rich alpha-2 glycoprotein-1 (Lrg1) is known to function in protein-protein interactions, signaling and cell adhesion. However, little was known about involvement in particular molecular mechanisms and pathways until Wang et al. found an upregulation of Lrg1 in three different mouse models of retinal diseases. Wang et al. observed that Lrg1 is expressed in healthy mice but highly upregulated under pathologic conditions. Further investigation revealed that Lrg1 promotes tube formation and vessel branching while the blocking of Lrg1 inhibits intact tube formation in *in vitro* studies.[77]

Laser-induced choroidal neovascularization in Lrg1 knock-out mice exposed a crucial role for Lrg1 in pathologic angiogenesis. Co-immunoprecipitation experiments provided further evidence that Lrg1 is classified into the TGF-b pathway as it forms complexes with TβRII, ALK1, ALK5 and endoglin.[77]

The investigation of the role of TGF-β pathway components and their binding affinity to Lrg1 revealed that the presence of endoglin is needed for the binding of Lrg1 to ALK1, and that this complex is strengthened in the presence of TGF-β. ALK5 binding to Lrg1 is independent of endoglin, however, the presence of endoglin weakens Lrg1-ALK5 binding. The addition of TGF-β completely loosens Lrg1-ALK5 connection. Based on these findings, Wang et al. proposed a model on the influence of Lrg1 on TGF-β-mediated angiogenesis.[77]

Under healthy conditions TGF-β signals via TβRII -ALK5-Smad2/3 pathway, which maintains the quiescent status of endothelial cells. Pathologic conditions trigger the increased expression of Lrg1 and endoglin. Together with TGF-β, Lrg1 binds to TβRII/ALK1 and the co-receptor endoglin (ENG). Phosphorylation of Smad1/5/8 leads to the proangiogenic transcriptional response (**Figure 13**).[77]

Due to the recruitment function of ALK5, it is possible that there is an intermediate complex consisting of Lrg1/TβRII/ALK1/ENG/ALK5, that facilitates binding of ALK1 to TβRII. The subsequent binding of TGF-β results in the release of ALK5 from the transient complex.[77]

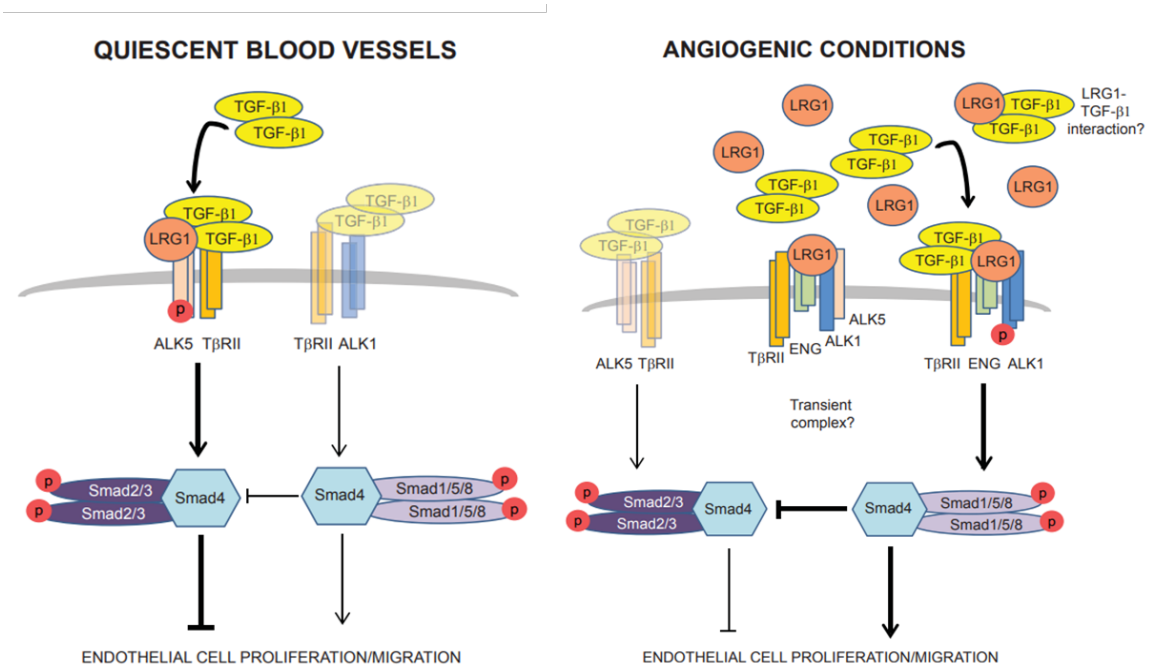

Figure 13. Proposed model of Lrg1-mediated TGFβ signaling in endothelial cells. ALK: activin receptor-like kinases, TGF-β1: transforming growth factor beta 1, TβRII: TGF-β receptor, Smad: small mothers against decapentaplegic, ENG: endoglin, LRG1: leucine-rich alpha-2-glycoprotein 1 (from Wang et al., 2013[77]).

Furthermore, experimental data indicate that Lrg1 is more involved in pathological than in developmental angiogenesis, making it a suitable therapeutic target not only for ocular diseases but also for other inflammatory diseases like aGVHD.[77]

Recent studies reported that serum concentration of Lrg1 is increased in patients under inflammatory conditions. This could be seen in patients suffering from diseases with known involvement of pathologic angiogenesis including inflammatory bowel disease[78], rheumatoid arthritis[79], appendicitis[80] or various types of tumors.[81-83]

1.5.7 Specific characteristics of lymph vessels

The main functions of lymph vessels are maintenance of tissue fluid homeostasis, regulation of immune cell trafficking, and the absorption of dietary fats. Based on these specific functions, the structure of lymph vessels differs from blood vessels in several components.[67,84] Lymphatic capillaries compose of one single layer of lymphatic endothelial cells (LECs) that are not supported by pericytes or smooth muscle cells and have no basement membrane. Further, cell-cell contacts of lymphatic capillaries allow interjunctional gaps (button junctions) that promote high permeability to support leukocyte entry and facilitate the uptake of humoral lymph components.[84,85] Lymph capillaries merge into pre-collecting and collecting vessels, whereby the transition is accompanied by decreasing permeability and increasing stability. Collecting lymphatics are fully covered with SMCs and show a continuous basement membrane. Contraction of SMCs and intraluminal valves mediate the unidirectional flow towards the large thoracic duct (**Figure 14**).[84,85] On its way to the thoracic duct, lymph passes draining lymph nodes that filter lymph for foreign or pathologic structures. The thoracic duct connects to the subclavian vein allowing the backflow of filtered lymph to the systemic circulation.[86]

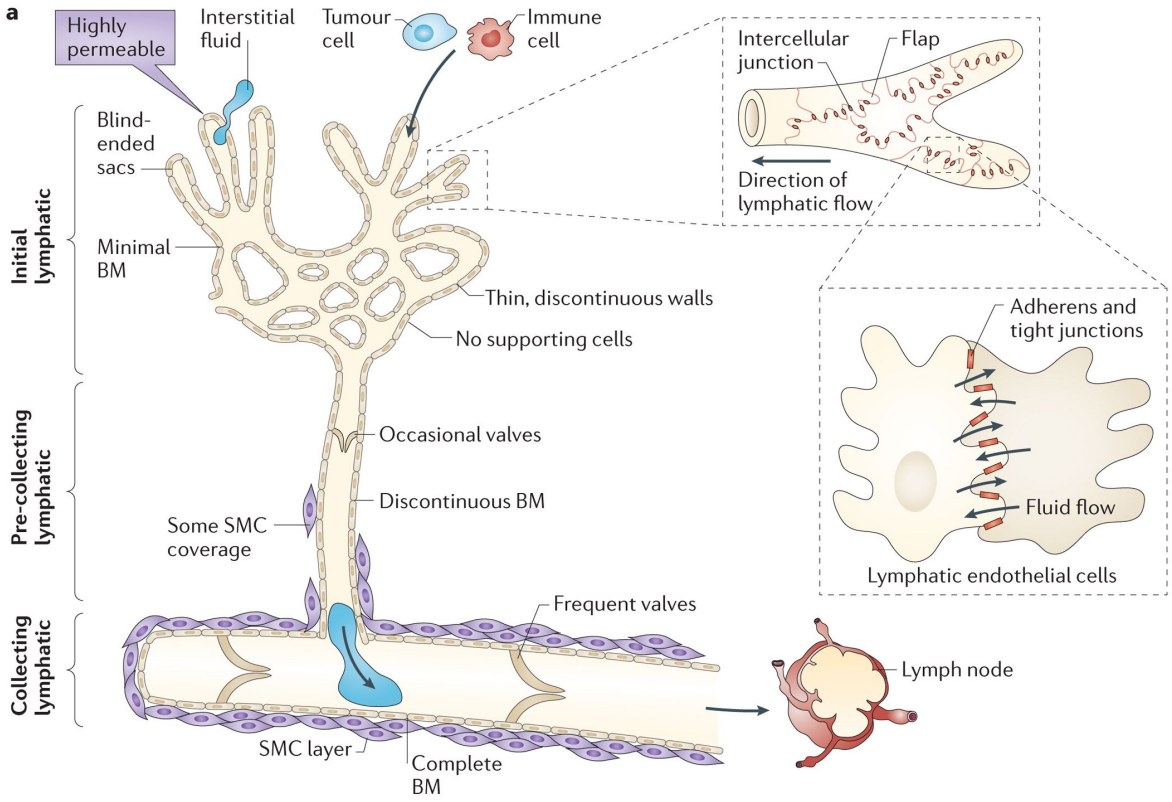

Figure 14. Structure of lymphatic vessels. SMC: smooth muscle cell, BM: basement membrane (from Stacker et al., 2014[84]).

1.5.8 Mechanisms of lymphangiogenesis

As described under **1.5.2**, lymph vessels emerge from the embryonic vein during development. LEC commitment starts with the expression of prospero-related homeobox-1 (PROX-1) transcription factor by a cluster of venous ECs, leading to the upregulation of lymphatic-specific genes (lymphatic vessel endothelial hyaluronan receptor 1 (LYVE1), VEGFR3, CCL21) and the suppression of blood vessel-specific genes. The separation process of LECs from the embryonic vein is probably mediated by spleen tyrosine kinase (SYK) and SH2 domain containing leukocyte protein of 76kDa (SLP76) (and fast-induced adipose factor (FIAF) in the intestine), though the molecular mechanisms remain unclear.[87] Subsequently to the initial specification and budding of lymphatic endothelial cells, lymphangiogenesis is induced by VEGF-C activated VEGFR3 signaling, the most important signaling axis in lymphangiogenesis.[85] The axon guidance protein neuropilin-2 (NRP2) and the collagen- and calcium-binding EGF domain-containing protein 1 (CCBE1) further enhances VEGFR3 signaling and promote proliferation and sprouting.[67,85,87,88] The differentiation of lymphatic plexi into lymphatic capillaries, precollectors and collecting vessels is mediated by the transcription factor forkhead box protein C2 (FOXC2), the mucin-type sialoglycoprotein podoplanin (PDPN) and the ligands ephrin-B2

and ANG2 that are responsible for the recruitment of pericytes and SMCs.[67,85] Further, the interaction between FOXC2 and the nuclear factor of activated T cells-1, cytoplasmic 1 (NFATc-1) and the FOXC2-mediated expression of the gap junction protein connexin 37 are required for the formation of valves.[85,87]

To induce lymphatic vessel sprouting, the binding of VEGF-C or VEGF-D promotes the homodimerization of VEGFR3 or heterodimerization of VEGFR2 and VEGFR3 and the activation of downstream signaling (**Figure 15**).[87,89] The major mechanism driving lymphangiogenesis is the VEGFR3-mediated phosphorylation of the tyrosine kinases AKT and ERK that results in LEC proliferation, migration and survival, while PI3K contributes to tube formation and enhances migration potential. Similar to the co-receptor signaling of NRP1 in blood vessel angiogenesis, NRP2 enhances VEGFR3 activation by promoting the binding of VEGF-C/-D to VEGFR3.[85,89]

Though VEGF-D and VEGFR2 are involved in lymphangiogenic processes, it is known that VEGF-D is not necessary for lymphangiogenesis during development[67] and signaling via VEGFR2 is less important for sprouting but results in lymph vessel enlargement.[67,85,87] Further, impaired lymphangiogenesis due to a lack of VEGFR3 cannot be rescued by VEGFR2 signaling.[85]

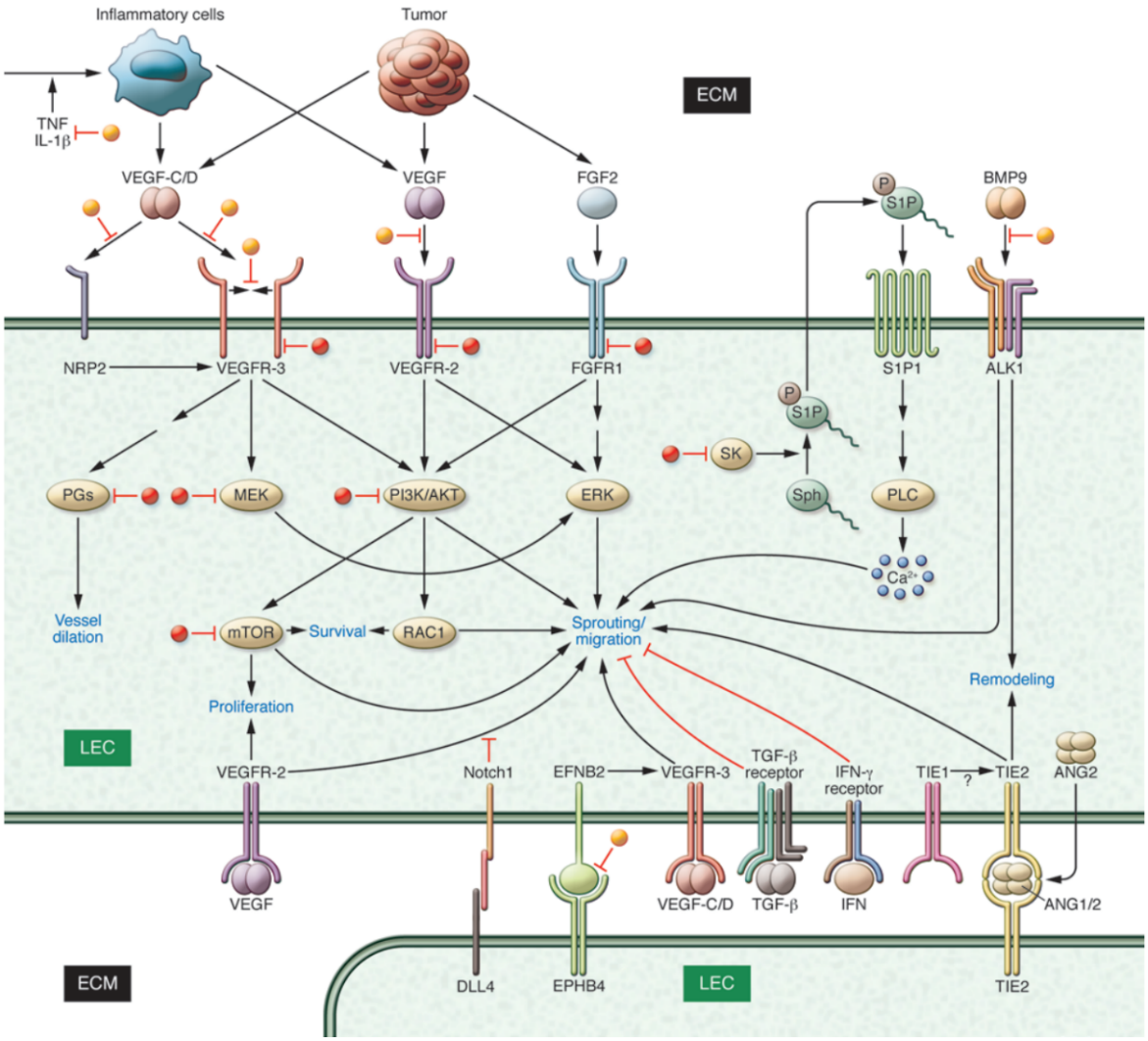

Figure 15. Signaling pathways involved in lymphangiogenesis. ECM: extracellular matrix, LEC: lymphatic endothelial cell, TNF: tumor necrosis factor, IL: interleukin, VEGF: vascular endothelial growth factor, FGF: fibroblast growth factor, PGs: prostaglandins, MEK: also known as MEP2K, mitogen-activated protein kinase kinase, PI3K/AKT(PKB): phosphoinositid-3-kinase/protein kinase B, ERK: extracellular signal–related kinase, SK: sphingosine kinase, S1P: sphingosine 1-phosphate, BMP9: bone morphogenic protein 9, ALK1: activin receptor-like kinase 1, Sph: sphingosine, PLC: phospholipase C, EFNB2: ephrin-B2, TGF-β: transforming growth factor beta, IFN-γ: interferon gamma, TIE1/2: tyrosine kinase with immunoglobulin-like and EGF-like domains 1/2, ANG1/2: angiopoietin 1/2, DLL4: delta-like 4, EPHB4: ephrin type-B receptor 4 (adapted from Zheng et al., 2014[90]).

1.5.9 Lymphangiogenesis in inflammation

The involvement of lymphangiogenesis in inflammation was shown by several groups, though studies provide inconclusive results. Whereas the inhibition of lymphangiogenesis via suppression of VEGFR3 aggravates inflammation in inflammatory bowel disease, rheumatoid arthritis or skin inflammation[91,92], the inhibition of VEGFR3 results in decreased inflammation in diabetes.[92] The increased number of lymph vessel may promote the clearance of immune cells thereby decreasing inflammation[91,93] or it enhances immune cell transport to inflamed tissue,

further aggravating inflammation.[88,92] However, it is still not clear which mechanisms regulate distinct effects of lymphangiogenesis.

Besides the crucial role of VEGF-C/VEGFR3 signaling in the formation of new lymph vessels, several other signaling pathways may contribute to the regulation of lymphangiogenesis during inflammation.[85] These pathways include FGF2/FGF receptor 1 (FGFR1) signaling that promotes LEC proliferation, migration and survival, sphingosine-1-phosphate (S1P)/S1P receptor 1 (S1PR1) pathway that contributes to lymphangiogenesis and normal lymphatic patterning, and morphogenetic protein 9 (BMP9)/ALK1 signaling that plays a role in lymphatic capillary growth and valve formation (**Figure 15**).[90,85]

Keratinocytes, stroma cells and immune cells, especially macrophages, are the main producers of VEGF-C.[91] Further, several inflammatory cytokines directly or indirectly (via the upregulation of VEGF-C expression), contribute to inflammatory lymphangiogenesis. IL-1, IL12, IL-17, IL-18, and TNF-α promote lymphangiogenesis, while IL-4, IL-5, IL-13 and IFN-γ show anti-lymphangiogenic activity.[91] Importantly, the mechanisms that are used by growth factors and cytokines to influence lymphangiogenesis are not fully understood, making it hard to distinguish between direct and indirect effects on vessel growth.[91] Besides the role of lymph vessels in tissue homeostasis, fluid drainage and lipid absorption, lymph vessels also influence immune cells during inflammation. Upon inflammation, LECs express chemokine receptors CCL21 to attract C-C chemokine receptor 7 (CCR7)-bearing dendritic cells and CCL27 to recruit CCR10-expressing B- and T cells.[88,92] LECs express adhesion markers like intercellular adhesion molecule 1 (ICAM-1), vascular cell adhesion protein 1 (VCAM-1) or endothelial-selectin (E-selectin) to mediate dendritic cell trafficking through lymph vessels. Subsequently, entered immune cells further promote lymphangiogenesis by the secretion of pro-lymphangiogenic factors.[92]

1.5.10 Lymphangiogenesis in transplantation

Lymphangiogenesis was also shown to be involved in solid organ transplantation. The investigation of angiogenesis in transplantation of usually avascular corneas, delivered important insights in the role of lymph vessel during graft rejection. By comparing the effect of pre-existing blood and lymph vessels on the outcome of cornea transplantation, lymph vessels were identified as main mediators of graft rejection. This may be explained by the role of LECs to attract APCs that subsequently activate alloreactive T cells.[92,94]

Though the mechanism is not fully understood, several preclinical studies suggest a critical role of lymph vessel in graft rejection.[94-97] Alitalo proposed a model of how lymphangiogenesis promotes graft rejection in solid organ transplantation[88] (**Figure 16**): Inflammatory cells like

macrophages activate LECs by the secretion of VEGF-C. In turn, activated LECs express the chemokine receptor CCL21 and enhance the flow of lymph containing soluble antigens and activated APCs. CCR7-bearing APCs enter lymph vessels, migrate to lymph nodes and via blood vessels to the spleen where they activate T cells to reject the allogeneic graft tissue. Thus, the increased number of APCs results in an enhanced allogeneic T cell response promoting rejection of the graft.[88]

Results from experimental inhibition of lymphangiogenesis support this hypothesis. In corneal transplants, the specific blocking of lymphangiogenesis led to prolonged graft survival without affecting blood vessels.[94,97,98] Further, experimental models of islet[99], tracheal[95] and cardiac[96] transplantation confirmed that the reduced number of VEGFR3 and CCL21 expressing lymph vessels prolonged graft survival.

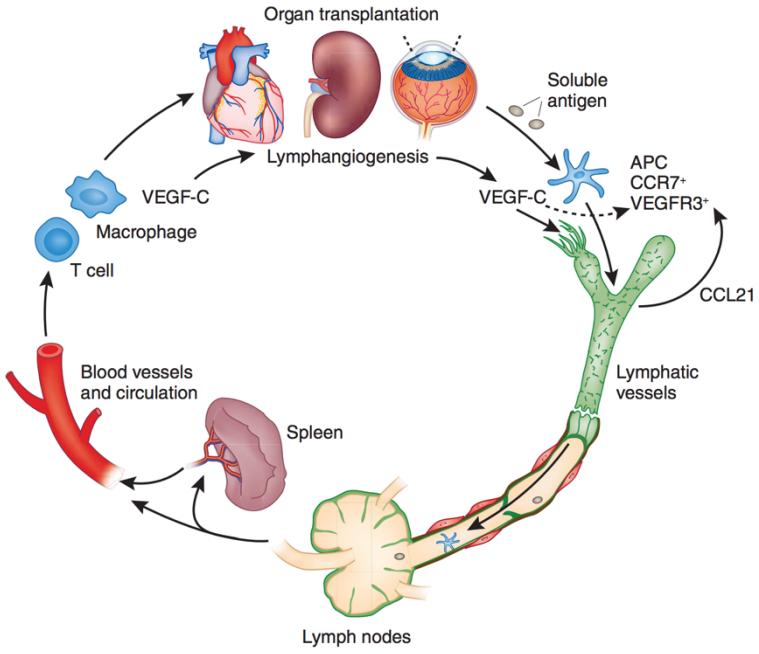

Figure 16. Model of lymphatic vessel function in organ transplantation. VEGF-C: vascular endothelial growth factor C, CCR7: C-C chemokine receptor type 7, VEGFR3: vascular endothelial growth factor receptor 3, CCL21: chemokine (C-C motif) ligand 21 (from Alitalo, 2011[88]).

1.5.11 Angiogenesis in aGVHD

As inner lining of blood vessels, the endothelium carries out many important functions in inflammation and hemostasis and serves as barrier between vessel lumen and surrounding tissue. In 1971, Judah Folkman was the first to state that cancer cells are able to trigger angiogenesis for their own oxygen and nutrient supply.[100] By now, it is well known that angiogenesis is a characteristic of various inflammatory diseases including inflammatory bowel disease, rheumatoid arthritis, appendicitis, psoriasis or retinopathies. However, several studies suggest that the endothelium also plays an important role in the pathogenesis of aGVHD.[101-104]

In vitro studies with serum from patients with and without aGVHD further support the importance of the endothelium considering the predictive role of endothelial biomarkers for the

development of aGVHD. 90% of patients with high serum levels of von Willebrand factor (vWF) and TNF receptor-1 (TNFR1) were predicted to develop aGVHD.[105]

Further, common complications that occur after allo-HSCT, including transplant-related microangiopathy, sinusoidal obstruction syndrome, idiopathic pneumonia syndrome, diffuse alveolar haemorrhage, engraftment syndrome and the capillary leak syndrome, are related to endothelial damage.[16,106]

Penack and Holtan proposed a model of the interaction between the endothelium and the development of aGVHD (**Figure 17**). Individual transplant- or patient-related predispositions influence the risk for the development and severity of aGVHD after allo-HSCT.[107] The conditioning regimen is the initial cause of endothelial damage, mainly in endothelial cells and epithelial cells of the gastrointestinal tract. The resulting release of cytokines, chemokines, DAMPs and PAMPs activates the patients' innate immune system. Subsequently, infused donor cells recognize foreign antigens and trigger alloreactive immune responses. Together, the activation of the innate immune system and alloreactive donor T cells induce angiogenesis as a key characteristic of early aGVHD.[107] Riesner et al. were able to confirm that angiogenesis is an early event in the development of aGVHD and proceeds immune cell infiltration in target organs. The increase of blood vessels was already profound on day +2 after allo-HSCT whereas the earliest time point to detect leukocyte infiltration was day +7 after allo-HSCT.[108] Thus, angiogenesis may be a trigger of aGVHD rather than a consequence. However, early angiogenic processes were not mediated via the classical VEGF-A/VEGFR2 pathway but seem to use different mechanisms to induce proliferation, migration and survival of ECs.[108]

The exact mechanisms describing the interplay between angiogenesis and aGVHD are still controversial and subject to further investigations.

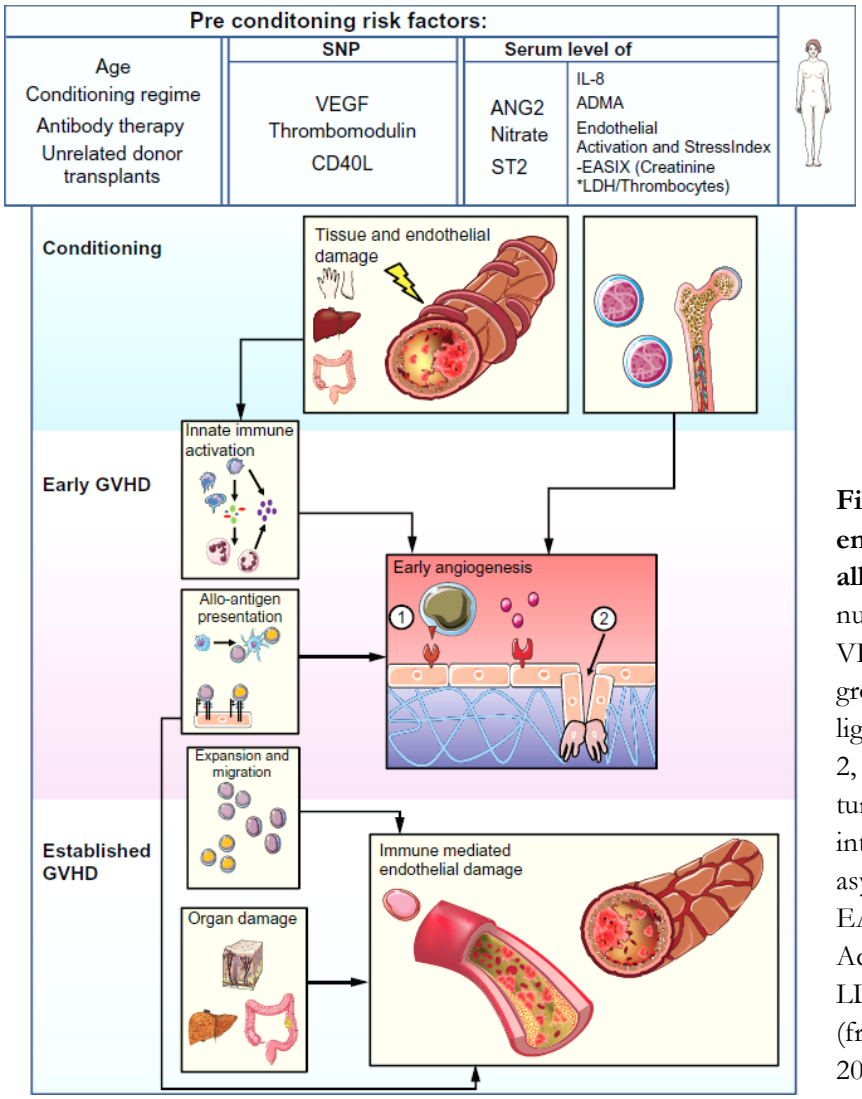

Figure 17. Schematic of endothelial damage during allo-HSCT. SNP: single-nucleotide polymorphism, VEGF: vascular endothelial growth factor, CD40L: CD40 ligand, ANG2: angiopoetin-2, ST2: suppression of tumorigenicity 2, IL-8: interleukin 8, ADMA: asymmetric dimethylarginine, EASIX: Endothelial Activation and Stress Index, LDH: lactate dehydrogenase (from Penack and Holtan, 2019[107]).

1.6 Objectives of the present study

Despite current treatment options, up to 50% of patients who received HLA-matched transplants develops any grade of aGVHD and still 30% of deaths after allo-HSCT are due to aGVHD and aGVHD-related complications.[109] All available standard therapies that are in clinical use aim at the suppression of effector T cells, which in turn promotes other complications like the increased risk for infections and tumor relapse. Therefore, the development of new therapeutic approaches that act independently of T cells is of high importance.

The influential role of the endothelium during aGVHD was shown in various studies by the confirmation of increased vessel density in aGVHD target organs or the discovery that angiogenesis occurs prior to immune cell infiltration. Angiogenesis and inflammation are two highly regulated processes that interact and influence each other. The hypothesis that

angiogenesis is an initiating event of inflammation in aGVHD, suggests that the endothelium is a promising target for new treatment options.

The general aim of the study was to further investigate mechanisms of angiogenesis during aGVHD to identify new potential therapeutic targets. Our research focus was not only on the blood vasculature, but we also examined the role of the second important vascular system, the lymphatic system, in the development of aGVHD.

The first part of this study examines the importance of lymph vessels during aGVHD. Though lymph vessels are known to bear important functions during inflammation, their role in aGVHD is not clear so far. This study aims to identify the involvement of lymphangiogenesis in the course of aGVHD.

The second part of this work describes our findings about the role of TGF-β signaling in aGVHD. As previous work of our group declined a central role of VEGF-A/VEGFR2 signaling in angiogenesis during aGVHD, the examination of alternative pathways is crucial for the identification of therapeutic targets. In experimental models of ocular diseases, TGF-β signaling that is mediated by the glycoprotein Lrg1 promoted particularly pathologic angiogenesis. Our purpose was to determine the role of Lrg1-regulated TGF-β signaling in aGVHD.

2 Materials and Methods

2.1 Mice

Female C57BL/6 (B6) (H-2K^{b}), LP/J (LP) (H-2K^{b}) and 129S2/SVPasCrl (129) (H-2K^{b}) mice were purchased from Charles River Laboratories (Sulzfeld, Germany). Female BALB/c (H-2K^{d}) mice were purchased from Janvier Laboratory (Saint-Berthevin, France). Lrg1 knockout (Lrg1 KO = Lrg1$^{-/-}$, H-2K^{b}) mice were a gift from Prof. John Greenwood (UCL, London, England) and were generated by the knockout mouse project (KOMP) repository (University of California, Davies, USA; http://www.komp.org/).[77] Mice were heterogeneously bred (Lrg1$^{+/-}$ x Lrg1$^{+/-}$) resulting in 25% homozygous Lrg1$^{-/-}$, 25% Lrg$^{+/+}$ (wildtype littermates) and 50% heterozygous Lrg1$^{+/-}$ mice. Wildtype (WT) littermates served as control mice for Lrg1 KO mice. Animals used in bone marrow transplantation (BMT) experiments were 10 to 12 weeks old and housed in the Charité University Medicine Animal Facility under pathogen-free controlled conditions and a 12-hour light/dark cycle. All experiments were approved by the Regional Ethics Committee for Animal Research.

2.2 GVHD models and characterization

2.2.1 Conditioning

For aGVHD experiments, different minor and major mismatch mouse models with different conditioning regimens were used (see **Table 4**).

Chemotherapy started 7 days before bone marrow transplantation (BMT) and consisted of daily intraperitoneal (i.p.) injections of busulfan (day -7 to day -3) and cyclophosphamide (day -7 and day -6). A stock solution of 40mg/ml busulfan (Sigma-Aldrich, St. Louis, Missouri, USA) in dimethyl sulfoxide (DMSO) (Carl Roth, Karlsruhe, Germany) was diluted in sterile phosphate-buffered saline (PBS) (Gibco; Thermo Fisher Scientific, Waltham, Massachusetts, USA) and injected at a concentration of 20mg/kg. Cyclophosphamide (Carl Roth) was diluted in sterile water and injected at a concentration of 100mg/kg. A time interval of 6 hours (h) was maintained between the two injections. The conditioning cycle was followed by 2 days of resting. On day 0, bone marrow cells and splenic T cells were isolated from donor mice and injected into the tail vein of recipient mice.

In contrast, split dose irradiation from a ^{137}Cs source was performed on the day of BMT (day 0). Recipient mice were irradiated in the morning, followed by a resting phase of at least 4h. Meanwhile, bone marrow (BM) and splenic T cells were isolated from donor mice. After the second dose of irradiation, BM cells and T cells were injected into the tail vein of recipient mice.

For syngeneic transplantation (e.g. B6 → B6), independent of conditioning, only BM cells were injected in the same amount as indicated for allo-HSCT.

Donor	Recipient	Contidioning	Cell numbers	Type of mismatch
LP	B6	chemotherapy: day -7 to -3: 20mg/mg/day busulfan day -7 and -6: 100mg/kg/day cyclophosphamide	1.5 x 10^7 BM cells 2 x 10^6 splenic T cells	minor mismatch (H-2K^b, H-2K^b)
129	B6	chemotherapy: day -7 to -3: 20mg/mg/day busulfan day -7 and -6: 100mg/kg/day cyclophosphamide	1.5 x 10^7 BM cells 2 x 10^6 splenic T cells	minor mismatch (H-2K^b, H-2K^b)
129	Lrg1	chemotherapy: day -7 to -3: 20mg/mg/day busulfan day -7 and -6: 100mg/kg/day cyclophosphamide	1.5 x 10^7 BM cells 2 x 10^6 splenic T cells	minor mismatch (H-2K^b, H-2K^b)
B6	BALB/c	radiation: 850cGY, split dose	5 x 10^6 BM cells 1 x 10^6 splenic T cells	major mismatch (H-2K^b, H-2K^d)
Lrg1	BALB/c	radiation: 850 cGy, split dose	5 x 10^6 BM cells 5 x 10^5 splenic T cells	major mismatch (H-2K^b, H-2K^d)

Table 4. Overview of mouse models for allo-HSCT experiments. Described are donor and recipient strain, specific conditioning, cell numbers and the type of mismatch. LP: LP/J, B6: C57BL/6, 129: 129S2/SVPasCrl.

2.2.2 Cell isolation from bone marrow and spleen

For the isolation of BM cells and splenic T cells, donor mice were sacrificed by cervical dislocation. Further processing was performed under sterile conditions. Femur, tibia and humerus were harvested and BM was flushed out with isolation buffer (PBS/2% FCS/1mM EDTA). Bone marrow was gently passed through a 70µm cell strainer using a 23G needle. Next, erythrocytes were lysed with ammonium-chloride-potassium (ACK) lysis buffer (150mM NH_4Cl/10mM $KHCO_3$/0.1mM Na_2EDTA), followed by two washing steps with isolation buffer and passaging over a 70µm cell strainer. Cell number was determined via Trypan blue staining and cells were counted with a Neubauer counting chamber (Marienfeld Superior Germany, Lauda-Königshofen, Germany). Finally, cell number was adjusted to the required cell number for the following transplantation.

For the isolation of T cells, spleens of donor mice were meshed through a 40µm cell strainer, followed by an erythrocyte lysis with ACK lysis buffer. The cell suspension was washed with isolation buffer and passed through a 40µm cell strainer twice more. Splenic T cells were isolated using the Pan T cell isolation kit II from Miltenyi (Miltenyi Biotec, Bergisch Gladbach, Germany) according to the manufacturer's instructions. The purity of the obtained T cell suspension was tested by $CD3^+$ staining and fluorescence-activated cell sorting (FACS) analysis. According to the percentage of $CD3^+$ cells in the suspension, the required cell number for the later transplantation was calculated.

2.2.3 Transplantation

The required amount of BM cells and T cells was resuspended in 100µl PBS each, resulting in a total injection volume of 200µl. For intravenous (i.v.) injection, recipient mice were placed under a heat lamp for 10 minutes (min) prior to the injection. Subsequently, mice were placed in a tailveiner restrainer (TV-150 small, Braintree Scientific, USA) and BM cells and T cells were injected into the tail vein.

For tumor experiments, tumor cells were injected together with BM cells and T cells in a total volume of 200µl.

2.2.4 Chimerism analysis

To check successful engraftment of donor cells, chimerism analysis was performed via FACS measurements. Around day +15 after BMT, 50µl blood was taken via retro-orbital bleeding from recipient mice. Erythrocyte lysis was performed with ACK lysis buffer before cells were stained against CD3 and donor specific minor antigens (H-2K^{b}, H2-K^{d}, Ly 9.1). Positive engraftment was defined as 80-90% donor cells in the CD3^{+} fraction of recipients' blood samples.

2.2.5 GVHD monitoring

Allo-HSCT recipients were individually scored for five clinical parameters (posture, activity, fur, skin, and weight loss) on a scale from 0 to 2 according to Cooke et al..[110] Clinical GVHD score was assessed by summation of these parameters. Animals were sacrificed when exceeding a total score of 6 or a score of 2 in one of the parameters. GVHD scoring started around day +8 after allo-HSCT and was performed twice per week. Survival was monitored on a daily basis.

2.3 Tumor models

For tumor experiments, recipient mice were conditioned with total body irradiation from a ^{137}Cs source as split dose with at least 4h in between the two doses. Recipient mice were sacrificed by cervical dislocation and bones (femur, tibia, humerus) and spleen were harvested. BM cells and splenic T cells were isolated (see **2.2.2**) and injected simultaneously with tumor cells. The two different tumor cell lines were A20 (BALB/c B cell lymphoma line), and EL4 (C57BL/6 T cell lymphoma line), both cell lines stably expressed firefly luciferase. Tumor cell lines were received from Dr. Evelyn Ullrich from Frankfurt, Germany. Tumor growth was measured weekly by bioluminescence imaging (see **2.6.1**). Tumor experiments were performed in combination with anti-lymphangiogenic treatment according to **2.6.3**.

Donor	Recipient	Contidioning	Cell numbers	Type of mismatch
B6	BALB/c	radiation: 800cGy, split dose	5×10^6 BM cells 3×10^5 splenic T cells 5×10^5 A20 tumor	major mismatch (H-2K^b, H-2K^d)
BALB/c	B6	radiation: 13 cGy, split dose	1.5×10^7 BM cells 3×10^5 splenic T cells 5×10^5 EL4 tumor	major mismatch (H-2K^b, H-2K^d)

Table 5. Overview of tumor models. Described are donor and recipient strain, specific conditioning, transplanted cell numbers and type of mismatch. B6: C57BL/6, BM: bone marrow.

2.4 Patient material and podoplanin staining

The protocol for collecting human samples was approved by the institutional ethics committee of the Charité University Medicine Berlin and was in accordance with the Declaration of Helsinki. Intestinal biopsies were collected from patients with suspected intestinal aGVHD after written informed consent was obtained. Intestinal biopsies of patients with aGVHD versus no GVHD taken after allo-HSCT (performed between 2007 and 2016) were identified by a search in the biobank of the institute for Pathology at the Charité University Medicine Berlin. Formalin-fixed, paraffin-embedded biopsies were assessed for histologic GVHD scores according to Lerner´s criteria.[111] Lymph vessels were stained with a monoclonal mouse anti-human podoplanin antibody (Clone D2-40, DAKO, Hamburg, Germany). For quantification, lymph vessels in 10 microscopic high-power fields per sample were counted.

2.5 Mouse models of inflammation

2.5.1 DSS-induced colitis mouse model

Experimental colitis was induced by the administration of 2.5% dextran sulfate sodium (DSS; MP Biomedicals, Santa Ana, California, USA) dissolved in autoclaved drinking water. DSS-containing drinking water was prepared freshly every second day. DSS treatment was performed on 7 consecutive days followed by one day with normal drinking water (without DSS). Disease activity score (DAI) was determined every second day. DAI consisted of the parameters weight loss, stool consistency and rectal bleeding. For the detection of occult blood, feces were collected and tested with the hemoCARE slide test (HemoCare; Care Diagnostica, Voerde, Germany). On day +9 mice were sacrificed and organs were harvested for further analyses.
As there is no standardized scoring sheet, DAI score for Lrg1 KO mice and WT littermates was adopted from different publications and based on our observations.[112-115]

Score	0	1	2	3	4
weight loss	no loss	1-5%	5-10%	10-15%	15-20%
stool consistency	normal	semi-solid	soft	diarrhea	
bleeding	no blood	Hemoccult positive	Hemoccult positive and visual		

Table 6. DAI scoring sheet for the evaluation of colitis severity.

For evaluation the of histopathologic score, colon samples were frozen in tissue Tissue-Tek® O.C.T.™ (Sakura Finetek, Alphen aan den Rijn, Netherlands) and 7µm thick sections were stained according to **2.7.2**. Histoscore was determined via the two parameters inflammation (score 1) and tissue damage (score 2). The assessment of the inflammation was based on severity and extent of the inflammation (0-3), the assessment of tissue damage on epithelial changes and mucosal architecture (0-3). Histological score was determined as summation of score 1 and score 2 (maximum score of 6).[116]

2.5.2 Paw edema mouse model

For paw edema experiments, mice received preemptive 0.03mg/kg buprenorphine (Temgesic; Invidia, North Chesterfield, Virginia, USA) subcutaneously one hour prior to the footpad injection. For the induction of paw edema, mice were transferred to an induction chamber and anesthetized with 1-2% isoflurane in oxygen. Anesthetized mice were injected with 30µl of 1% λ-Carrageenan (Sigma-Aldrich) in 0.9% saline into the right footpad. The left footpad served as control and was injected with 30µl of 0.9% saline only.[117] Footpad thickness of both paws was measured at different time points after the injection. After 3h or 6h mice were sacrificed and biopsies were punched out of the footpads using a 6mm biopsy punch (Stiefel, Research Triangle Park, North Carolina, USA). Footpad biopsies and harvested spleens were weighed and embedded in Tissue-Tek® O.C.T.™ (Sakura Finetek) for histologic examinations.

2.6 *In vivo* methods

2.6.1 Bioluminescence imaging

For bioluminescence imaging, 100µl of 30 mg/ml D-Luciferin (Cayman Chemicals, Ann Arbor, Michigan, USA) were injected i.p. into each mouse before imaging. Mice were transferred to an induction chamber and anesthetized with 1-2% isoflurane in oxygen. Anesthetized mice were imaged in an IVIS Lumina II system (PerkinElmer, Waltham, Massachusetts, USA). Living Image 3.1 software (PerkinElmer) was used to set regions of interest (ROI) and integrate the total bioluminescence signal into each ROI. Data was analyzed using average radiance (photons/second/square centimeter/steradian = $p/s/cm^2/sr$)) in ROIs and was normalized to background signal.

2.6.2 Evans blue assay

For Evans blue assays, mice were injected i.v. with a 0.5% solution of Evans blue (Sigma-Aldrich) diluted in PBS 30min prior to the end of the experiment. 30min later, mice were sacrificed by cervical dislocation and footpad biopsies and spleens were harvested. Organs were weighed and subsequently transferred to a 1.5ml Eppendorf tube containing 500µl formamide (Carl Roth). Subsequently, tissue samples were incubated on a shaker at 55°C for 24h to extract albumin-bound Evans blue. After 24h, the supernatant was taken and the Evans blue concentration was determined via absorbance measurement at 610mn on SpectraMax i3x microplate reader (Molecular Devices, LLC., San Jose, California, USA) using the SoftMax Pro Software (Molecular Devices). The amount of extravasated Evans blue per mg tissue provided information about vessel permeability.

2.6.3 Treatment

After allo-HSCT on day 0, mice received i.p. injections of mF4-31c1 antibody (Eli Lilly & Co., Indianapolis, Indiana, USA) or rat-IgG control antibody (Sigma-Aldrich) at a dose of 1mg/mouse/shot. Mice were injected every second day until day +16 after allo-HSCT or until organ harvesting.

2.7 *Ex vivo* methods

2.7.1 Retina flat mount analysis

Retina isolation and flat mount analysis were performed in cooperation with Dr. Nadine Reichhart from the clinic for ophthalmology at the Charité University Medicine Berlin.
Eyes were fixated in a 4% paraformaldehyde (PFA) solution for 15min and retinas were carefully dissected. Tissue was incubated with isolectin GS-IB_4 from Griffonia simplicifolia (Invitrogen, Carlsbad, California, USA) at a dilution of 1:200 in Tris-buffered saline (TBS) to stain blood vessels. Flat mounts were fixed onto glass slides and imaged using a Zeiss ApoTome.2 microscope (Carl Zeiss Microscopy, Thornwood, NY, USA). Images were processed using the Zen Lite 2010 software (Zeiss) and analyzed with Fiji Software (http://fiji.sc/Fiji).

2.7.2 Histology

For blinded histopathological analysis after Lerner criteria,[111] cryosections of colon and liver taken from allogeneic transplanted mice were stained with hematoxylin and eosin (Carl Roth). At the indicated time point after allo-HSCT, mice were sacrificed by cervical dislocation and organs were harvested. Colon and liver samples were embedded in Tissue-Tek® O.C.T.™ (Sakura Finetek) and frozen at -80°C. For staining, 7µm tissue sections were generated on the CryoStar™ NX70 cryostat (Thermo Fisher Scientific, Waltham, Massachusetts, USA). 7µm-sections were acetone-fixed for 10min at -20°C. Sections were stained with hematoxylin and eosin (Carl Roth) and scored after Lerner criteria.

For immunofluorescence staining 7µm thick cryosections were generated as described above. Sections were blocked with blocking buffer (PBS/3% BSA/5% FCS) for 1 hour at room temperature. Subsequently, primary antibodies were diluted in blocking buffer and applied onto the sections. **Table 7** shows all used primary antibodies and according dilutions. Sections were washed three times with PBS, secondary antibodies were applied onto the sections and incubated for 2h at room temperature. Secondary antibodies are listed in **Table 8**. For nuclear counterstaining, 4',6-Diamidino-2-phenylindole (DAPI) from Sigma-Aldrich was used. To determine positive stained area, five to six representative pictures per section were taken with a Moticam Pro 285B camera (Motic, Hong Kong) on a Motic BA410 epifluorescence microscope (objectives 10x/0.30 and 20x/0.50). Area was assessed by quantification of positive area to total area with a predetermined threshold using Fiji Software (http://fiji.sc/Fiji).

Antibody	Clone	Host species	Dilution	Supplier	
Lyve1	223322	rat	1:200	R&D systems	Minneapolis, Minnesota, USA
CD31	Mec13.3	rat	1:400	BD Biosciences	San José, California, USA
CD11b	M1/70	rat	1:200	BD Biosciences	San José, California, USA
F4/80	CI:A3-1	rat	1:200	Bio-Rad	Raleigh, North Carolina, USA
CD3	SP7	rabbit	1:300	Thermo Fisher Scientific	Waltham, Massachusetts, USA
IgG	eBR2s	rabbit	1:200	ebioscience	San Diego, California, USA
IgM	MM-30	rabbit	1:200	Bio Legend	San Diego, California, USA
ZO-1	polyclonal	rabbit	1:250	Thermo Fisher Scientific	Waltham, Massachusetts, USA
NG2	polyclonal	rabbit	1:200	Merck Millipore	Darmstadt. Germany
Lyve1	polyclonal	rabbit	1:1000	Reliatech	Wolfenbüttel, Germany
αSMA	1A4	mouse	1:250	Sigma-Aldrich	St. Louis, Missouri, USA

Table 7. Primary antibodies. Primary antibodies and according dilutions used for immunofluorescence staining of murine tissue. CD: cluster of differentiation, Ig: immunoglobulin, ZO-1: zonula occludens 1, NG2: Neural/Glial antigen 2, αSMA: alpha smooth muscle actin.

Antibody	Conjugate	Dilution	Supplier	
donkey anti-rat	Alexa Fluor 488	1:1000	Invitrogen	Carlsbad, California, USA
donkey anti-rabbit	Alexa Fluor 488	1:1000	Invitrogen	Carlsbad, California, USA
goat anti-rat	Cy3	1:1000	BioLegend	San Diego, California, USA

Table 8. Secondary antibodies. Secondary antibodies and according dilutions used for immunofluorescence staining of murine tissue.

2.7.3 Preparation of single cell suspensions of lymph nodes

Lymph nodes were put in ice-cold Hank's balanced salt solution (Thermo Fisher Scientific) and cut into small pieces, transferred to a 15ml falcon and centrifuged. The supernatant was carefully taken and used for lymphocyte staining. The pellet was further processed with a 0.6% collagenase II (Worthington, Lakewood, New Jersey, USA)/0.4% DNase (Sigma-Aldrich) solution to isolate endothelial cells. After a washing step with PBS, cells were collected in MACS buffer (PBS/ 0.5% BSA/1mM EDTA) before the staining for subsequent flow cytometry analysis.

2.7.4 Liver sinusoidal endothelial cell isolation

Anesthesia was prepared in 1:1:2 dilution with 100mg/ml Ketavet (Pfizer, New York City, New York, USA), 2% Rompun (Bayer Vital GmbH, Leverkusen, Germany) and PBS. The anesthetic effect was checked by reflex testing at the footpads and tail base. Livers of anesthetized mice were perfused with PBS (Thermo Fisher Scientific) via the portal vein at a flow rate of 5ml/min for 2min. Subsequently, solution was switched to collagenase D solution prepared of 2mg/ml collagenase D (Roche Diagnostics, Rotkreuz, Switzerland) and 2µl/ml DNase (Sigma-Aldrich) in Krebs-Ringer Buffer (KRB; 154mM NaCl/5.6mM KCl/5.5mM Glucose/20.1mM HEPES/25mM $NaHCO_3$, pH 7,4). Liver tissue was perfused with collagenase solution for

another 3min at a flow rate of 5ml/min. For further processing, liver was harvested and incubated in collagenase D solution at 37°C under continuous shaking for 45min. Digested liver tissue was passed over a 70µm cell strainer two times. Further enrichment of liver endothelial cells was achieved with 30% Histodenz (Sigma-Aldrich) density gradient centrifugation. The endothelial cell containing interphase was purified via magnetic activated cell sorting (MACS) using CD146 (LSEC) microbeads (Miltenyi Biotec) according to the manufacturer's instructions. Purity of sorted cells was determined via FACS analysis of ICAM1 and CD31 positive cells. For the analysis of lymph vessels, the lymph vessel specific marker podoplanin (gp38) and peripheral lymph node addressin (PNAd) were integrated.

2.7.5 Flow cytometry staining

For flow cytometry measurements, single cell suspension was generated as described under **2.2.2** and under **2.7.4** (endothelial cells). Antibody mixes were prepared in MACS buffer (PBS/ 0.5% BSA/1mM EDTA). Cells suspensions were centrifuged, resuspended in the prepared antibody mixes and stained for 20min at 4°C. All antibodies used for FACS stainings are listed in **Table 9**. After the incubation period, cells were washed twice with PBS, resuspended in MACS buffer and analyzed on FACSCanto II (BD Biosciences). For regulatory T cell staining, anti-mouse/rat FoxP3 Staining Set APC (eBioscience, San Diego, CA, USA) was used following the manufacturer's instructions. Data was analyzed with FlowJo 7.6.5 Software (TreeStar Inc., Ashland, OR, USA).

2.7.6 RNAScope

For RNAScope analyses, fresh frozen tissue sections were fixed with 4% PFA for 15min at 4°C. Subsequently sections were washed with PBS two times before they were exposed to increasing ethanol (Carl Roth) concentrations (50%, 70%, 100%) and incubated for 5min at room temperature for each concentration. Next, slides were stored in fresh 100% ethanol solution for shipping. RNAScope analysis was done by Dr. Marie O'Connor in the laboratory of Prof. Greenwood at the UCL Institute of Ophthalmology in London. Podocalyxin and Lrg1 antibodies were provided by the group of Prof. Greenwood.

RNAScope technique is based on the hybridization of a probe to target mRNA and the binding of a cascade of signal amplification molecules. Signal detection and analysis was done with fluorescent microscopy.

Antibody	Clone	Fluorochome	Dilution	Supplier	
Ly9.1	30C7	PE	1:100	BD Biosciences	San José, California, USA
CD8a	53-6.7	APC	1:200	BD Biosciences	San José, California, USA
Ly-6G/Ly-6C (Gr1)	RB6-8C5	APC	1:200	BD Biosciences	San José, California, USA
CD45R/B220	RA3-6B2	PerCP-Cy5.5	1:100	BD Biosciences	San José, California, USA
CD45	30F11	PerCP-Cy5.5	1:200	BD Biosciences	San José, California, USA
H2kb	AF6-88.5	FITC	1:50	BD Biosciences	San José, California, USA
CD4	RM4-5	PE-Cy7	1:800	BD Biosciences	San José, California, USA
CD11c	HL3	PE-Cy7	1:400	eBioscience	San Diego, California, USA
CD11b	M1/70	APC-Cy7	1:400	BD Biosciences	San José, California, USA
CD25	PC61	PerCP-Cy5.5	1:200	BD Biosciences	San José, California, USA
Podoplanin/gp38	8.1.1	FITC	1:50	Bio Legend	San Diego, California, USA
Podoplanin/gp38	8.1.1	PE	1:200	Bio Legend	San Diego, California, USA
VEGFR3	AFL4	PE	1:200	Novus Biologicals	Contennial, Colorado, USA
rat IgG 2a,κ	R35-95	PE	1:200	BD Biosciences	San José, California, USA
CD31	MEC13.3	PE	1:200	BD Biosciences	San José, California, USA
PNAd	MECA-79	FITC	1:50	Santa Cruz Biotechnology	Santa Cruz, California, USA

Table 9. FACS antibodies. FACS antibodies and according dilutions.

2.8 Molecular biological methods

2.8.1 Quantitative real-time PCR

RNA was extracted from about 30mg mouse tissue using the RNeasy Mini Kit (QIAGEN, Venlo, Netherlands). RNA concentration and purity were determined by NanoDrop 1000 spectrophotometry (PEQLAB, Erlangen, Germany) measurement. cDNA was synthesized from 1µg of total RNA using QuantiTect Reverse Transcription Kit (QIAGEN) following the manufacturer's instructions. Quantitative real-time polymerase chain reaction (qPCR) was performed using the TaqMan probe-based assay. Primers and probes were designed using the Primer Express 1.5 software (Thermo Fisher Scientific) and were ordered from BioTez GmbH (Berlin, Germany).

qPCR amplification reaction was performed on DNA Engine Opticon (BioRad, Hercules, California, USA) using the TaqMan Gene Expression Master Mix (Thermo Fisher Scientific) according to the manufacturer's instructions. Thermal cycling conditions were as follows: 50°C for 2min, 95°C for 10min followed by 49 cycles of 95°C for 10s, and 60°C for 1min. Data were collected and analyzed with the Opticon Monitor 3.1 analysis software (BioRad) and the comparative CT Method (ΔΔCT Method). All used primers and probes are listed in **Table 10**.

Gene		GAPDH
MGI/Gene No.		NM_008084.2
Amplicon Length		70
Amount of Exons		7
Primer	Forward	5'-GGCAAATTCAACGGCACAGT-3'
	Reverse	5'-AGATGGTGATGGGCTTCCC-3'
	Probe	FAM-5'-AGGCCGAGAATGGGAAGCTTGTCATC-3'-TAMRA

Gene		Lrg1
MGI/Gene No.		NM_029796.2
Amplicon Length		94
Amount of Exons		2
Primer	Forward	5'-TAGAGGAGCAGCTATGGTCTCTTG-3'
	Reverse	5'-CAAGAGGGCCAGGAGAAACA-3'
	Probe	FAM-5'-CAGCATCAAGGAAGCCTCCAGGATCTC-3'-TAMRA

Gene		ALK1
MGI/Gene No.		NM_001277255
Amplicon Length		82
Amount of Exons		11
Primer	Forward	5'-TGGTCAAGAGTAACTTGCAGTGTTG-3'
	Reverse	5'-ATATCCAGGTAATCGCTGCTTTGT-3'
	Probe	6-FAM-AGACCTGGGACTGGCTGTGATGCAC-TAMRA

Gene		ALK5
MGI/Gene No.		NM_009370
Amplicon Length		85
Amount of Exons		9
Primer	Forward	5'-GGGCGAAGGCATTACAGTGT-3'
	Reverse	5'-ACTGAGACAAAGCAAAGACCATCTG-3'
	Probe	6-FAM-TCTGCCACCTCTGTACAAAGGATAATT-TAMRA

Gene		Vegf C
MGI/Gene No.		NM_009506.2
Amplicon Length		79
Amount of Exons		7
Primer	Forward	5'-CTCAGCAAGACGTTGTTTGAAATTA-3'
	Reverse	5'-GTGATTGGCAAAACTGATTGTGA-3'
	Probe	6-FAM-CTCTCTCACAAGGCCCCAAACCA-TAMRA

Table 10. Primer and probes used for quantitative polymerase chain reaction. (FAM: 6-carboxyfluorescein; TAMRA: 6-caboxytetramethyl-rohdamine).

2.8.2 Proteomics

2.8.2.1 Protein isolation

Snap frozen liver tissue was grid to a fine powder with pre-cooled mortar and pestle, mixed with denaturation buffer (6M urea/2M thiourea/20mM HEPES (Sigma-Aldrich), pH 7.5) and shaked for 20min at room temperature to extract proteins. After centrifugation at 100,000g for 30min, the supernatant was taken for protein quantification. The protein quantification and analysis were performed at the mass spectrometry-based proteomics facility of the Max Delbrück Center for Molecular Medicine and are briefly described below. A detailed description is given in the supplementary section of *Initiation of acute graft-versus-host disease by angiogenesis*, Riesner et al., 2017[108].

2.8.2.2 Protein quantification by dimethylation labeling

The protein concentration was determined by Bradford protein assay. Samples were digested with Trypsin (Promega, Walldorf, Germany) for 16h and subsequently digestion was stopped by acidifying each sample to pH<2.5 by adding 10% trifluoroacetic acid solution. The resulting peptide extracts were purified and stored on stage tips according to Rappsilber et al.[118] Next, samples were reconstituted in 100µl of 20mM HEPES buffer, pH 7.5. The samples were differentially labelled by adding light label formaldehyde (Pierce, Thermo Fisher Scientific) (+28Da), medium label formaldehyde (Cambridge Isotope Laboratories) (+32Da) and heavy label formaldehyde (Sigma-Aldrich) (+36Da) cells. The reaction was quenched after 1 hour by adding 30µl of 1% ammonia solution. All the samples were mixed and acidified to pH<2.5 by adding 10% trifluoroacetic acid solution.

2.8.2.3 High throughput LC-MS/MS analysis

Peptides were separated on an Eksigent nLC-415 system (Eksigent Technologies, Dublin, California, USA) and MS and MS/MS spectra were analyzed coupled to a QExactive mass spectrometer (Thermo Fisher Scientific) by a gradient from 4 to 42% B in 240min. The mass spectrometer was operated in a data-dependent acquisition mode with dynamic exclusion enabled (30s). Survey scans (mass range 300-1700 Th) were acquired at a resolution of 70,000 with the ten most abundant multiply charged ($z \geq 2$) ions selected with a 4 Th isolation window for HCD fragmentation. MS/MS scans were acquired at a resolution of 17,500 and injection time of 60ms.

2.8.2.4 Processing of mass spectrometry data

Protein and peptide quantitation information were extracted from MaxQuant 1.2.2.5[119] All samples were searched against the IPI mouse database version 3.84 with 60.012 entries (ftp://ftp.ebi.ac.uk/pub/databases/IPI). Cleavage specificity was set for trypsin/P. Search parameters were two missed cleavage sites, cysteine carbamidomethylation as fixed modification and methionine oxidation as variable modification. Quantification data of labeled peptides were measured considering N-termini and lysine dimethylation on light (+28Da), medium (+32Da) or on heavy (+36Da) modification per free primary amine.[120] The results were filtered to 1% false discovery rate at peptide level by MaxQuant. Normalized ratios were used for differential expression analysis (up ≥1.3 or down ≤0.44).

2.9 Statistics

Survival data was analyzed using the Kaplan-Meier method and compared with the Mantel-Cox log-rank test. For statistical analysis of all other data, the unpaired Student´s t test and Mann-Whitney U test were used. Values are presented as mean ± SEM; values of $P \leq .05$ were considered statistically significant. All statistical analyses were performed using GraphPad Prism software (GraphPad Software Inc., La Jolla, California, USA).

2.10 Devices

Name	Supplier	
BD FACSCanto II	BD Biosciences	San José, California, USA
CryoStar™ NX70 cryostat	Thermo Fisher Scientific	Waltham, Massachusetts, USA
DNA Engine Opticon	BioRad	Hercules, California, USA
Heraeus Megafuge 1.0 R	Heraeus	Hanau, Germany
Heraeus Pico 17 Centrifuge	Heraeus	Hanau, Germany
Irradiation device GSR D1	Gamma-Service Medical GmbH	Leipzig, Germany
Laboratory peristaltic pump PLP 380	behr Labor-Technik	Düsseldorf, Germany
Motic AE31 inverted microscope	Motic	Hong Kong, Japan
Motic BA410 epifluorescence microscope	Motic	Hong Kong, Japan
Nanodrop 1000 spectrophotometry	PEQLAB	Erlangen, Germany
Ultra turrax t25 basic	IKA®-Werke GmbH & CO. KG	Staugen im Breisgau, Germany

Table 11. List of devices.

2.11 Routinely used reagents and consumables

Reagents	Supplier	
4-(2-Hydroxyethyl)piperazine-1-ethanesulfonic acid, N-(2-Hydroxyethyl)piperazine-N'-(2-ethanesulfonic acid) (HEPES)	Sigma-Aldrich	St. Louis, Missouri, USA
Aceton	Sigma-Aldrich	St. Louis, Missouri, USA
Albumin fraction V (BSA)	Carl Roth	Karlsruhe, Germany
Busulfan	Sigma-Aldrich	St. Louis, Missouri, USA
Chloroform	Carl Roth	Karlsruhe, Germany
Cyclophosphamide	Carl Roth	Karlsruhe, Germany
D(+)-Glucose	Merck	Darmstadt, Germany
DEPC-H_2O	Ambion; Thermo Fisher Scientific	Waltham, Massachusetts, USA
dimethyl dimethyl sulfoxide (DMSO)	Carl Roth	Karlsruhe, Germany
Disodium ethylenediaminetetraacetate dihydrate (Na2EDTA)	Sigma-Aldrich	St. Louis, Missouri, USA
Dulbecco's Phosphate-Buffered Saline (DPBS; PBS)	Gibco; Thermo Fisher Scientific	Waltham, Massachusetts, USA
Ethanol Rotipuran >99,8%	Carl Roth	Karlsruhe, Germany
Ethylenediaminetetraacetic acid (EDTA)	Sigma-Aldrich	St. Louis, Missouri, USA
Fetal calf serum (FCS)	Invitrogen	Carlsbad, California, USA
Formalin solution	Carl Roth	Karlsruhe, Germany
Histodenz	Sigma-Aldrich	St. Louis, Missouri, USA
Isopropanol	J.T. Baker; Thermo Fisher Scientific	Waltham, Massachusetts, USA
$KHCO_3$ Potassium hydrogen carbonate	Merck	Darmstadt, Germany
MACS Quant running buffer	Miltenyi Biotec	Bergisch Gladbach, Germany
$NaHCO_3$	Fluka Chemie	Buchs, Switzerland
NH_4Cl (ammonium chloride)	Sigma-Aldrich	St. Louis, Missouri, USA
Paraformaldehyd (PFA)	Sigma-Aldric	St. Louis, Missouri, USA
Potassium chloride (KCl)	Carl Roth	Karlsruhe, Germany
RPMI	Gibco; Thermo Fisher Scientific	Waltham, Massachusetts, USA
Sodium chloride (NaCl)	Carl Roth	Karlsruhe, Germany
ß-mercaptoethanol	Sigma-Aldrich	St. Louis, Missouri, USA
TRI reagent	Ambion; Thermo Fisher Scientific	Waltham, Massachusetts, USA
Trypan blue solution 0.4%	Sigma-Aldrich	St. Louis, Missouri, USA

Table 12. List of reagents.

Consumables	Supplier	
40um cell strainer	BD Biosciences	San José, California, USA
70um cell strainer	BD Biosciences	San José, California, USA
BZO seal film	Biozym Scientific GmbH	Hessisch Oldendorf, Germany
Cell culture dishes, 60x15mm	Greiner Bio-One	Kremsmünster, Austria
Falcon 50ml	VWR	Darmstadt, Germany
Falcons 15ml	VWR	Darmstadt, Germany
Tailveiner Restrainer for mice TV-150 small	Braintree Scientific, Inc.	Massachusetts, USA
MACS separation columns, MS columns	Milteny Biotec	Bergisch Gladbach, Germany
Needles (20G, 23G, 27G)	Braun	Germany
Neubauer Counting Chamber	Marienfeld Superior Germany	Lauda-Königshofen, Germany
Pasteur pipettes	VWR	Darmstadt, Germany
PCR 96-well plates	Biozym Scientific GmbH	Hessisch Oldendorf, Germany
Serological pipettes 10ml	Sarstedt	Nümbrecht, Germany
Serological pipettes 25ml	Sarstedt	Nümbrecht, Germany
Serological pipettes 5ml	Sarstedt	Nümbrecht, Germany
Syringe 1ml	B. Braun Melsungen AG	Melsungen, Germany
Syringe 5ml	B. Braun Melsungen AG	Melsungen, Germany
Trypan Blue Solution 0,4%	Sigma-Aldrich	St. Louis, Missouri, USA

Table 13. List of consumables.

3 Results

3.1 Lymphangiogenesis in GVHD

It is well known that angiogenesis is a major characteristic in the progress of aGVHD. Usually, this refers to hemangiogenesis. Besides the increased blood vessel formation, we looked closer to the importance of lymph vessels in the course of aGVHD. The following results describe the alteration of the lymphatic vasculature during aGVHD and show a promising therapeutic approach addressing the vascular endothelial growth factor receptor VEGFR3.

Partial results of this thesis, including figures and figure legends, have already been published in: Lymphangiogenesis is a feature of acute GVHD, and VEGFR3 inhibition protects against experimental GVHD. Blood. 2017 Mar 30;129(13):1865-1875.[121]

3.1.1 Lymph vessel density in GVHD target organs

To evaluate the role of lymphangiogenesis during aGVHD we determined the lymph vessel density in aGVHD target organs using a murine allo-HSCT model. To ensure that our results are close to the clinic, most data was generated in a major histocompatibility complex-matched (MHC-matched), minor histocompatibility antigen-mismatched (miHA-mismatched) allo-HSCT model (LP/J → C57BL/6, 129/SV → C57BL/6). We determined lymph vessel density on aGVHD target organs colon and liver by immunofluorescent staining against the lymph vessel marker Lyve1. The exclusive detection of lymphatic endothelial cells was tested beforehand (**Figure S1**). As shown by exemplary pictures in **Figure 18A**, we found more lymph vessels in the colon of mice with aGVHD than in those of control mice without GVHD. These observations could be confirmed by the quantification of Lyve1 positive area of mice with and without GVHD (**Figure 18B**). In the liver, we also found significantly more lymph vessels in allogeneic transplanted mice than in syngeneic transplanted mice which did not develop aGVHD. (**Figure S2**). Nevertheless, the quantification of lymph vessels by Lyve1 staining in liver tissue during aGVHD may not be reliable. In the liver, the expression of Lyve1 is not restricted to lymph vessels, and furthermore its expression pattern in liver blood sinusoids differs under disease conditions like inflammation.[122,123]

Another organ that is widely used to study lymphatics is the small bowel mesentery. The thin fan-shaped membrane is located between the loops of the small intestine and contains a high amount of lymph vessels and intestinal draining lymph nodes. We stained the mesentery of mice with aGVHD vs. syngeneic control mice without GVHD and quantified lymph vessels of mesenteric windows. We detected a tendency towards a higher Lyve1 positive area occurring

during aGVHD vs. syngeneic controls without GVHD, which did not reach statistical significance (**Figure 18C, D**).

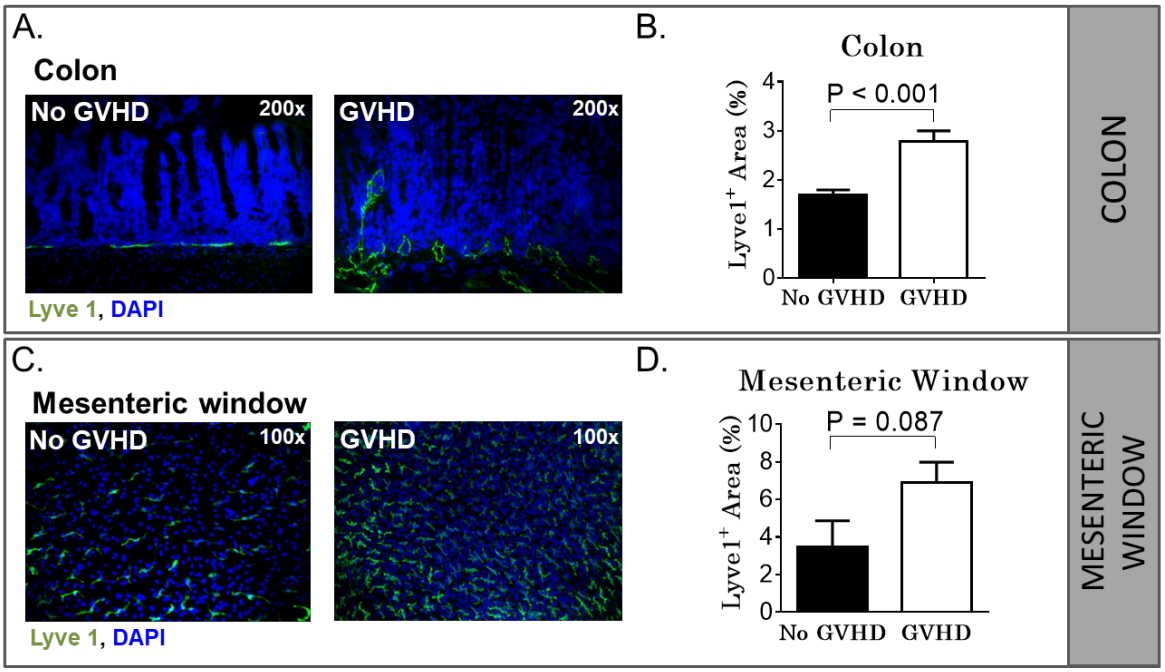

Figure 18. Acute GVHD is associated with lymphangiogenesis during experimental GVHD. (A) Representative images of increased lymphangiogenesis in the colon during aGVHD (right) versus no GVHD (left) on day +15 after HSCT. Colon sections of HSCT recipients with aGVHD and without GVHD were stained with Lyve1 antibody (green) and counterstained with the nuclear stain 4´,6-diamidino-2-phenylindole (DAPI). (B) Quantification of the Lyve1 positive area in the colon on day +15 after HSCT (n = 5 per group). (C) Lymph vessels in the mesenteric window during GVHD (right) versus no GVHD (left) on day +15 after HSCT. Isolated mesenteric windows of HSCT recipients with aGVHD versus no GVHD were stained with Lyve1 antibody (green) and counterstained with DAPI. (D) Quantification of the Lyve1 positive area in the mesenteric window on day +15 after HSCT. Transplantation was performed in the LP/J → C57BL/6 model. n = 4 no GVHD, n = 5 GVHD; error bars indicate mean ± SEM, significance was tested with an unpaired Student´s t-test.

Further, we collected mesenteric as well as peripheral lymph nodes from allo-HSCT recipients with aGVHD vs. no GVHD and quantified the number of lymphatic endothelial cells by flow cytometry using an antibody against podoplanin (gp38).[124] The analysis of mesenteric lymph nodes showed a trend towards an increased number of gp38 positive endothelial cells in mesenteric lymph nodes of allo-HSCT recipients with aGVHD compared to syn-HSCT recipients without GVHD (**Figure 19A**). The number of gp38 positive endothelial cells was significantly higher in recipients with aGVHD compared to mice without GVHD (**Figure 19B**). Besides gp38, we also investigated the expression of peripheral lymph node addressin (PNAd), also termed MECA79, that is expressed on high endothelial venules (HEVs) of lymphoid tissue including peripheral and mesenteric lymph nodes.[125] The interaction between PNAd and leukocyte-selectin (L-selectin) on lymphocytes initiates the homing of lymphocytes to peripheral

lymph nodes. We detected significantly increased numbers of PNAd positive endothelial cells in allo-HSCT recipients with aGVHD compared to syn-HSCT control mice without GVHD (**Figure 19C**). Exemplary FACS plots for the identification of lymphatic endothelial cells and PNAd positive cells are shown in **Figure S3**.

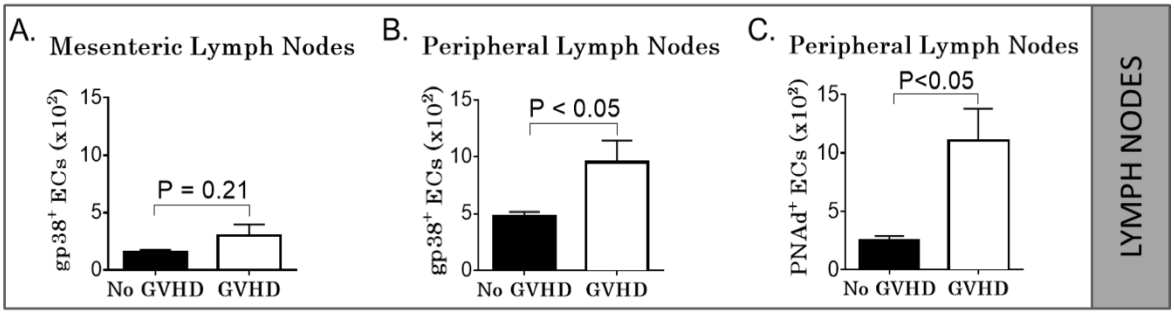

Figure 19. Acute GVHD is associated with lymphangiogenesis in lymph nodes. (A, B) Quantification of lymphatic endothelial cells (gp38$^+$ ECs) via fluorescence-activated cell sortering (FACS). Endothelial cells were isolated from mesenteric (n = 6 per group) (A) and peripheral (n = 3 per group) (B, C) lymph nodes of HSCT recipients with aGVHD versus no GVHD on day +7 after HSCT. (C) Quantification of peripheral lymph node addressin (PNAd)–positive endothelial cells in peripheral lymph nodes of HSCT recipients with aGVHD versus no GVHD. Transplantation was performed in the C57BL/6 → BALB/c model. n = 3 per group; error bars indicate mean ± SEM, significance was tested with an unpaired Student´s t-test.

On mRNA level, we checked the expression of the VEGFR3 ligand VEGF-C in syngeneic and allogeneic transplanted mice in the aGVHD target organs liver and colon. We didn´t see an increase in VEGF-C expression in liver or colon of allo-HSCT recipients on d+7 or d+15 after transplantation (**Figure 20**).

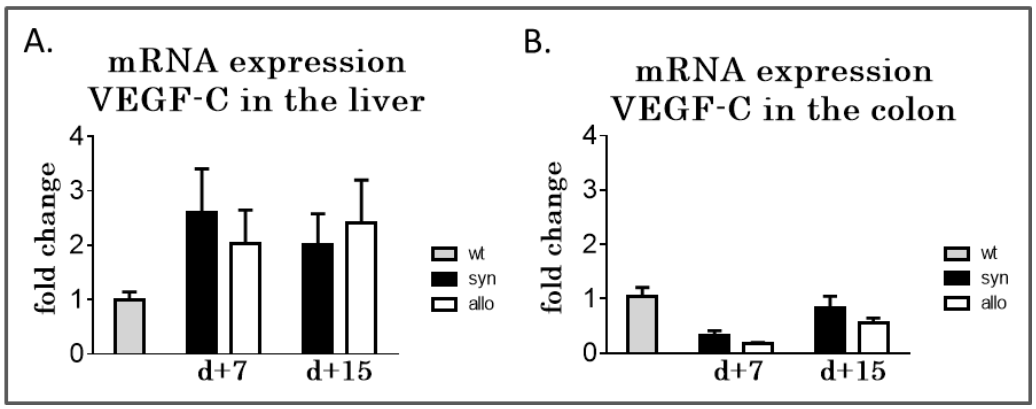

Figure 20. mRNA expression of VEGF-C in the liver (A) and in the colon (B). Transplantation was performed in the LP/J → C57BL/6 model. n = 4-5 per group; error bars indicate mean ± SEM, significance tested by unpaired Student´s t-test. wt: wildtype; syn: syngeneic transplanted, allo: allogeneic transplanted, d: day (post bone marrow transplantation).

Based on these findings we conclude that increased lymphangiogenesis in colon, the mesentery and peripheral lymph nodes are characteristics of aGVHD. We assume that increased lymphangiogenesis occurs also in the liver, although we cannot rely on the immunohistologic evaluation. Regarding the VEGF-C concentration, the analysis of isolated endothelial cells would be more useful than the evaluation of the whole tissue due to the high amount of mRNA expression in the organs.

3.1.2 Lymph vessels are increased in small intestinal lesions during GVHD in humans

The next very important step was to validate our findings in the clinical situation. We received small intestinal biopsies from patients suffering from aGVHD vs. no GVHD and examined lymph vessel density in tissue sections. Samples were immunostained against the human lymph vessel marker podoplanin and analyzed microscopically. **Figure 21** demonstrates typical examples of anti-podoplandin staining in duodenal biopsies. **Figure 21A** shows villous duodenal tissue without GVHD, displaying orthotopic lymph vessels at the mucosal and submucosal level. In contrast, biopsies of severe aGVHD (Lerner Grade III)[111], showed degenerated mucosal tissue with highly increased lymph vessel density, that is concentrated at the former mucosal level and was formed as a result of regenerative vascular proliferation. (**Figure 21B**). Quantification of lymph vessels of duodenum and colon biopsies taken from patients after allo-HSCT without GVHD (GVHD 0) and patients with histological grades III-IV aGVHD (**Figure 21C, D**) was done microscopically. Both analyses revealed a highly increased number of lymph vessels in patients with grade III-IV aGVHD compared to patients without GVHD.

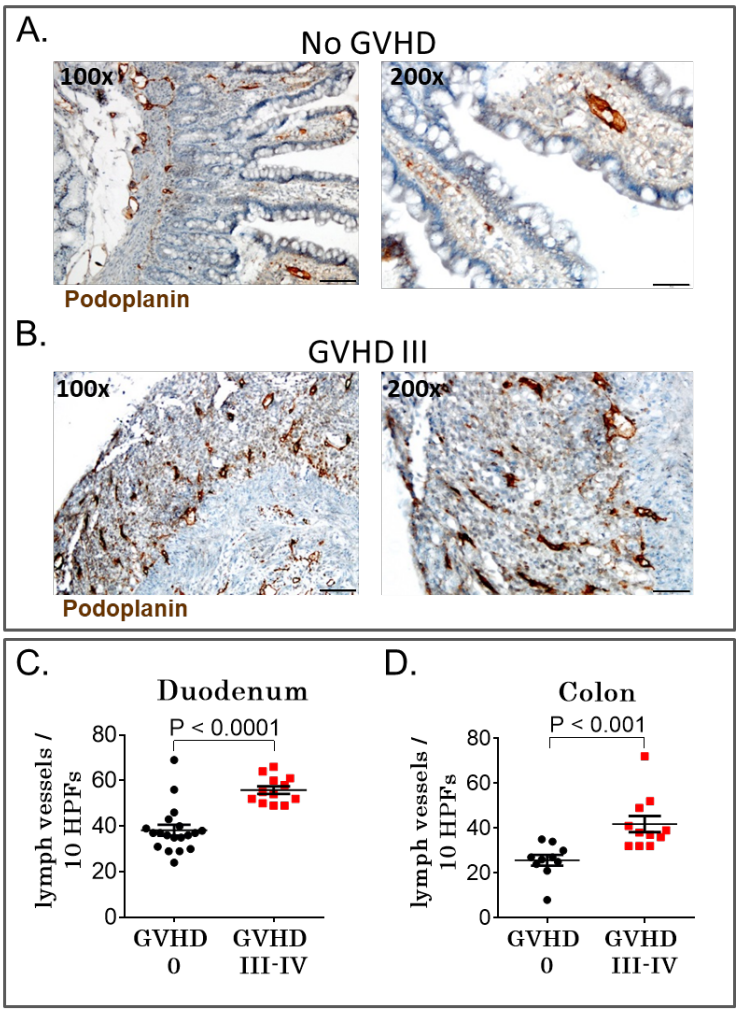

Figure 21. Lymph vessels are increased in intestinal lesions during GVHD in humans. Representative images of lymph vessels in the duodenum of patients without intestinal GVHD (A) and with grade III intestinal GVHD (B). Sections were stained with podoplanin antibody (brown), which is specifically expressed by lymphatic endothelial cells. Destructive mucosal lesions during severe GVHD are associated with lymphatic vascular proliferation. Quantification of lymph vessels in duodenum (C) and colon (D) biopsies from patients after allo-SCT without GVHD (GVHD 0) and patients with histological aGVHD grades III-IV. Number of lymph vessels in 10 high-power fields (HPFs) was determined. Bars in x100 magnification, 100 µm; and in x200 magnification, 50 µm. n = 12-19 (C); n = 10-11 (D). Error bars indicate mean ± SEM, significance was tested by the Mann-Whitney U test.

Further, we compared the analyses in human and murine tissue biopsies and found a common structural characteristic: lymph vessel proliferation occurs substantially in degenerated mucosal tissue and ulcerations (**Figure 22**).

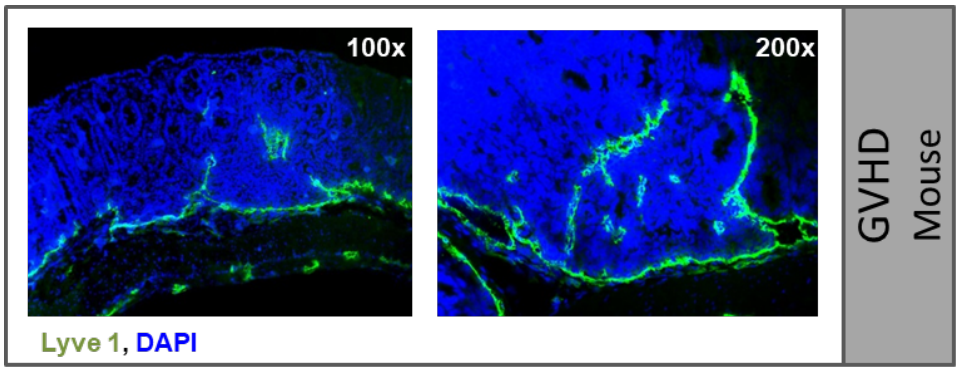

Figure 22. Destructive mucosal lesions in the colon of mice with GVHD. Representative images of lymph vessels in destructive mucosal lesions. Colon sections were stained against the lymph vessel marker Lyve1 (green) and counterstained with the nuclear stain DAPI. Transplantation was performed in the LP/J → C57BL/6 model.

Based on these results we believe that our findings in murine tissue correlate to the human situation and severe human intestinal aGVHD is also associated to increased lymphangiogenesis.

3.1.3 Anti-VEGFR3 treatment results in inhibition of GVHD-associated lymphangiogenesis

The next approach after confirming increased lymph vessel density in murine and human biopsies was to selectively inhibit lymphangiogenesis during aGVHD. We used the anti-VEGFR3 monoclonal antibody mF4-31c1 that specifically antagonizes the binding of VEGF-C to VEGFR3.[126,127] For inhibition studies we used the MHC-matched, miHA-mismatched LP/J → C57BL/6 model. The antibody mF4-31c1 or control antibody (rat-IgG) were injected at a dose of 1mg per mouse every second day starting from day 0 (day of transplantation) and organs were harvested on day +15, during the peak of aGVHD. Colon and mesenteric window were used for immunofluorescence staining against the lymph vessel marker Lyve1 (**Figure 23A, C**). In the colon, quantification of Lyve1 positive area showed a significant reduction of lymph vessel density in mF4-31c1-treated mice compared to control antibody-treated mice (**Figure 23B**). In the mesentery, we found a non-significant trend towards reduced lymph vessel density in mF4-31c1-treated allo-HSCT recipients vs. control antibody-treated allo-HSCT recipient mice during aGVHD (**Figure 23D**).

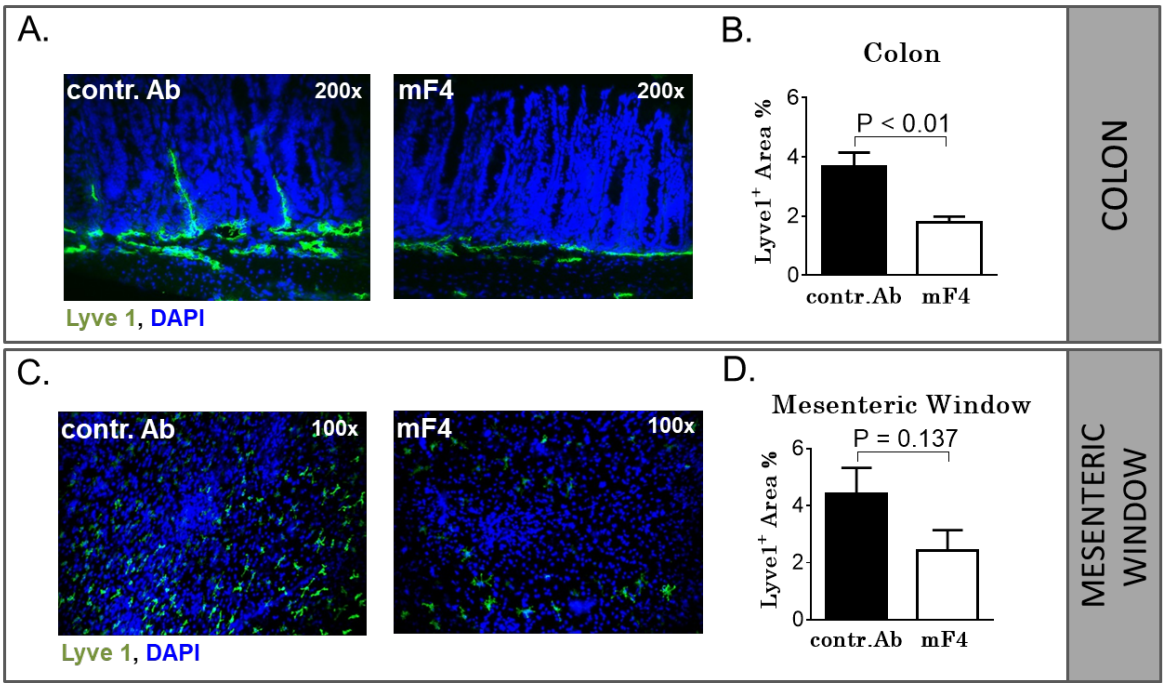

Figure 23. Anti-VEGFR3 treatment results in inhibition of GVHD-associated lymphangiogenesis. Allo-HSCT recipients received i.p. injections of 1mg/mouse/shot anti-VEGFR3 antibody (mF4-31c1) or control antibody every second day from day 0 to day +10 or day +14. Colon sections and mesenteric windows of mice treated with control antibody or mF4-31c1 were stained against Lyve1 (green) and counterstained with DAPI. Transplantation was performed in the 129/SV → C57BL/6 model. (A) Visualization of the reduction of lymphangiogenesis after anti-VEGFR3 treatment in the colon on day +15 after allo-HSCT. (B) Quantification of Lyve1 positive area in the colon after control antibody or mF4-31c1 treatment on day +15 after allo-HSCT (n = 4 per group). (C) Representative images of lymph vessels in the mesenteric window of mF4-31c1 antibody versus control antibody-treated allo-HSCT recipients on day +11 after allo-HSCT. (D) Quantitative analysis of Lyve1 positive area of mesenteric windows from control antibody and mF4-31c1-treated allo-HSCT recipients on day +11 post allo-HSCT. n = 4 per group; error bars indicate mean ± SEM, significance was tested with an unpaired Student´s t-test. contr. Ab: control antibody, mF4: mF4-31c1.

We further analyzed the amount of lymphatic endothelial cells (gp38$^+$ ECs) in mesenteric as well as peripheral lymph nodes via FACS analysis. In mesenteric lymph nodes we found no significant difference in lymph vessel density between the analyzed groups. In peripheral lymph nodes we found a trend towards a reduced number of lymphatic endothelial cells but again, without reaching statistical significance (**Figure 24**).

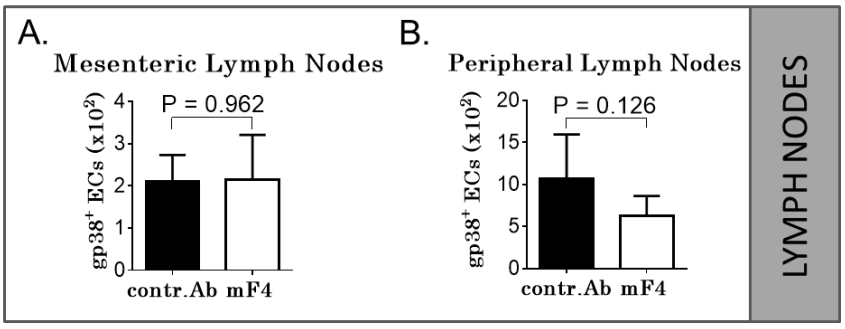

Figure 24. Anti-VEGFR3 treatment results in inhibition of GVHD-associated lymphangiogenesis. Allo-HSCT recipients received intraperitoneal injections of 1mg/mouse/shot anti-VEGFR3 antibody (mF4-31c1) or control antibody every second day from day 0 to day +10 or day +14. Endothelial cells were isolated from mesenteric and peripheral lymph nodes of control antibody- and mF4-31c1-treated allo-HSCT recipients on day +11. Transplantation was performed in the 129/SV → C57BL/6 model. (A, B) Quantification of lymphatic endothelial cells (gp38$^+$ ECs) in mesenteric (A) and peripheral (B) lymph nodes determined via FACS analysis. n = 5 per group; error bars indicate mean ± SEM, significance was tested with an unpaired Student´s t-test. contr. Ab: control antibody, mF4: mF4-31c1.

Before using the mF4-31c1 antibody therapeutically, we clarified if the antibody acts on lymphangiogenesis exclusively or if it has any effects on hemangiogenesis. We stained fresh frozen colon and liver sections from control antibody- and mF4-31c1 antibody-treated allo-HSCT recipients with aGVHD against the blood vessel marker CD31 (**Figure 25A, C**). In contrast to lymph vessels, the amount of blood vessels showed no significant difference in colon or liver samples of control antibody or mF4-31c1 antibody-treated animals (**Figure 25B, D**).

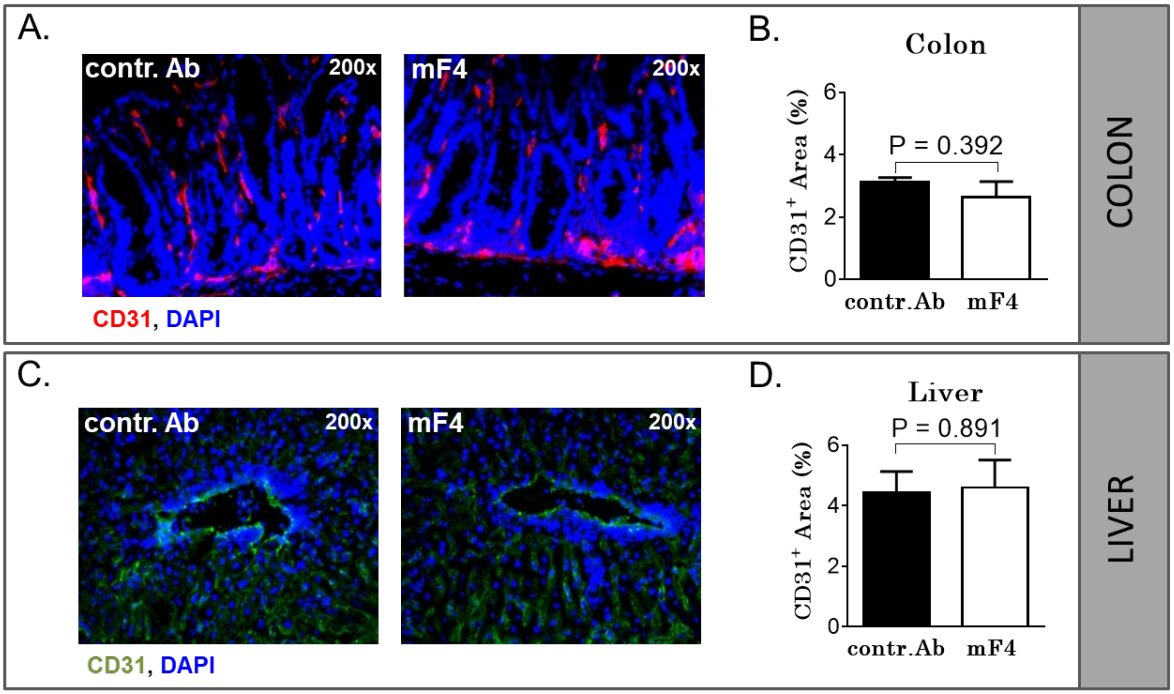

Figure 25. Anti-VEGFR3 treatment does not inhibit hemangiogenesis. Allo-HSCT recipients received i.p. injections of 1mg/mouse/shot mF4-31c1 or control antibody every second day from day 0 to day +11. Transplantation was performed in the 129/SV → C57BL/6 model. (A, C) Representative images of CD31 staining in colon (A) and liver (C) sections. DAPI was used for nuclear staining. (B, D) Quantification of CD31 positive area in colon (B) and liver (D) of control antibody- and mF4-31c1-treated allo-HSCT recipients on day +11. n = 4 per group; error bars indicate mean ± SEM, significance tested by unpaired Student´s t-test. contr. Ab: control antibody, mF4: mF4-31c1.

We conclude that treatment with the anti-VEGFR3 antibody mF4-31c1, is effective to inhibit GVHD-associated lymphangiogenesis in the colon and does not affect hemangiogenesis.

3.1.4 Anti-VEGFR3 treatment ameliorates lethal GVHD

Based on our findings that aGVHD is associated to increased lymphangiogenesis and the anti-VEGFR3 antibody mF4-31c1 effectively inhibits lymph vessel growth, the next step was to determine the effect of VEGFR3 inhibition on aGVHD. Allo-HSCTs were performed in two different well characterized minor mismatch models: 129/SV → C57BL/6 and LP/J →

C57BL/6.[128] We chose two mouse models with different GVHD progression patterns to mimic different clinical GVHD phenotypes. In both settings, the antibody administration started on the day of transplantation (day 0). We injected the anti-VEGFR3 antibody or the control antibody at a dose of 1mg per recipient every second day. The last shot was given on day +16 after allo-HSCT, which correlates with the acute phase of GVHD. As shown in **Figure 26A and C**, GVHD-related mortality was significantly reduced in mF4-31c1 treated allo-HSCT recipients compared to control antibody-treated recipients. We further assessed the clinical GVHD score, consisting of scores for the five parameters posture, activity, fur, skin and weight loss. In both tested mouse models the clinical GVHD scores were significantly lower in mF4-31c1 treated-animals at the peak of aGVHD (**Figure 26B, D**). We further harvested colon and liver samples from sacrificed animals of both cohorts for immunostaining. **Figure 26E** displays target organ aGVHD in colon and liver showing less tissue damage and immune cell infiltration in mf4-31c1-treated allo-HSCT recipients than in control antibody-treated allo-HSCT-recipients. Quantification of blinded histologic scoring revealed significantly diminished GVHD-associated tissue destruction of colon and liver tissue in anti-VEGFR3-treated animals than in control antibody-treated animals (**Figure 26F**). Immunofluorescent staining of liver sections further demonstrated less tissue-infiltrating $CD3^+$ T cells as a result of diminished lymphangiogenesis due to anti-VEGFR3 therapy (**Figure 26G, H**).

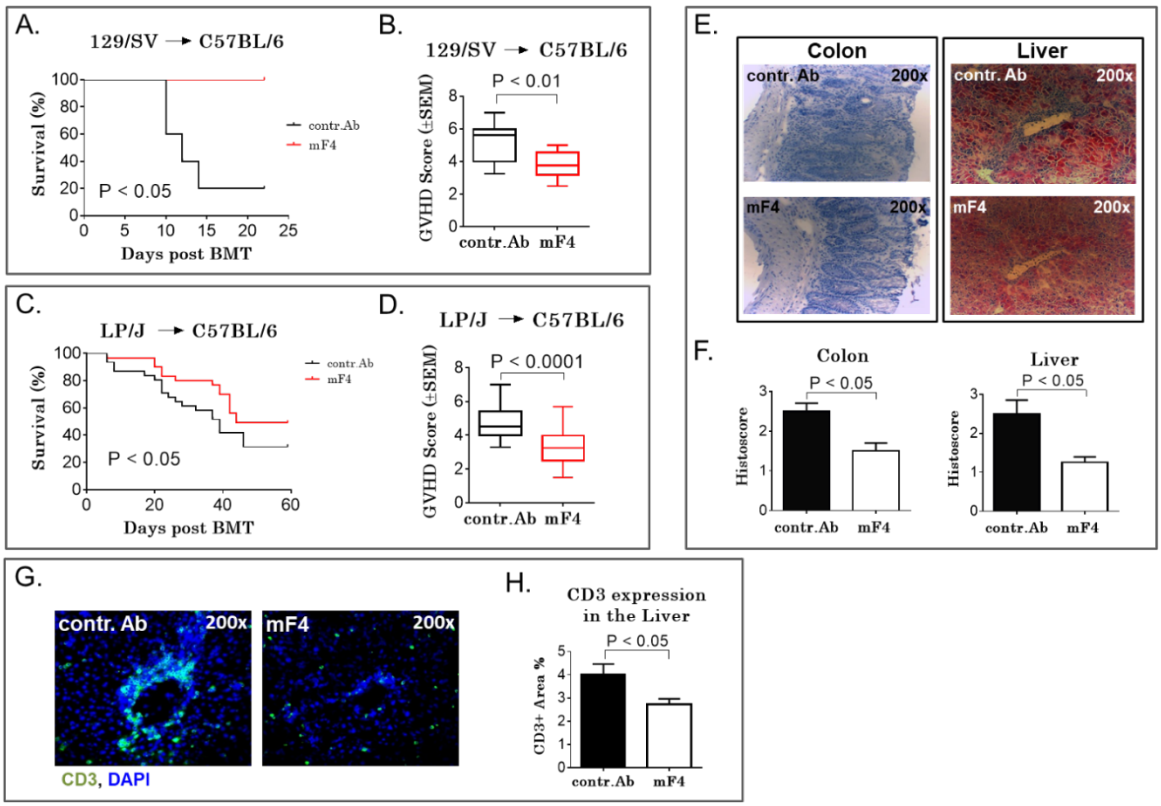

Figure 26. Anti-VEGFR3 treatment ameliorates lethal GVHD. Allo-HSCT recipients received i.p. injections of 1mg/mouse/shot mF4-31c1 or control antibody every second day from day 0 to day +16 after allo-HSCT. (A) Survival curve of control antibody- and mF4-31c1-treated allo-HSCT recipients using the 129/SV → C57BL/6 model (n = 5 per group). Data from one representative experiment are shown, analysis with the log-rank test. (B) GVHD scores of control antibody- and mF4-31c1-treated allo-HSCT recipients on day +14 using the 129/SV → C57BL/6 model. Data from one representative experiment are shown (n = 5 per group). (C) Survival curve in the LP/J → C57BL/6 model (n = 28 per group). Combined data from three independent experiments are presented. Analysis was performed with the log-rank test. (D) GVHD scores of control antibody- versus mF4-31c1-treated allo-HSCT recipients in the LP/J → C57BL/6 model on day +18 after HSCT (n = 28 per group). Combined data from three independent experiments are presented, analysis was performed with the log-rank test. (E) Representative images of histopathology in the colon and liver. Organs were taken on day +11 after allo-HSCT, histological staining was performed with hematoxylin and eosin (n = 4 per group). (F) Histopathological scores of colon and liver sections from control antibody- and mF4-31c1-treated allo-HSCT recipients on day +11 after allo-HSCT, scoring was done according to Lerner criteria (n = 4 per group). (G) Representative images of CD31 cell infiltration in the liver. Organs were taken on day +11, liver sections were stained against CD3 (green) and counterstained with DAPI. (H) Quantification of CD3 positive area in the liver of control antibody- or mF4-31c1-treated mice. n = 4 per group; error bars indicate mean ± SEM, significance was tested with an unpaired Student's t test. BMT, bone marrow transplantation, contr. Ab: control antibody, mF4: mF4-31c1.

According to our results we state that anti-VEGFR3 treatment inhibits lymphangiogenesis and subsequently reduces GVHD-associated target organ damage and mortality after allo-HSCT.

3.1.5 Effect of anti-VEGFR3 treatment on hematopoietic reconstitution after allo-HSCT

In previous approaches we performed anti-VEGFR1 or anti-VEGFR2 antibody treatments and were confronted with impaired donor cell engraftment due to the inhibition of VEGFR1 or VEGFR2.[129] Therefore, we investigated effects of anti-VEGFR3 therapy on hematopoietic engraftment. Allo-HSCT was performed in the 129/SV → C57BL/6 model. mF4-31c1 antibody or control antibody were given at a dose of 1mg per mouse every second day starting from day 0 (day of transplantation). On day +11, when donor cell engraftment is well advanced, recipient mice were sacrificed and blood and bone marrow were harvested for FACS analysis. Cells from donor and recipient mice can be differentiated via their chimerism markers: 129/SV mice express Ly9.1 and H2kb whereas C57BL/6 mice only express the H2kb antigen. As shown in representative dot plots in **Figure 27A and B**, the majority of cells from bone marrow as well as from peripheral blood of control antibody- and mF4-31c1 antibody-treated mice expressed both chimerism markers, Ly9.1 and H2kb. Quantification of donor cell percentages also revealed that there is no difference in donor cell engraftment between mF4-31c1- and control antibody-treated allo-HSCT recipients. In contrast to anti-VEGFR1/VEGFR2 therapy, the anti-VEGFR3 treatment had no impact on hematopoietic engraftment.

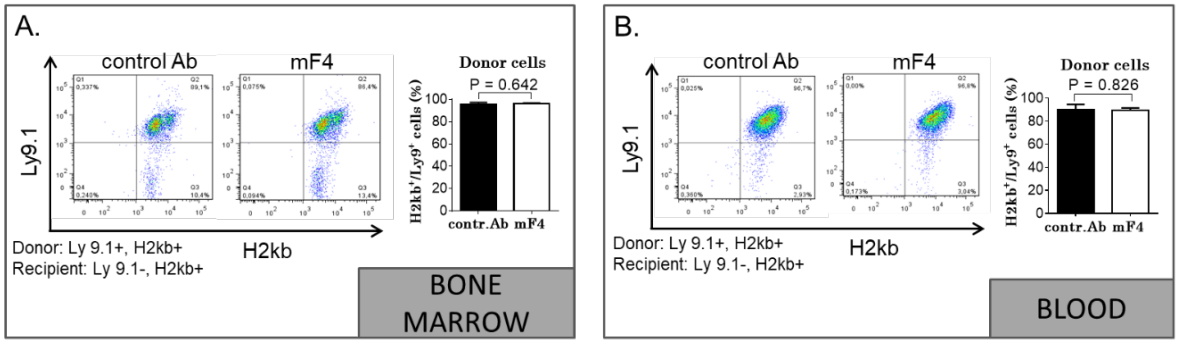

Figure 27. Effect of anti-VEGFR3 treatment on hematopoietic engraftment after allo-HSCT. Allo-HSCT recipients received i.p. injections of 1mg/mouse/shot mF4-31c1 or control antibody every second day from day 0 to day +10. On day +11, allo-HSCT recipients were sacrificed and organs were harvested for cell isolation and FACS analysis. Transplantation was performed in the 129/SV → C57BL/6 model. (A, B) Chimerism was analyzed by staining of bone marrow cells (A) and blood cells (B) against Ly9.1 and H2kb. n = 4 per group; error bars indicate mean ± SEM, significance was tested with an unpaired Student´s t-test. contr. Ab: control antibody, mF4: mF4-31c1.

We further examined the impact of mF4-31c1 on the recovery of different donor cell subsets. As shown in **Figure 28A**, the number of total donor leukocytes in the peripheral blood was significantly higher in mF4-31c1 antibody-treated allo-HSCT recipients than in control antibody-treated allo-HSCT recipients.

Looking closer to single myeloid cell subsets we found elevated cell counts in donor granulocytes (**Figure 28B**), monocytes (**Figure 28C**), dendritic cells (**Figure 28D**), B-cells (**Figure 28E**) and T cells (**Figure 28F – 28H**) of mF4-31c1-treated allo-HSCT recipients vs. control antibody-treated allo-HSCT recipients. T cells were further checked for $CD4^+$, $CD8^+$ and $CD4^+CD25^+FoxP3^+$ populations. All of them showed higher cell numbers in mF4-31c1-treated compared to control antibody-treated allo-HSCT recipients. Despite donor dendritic cells, all myeloid cell populations reached statistical significance.

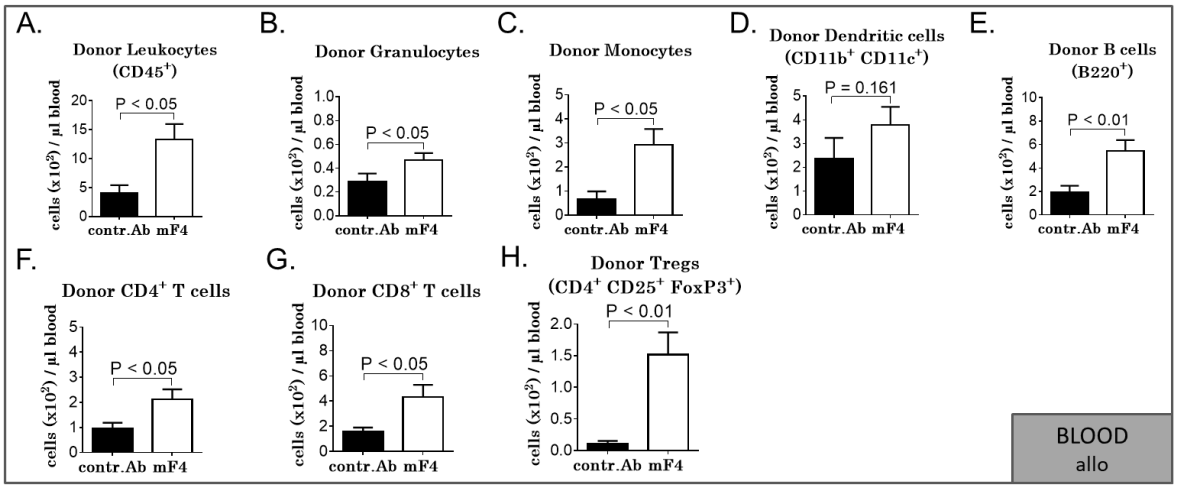

Figure 28. Effect of anti-VEGFR3 treatment on hematopoietic reconstitution after allo-HSCT. Allo-HSCT recipients received i.p. injections of 1mg/mouse/shot mF4-31c1 or control antibody every second day from day 0 to day +10. On day +11, allo-HSCT recipients were sacrificed and blood was harvested for cell isolation and FACS analysis. Transplantation was performed in the 129/SV → C57BL/6 model. (A-H) Cell counts of immune cells in the blood of control antibody- versus mF4- 31c1-treated animals measured by FACS. n = 4 per group; error bars indicate mean ± SEM, significance was tested with an unpaired Student´s t-test. Treg: regulatory T-cells, contr. Ab: control antibody, mF4: mF4-31c1.

To determine whether higher immune cell numbers result directly from anti-VEGFR3 therapy or are due to a secondary effect of reduced aGVHD, we tested the mF4-31c1 antibody in a syngeneic approach. C57BL/6 mice were transplanted with syngeneic C57BL/6 bone marrow and treated with mF4-31c1 or control antibody under the same conditions as in allogeneic experiments. Treatment after syngeneic transplantation revealed that none of the analyzed populations vary significantly between control antibody or mF4-31c1 antibody-treated mice (**Figure 29A – H**). Based on these finding we conclude that improved immune cell reconstitution in the allogeneic situation is a subsequent event to reduced bone marrow aGVHD[130] caused by anti-VEGFR3 therapy.

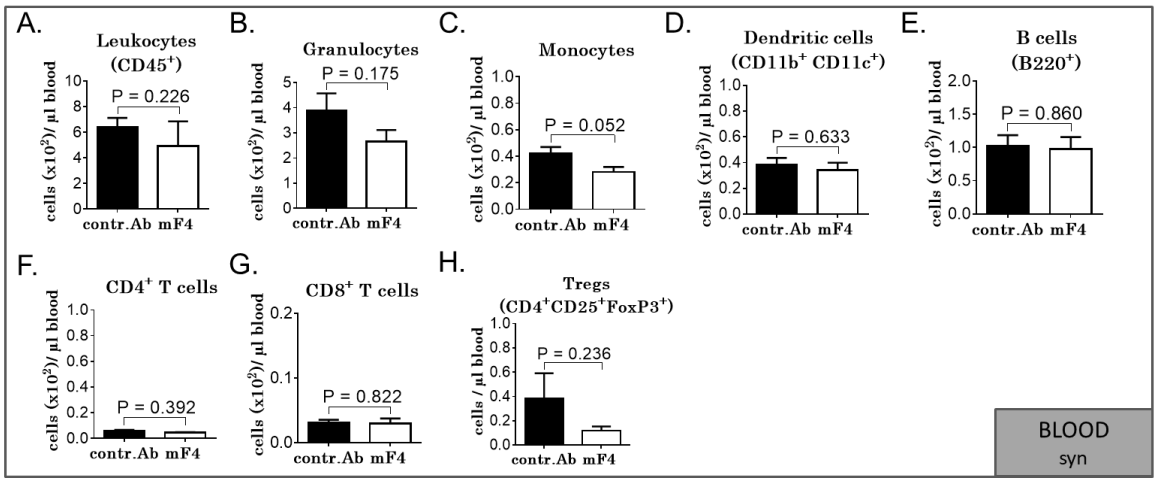

Figure 29. Effect of anti-VEGFR3 treatment on hematopoietic reconstitution after syn-HSCT. Syn-HSCT recipients received i.p. injections of 1mg/mouse/shot mF4-31c1 or control-antibody every second day from day 0 to day +10. On day +11, HSCT recipients were sacrificed and organs were harvested for cell isolation and FACS analysis. Transplantation was performed in the C57BL/6 → C57BL/6 model. (A-G) Cell counts of immune cells in the blood of control antibody- vs. mF4-31c1-treated animals measured by FACS. n=5 per group; error bars indicate mean ± SEM, significance tested by unpaired Student´s t-test. Treg: regulatory T cells, contr. Ab: control antibody, mF4: mF4-31c1.

3.1.6 Effect of anti-VEGFR3 treatment on tumor-associated mortality and tumor growth post allo- HSCT

As malignant lymphoma is a common indication for stem cell transplantation, we also wanted to elucidate the impact of anti-VEGFR3 therapy on lymphoma growth. We performed tumor experiments in two different aGVHD mouse models. In the C57BL/6 → BALB/c model we injected A20 B-cell lymphoma cells together with bone marrow cells and T-cells intravenously on day 0. To monitor tumor growth efficiently via *in vivo* bioluminescent signal intensity measurement we used luciferase expressing tumor cells. Exemplary pictures from *in vivo* imaging on the IVIS system are shown in **Figure S4**. The conditions for antibody treatment were the same as for aGVHD experiments: recipient mice received 1mg/mouse/shot of mF4-31c1 or control antibody every second day from day 0 to day +16 (**Figure 30A**).

In both tumor approaches we compared allo-HSCT recipients that received only bone marrow cells and allo-HSCT recipients that received bone marrow cells and additional splenic T cells. In the A20 tumor experiment, we found a significantly enhanced survival rate of mF4-31c1-treated mice in the bone marrow only group but no difference in the bone marrow plus T cells group (**Figure 30B, D**). Nevertheless, bioluminescence *in vivo* imaging on day +41 showed no significant difference of average radiance (p/s/cm2/sr) between mF4-31c1-treated mice and control antibody-treated mice in both transplantation settings (**Figure 30C, E**).

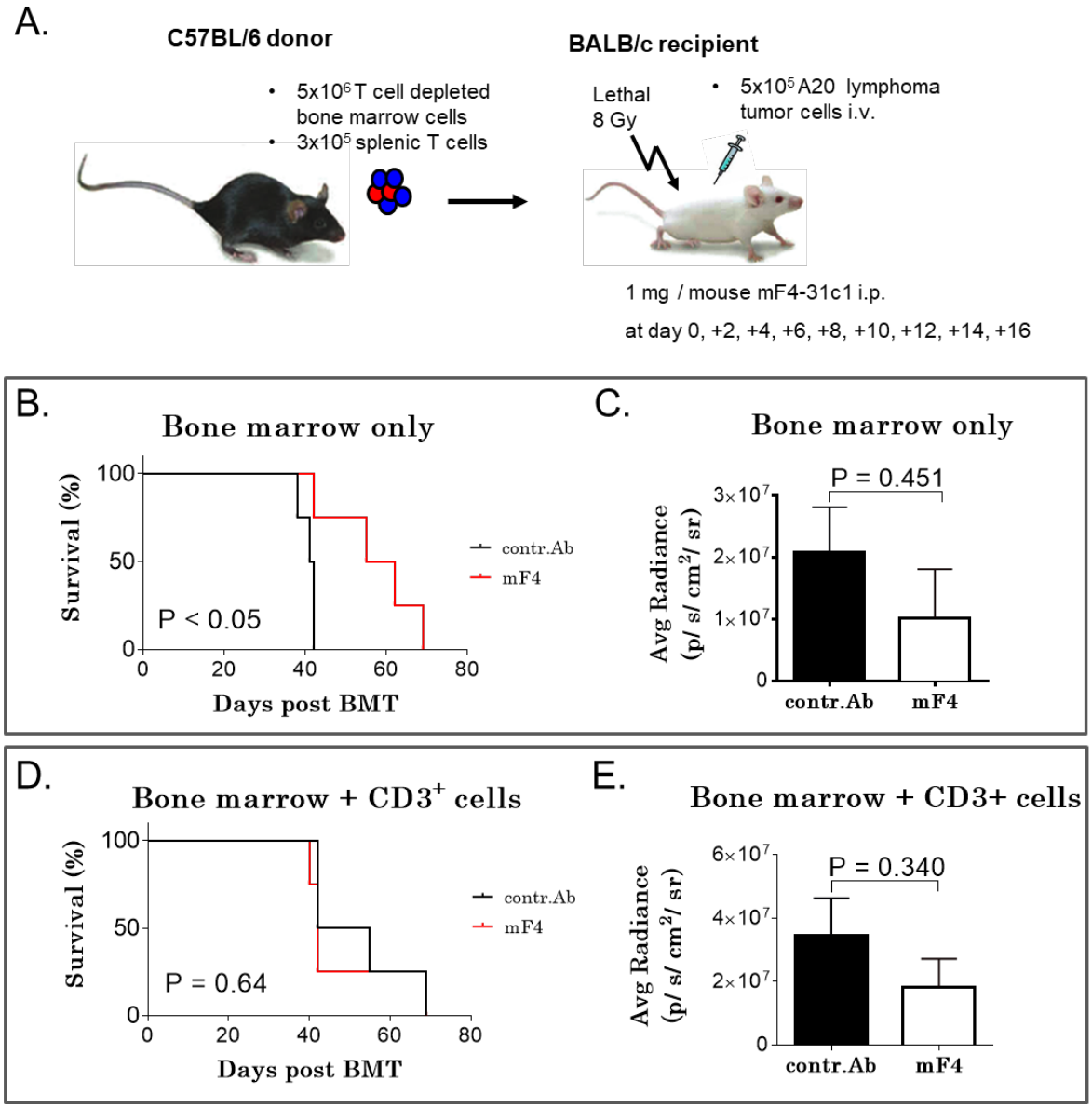

Figure 30. Effect of anti-VEGFR3 treatment on tumor-associated mortality and tumor growth post allo-HSCT in the C57BL/6 → BALB/c model. BALB/c allo-HSCT recipients were injected i.v. with 5 x 10^6 C57BL/6 bone marrow cells and 5 x 10^5 A20 tumor cells. 1 mg per mouse of control antibody or mF4-31c1 antibody was injected i.p. every second day from day 0 to day +16. (A) Schematic representation of the C57BL/6 → BALB/c aGVHD model used for tumor experiments. (B, C) Allo-HSCT with bone marrow only, no T cells were given. (B) Survival curve of control antibody- and mF4-31c1-treated allo-HSCT recipients (n = 4 per group). Data from one representative experiment are shown; analysis was done with the log-rank test. (C) Average radiance data of control antibody and mF4-31c1-treated allo-HSCT recipients (n = 4 per group). (D, E) Allo-HSCT with bone marrow and additional 3 x 10^5 donor splenic T cells. (D) Survival curve of control antibody- and mF4-31c1-treated allo-HSCT recipients (n = 4 per group). Data from one representative experiment are shown; analysis was done with the log-rank test. (E) Average radiance data of control antibody- and mF4-31c1-treated allo-HSCT recipients (n = 4 per group). Error bars indicate mean ± SEM, significance was tested with an unpaired Student´s t-test. BMT: bone marrow transplantation, Avg, average, contr. Ab: control antibody, mF4: mF4-31c1.

For experiments using the EL4 T cell lymphoma line the treatment conditions were the same as for the A20 tumor experiment: recipient mice received $5x10^5$ EL4 lymphoma cells and 1mg/mouse/shot of mF4-31c1 or control antibody per mouse every second day from day 0 to day +16 (**Figure 31A**). Experiments using the EL4 T cell lymphoma line revealed no significant survival difference between mF4-31c1-treated allo-HSCT recipients and control antibody-treated allo-HSCT recipients when transplanting bone marrow cells only (**Figure 31B**) or bone marrow and T-cells (**Figure 31D**). Again, we measured the average radiance (p/s/cm2/sr) of luciferase transfected tumor cells. On day +35 we found no significant difference in tumor growth between mF4-31c1-treated and control antibody-treated mice transplanted either with bone marrow only (**Figure 31C**) or bone marrow and additional T-cells (**Figure 31E**).

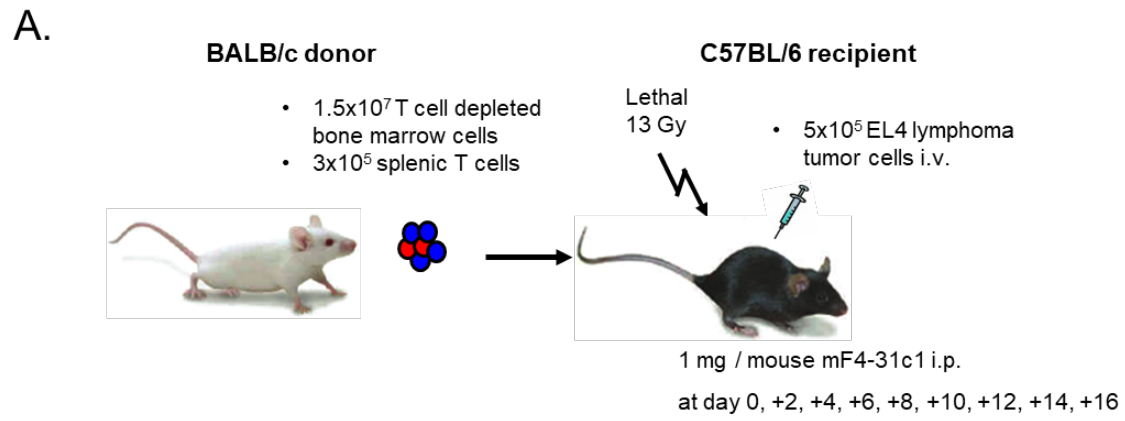

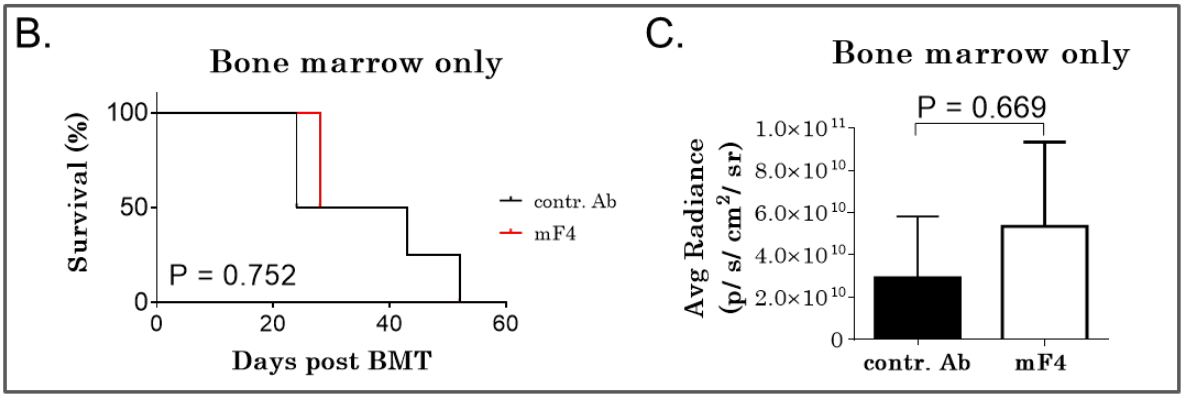

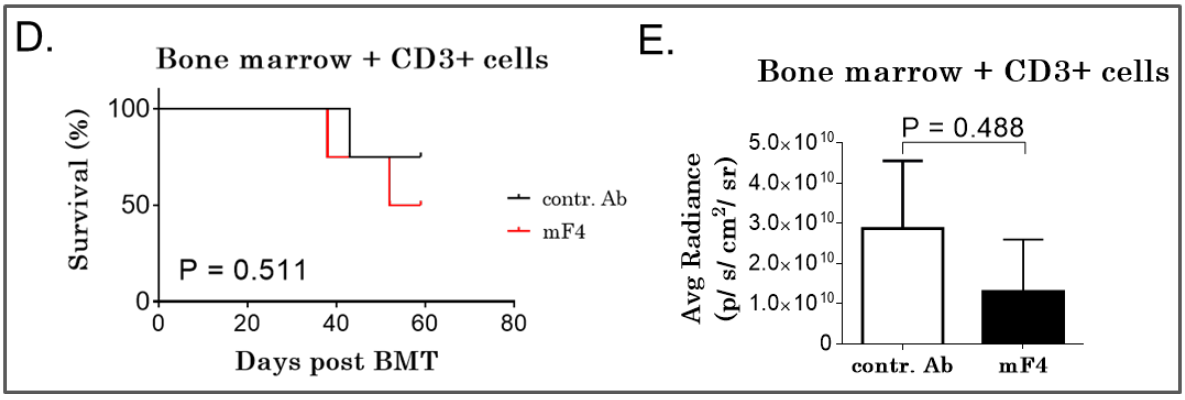

Figure 31. Effect of anti-VEGFR3 treatment on tumor-associated mortality and tumor growth post–allo-HSCT in the BALB/c → C57BL/6 model. C57BL/6 allo-HSCT recipients received i.v. injections of 1.5 x 10^7 BALB/c bone marrow cells and 5 x 10^5 EL4 tumor cells. 1 mg per mouse of control antibody or mF4-31c1 antibody was injected i.p. every second day from day 0 to day +16. (A) Schematic representation of the BALB/c → C57BL/6 GVHD model used for tumor experiments. (B, C) Allo-HSCT with bone marrow only, no T cells were given. (B) Survival curve of control antibody and mF4-31c1 treated allo-HSCT recipients (n = 4 per group). Data from one representative experiment are shown, analysis with the log-rank test. (C) Average radiance data of control antibody- and mF4-31c1–treated allo-HSCT recipients (n = 4 per group). (D, E) Allo-HSCT with bone marrow and additional 3 x 10^5 donor splenic T cells. (D) Survival curve of control antibody and mF4-31c1-treated allo-HSCT recipients (n = 4 per group). Data from one representative experiment are shown, analysis was done with the log-rank test. (E) Average radiance data of control antibody and mF4-31c1 treated allo-HSCT recipients (n = 4 per group). Error bars indicate mean ± SEM, significance was tested with an unpaired Student´s t-test. BMT: bone marrow transplantation, Avg, average, contr. Ab: control antibody, mF4: mF4-31c1.

Our findings suggest that anti-VEGFR3 treatment did not have any significant effects on malignant lymphoma growth in our murine allo-HSCT models.

3.2 Leucine-rich alpha-2-glycoprotein 1 in GVHD

Research interest in leucine-rich alpha-2-glycoprotein 1 (Lrg1) has increased since Greenwood et al. proposed a model of how Lrg1 is involved in Tfg-β-driven angiogenesis.[77] In contrast to other angiogenic factors, Lrg1 seems to be involved in pathologic angiogenesis rather than in physiologic angiogenesis, making it a promising therapeutic candidate for the treatment of angiogenesis-associated conditions, including various inflammatory diseases and cancer. In patients with angiogenesis-associated inflammatory diseases, such as inflammatory bowel disease, rheumatoid arthritis or appendicitis, serum levels of Lrg1 were elevated, suggesting a clinical significance.

We investigated the role of Lrg1 on pathologic angiogenesis and disease severity in experimental mouse models of aGVHD, colitis and rheumatoid arthritis.

Considering that the group of Prof. Greenwood is doing eye research and proved the important role of Lrg1 in pathologic retinal angiogenesis, we decided to check vessel density in retinas of mice during early aGVHD. As shown in **Figure 32**, vessel density was significantly increased in retinas of allogeneic transplanted mice with aGVHD than vessel density in mice without GVHD on day +2 after allo-HSCT.

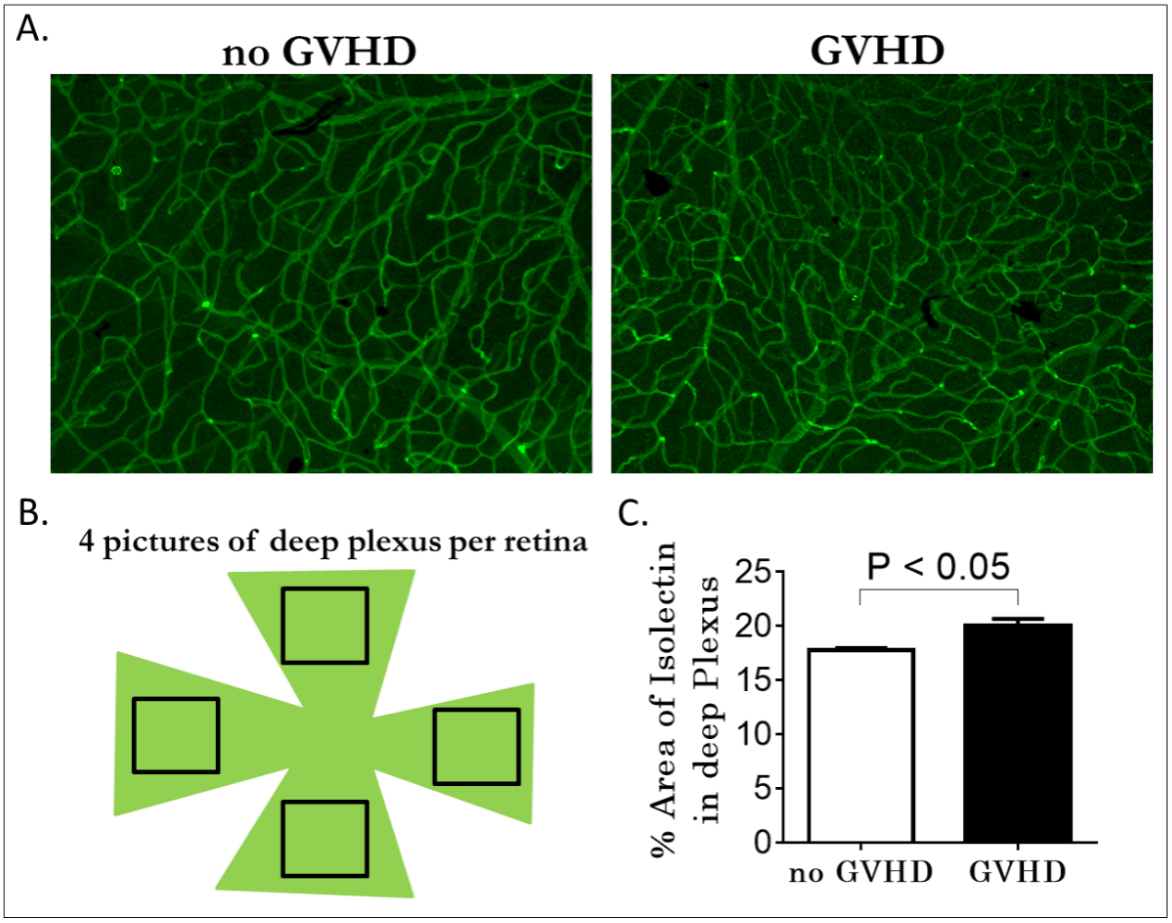

Figure 32. Vessel density in the retina of mice after syn- and allo-HSCT. Retinas of syngeneic (C57BL/6 → C57BL/6) and allogeneic (LP/J → C57BL/6) transplanted mice were harvested on day +2 after HSCT and stained against isolectin-IB_4. (A) Representative pictures of retinas from mice without GVHD (left, syngeneic transplantation) and with aGVHD (right, allogeneic transplantation). (B) Exemplary presentation of analysis. Four pictures of the deep plexus were taken per retina and the percentage of isolection-IB_4 was measured. (C) Quantification of isolectin-positive area in retinas of mice without GVHD or with aGVHD. n = 3 per group; error bars indicate mean ± SEM, significance was tested with an unpaired Student´s t-test.

3.2.1 Expression of Lrg1 in organs and endothelial cells

To define the role of Lrg1 in aGVHD we determined the expression level of Lrg1 in allo-HSCT recipients with aGVHD compared to syngeneic controls without GVHD (**Figure 33A**). We checked the mRNA expression level of whole liver tissue and freshly isolated liver sinusoidal endothelial cells on day +2 and day +15 after syn- vs. allo-HSCT. The expression level of Lrg1 was significantly increased in allogeneic transplanted animals already on day +2 after transplantation. During the peak of aGVHD, on day +15 post allo-HSCT, we detected lower levels of Lrg1 in general, with significantly increased Lrg1 expression in allogeneic liver tissue (**Figure 33A, left graph**). Liver sinusoidal endothelial cells (LSECs) still showed a trend towards higher Lrg1 expression in allogeneic transplanted animals (**Figure 33A, right graph**).

We further checked Lrg1 protein levels and found significantly higher protein expression in allo-HSCT recipients with aGVHD compared to syn-HSCT recipients without GVHD (**Figure 33B**). As described previously, Lrg1 signaling requires the contribution of different co-receptors, depending on whether proangiogenic (endoglin and ALK1) or angiostatic (ALK5) signaling is required. mRNA expression analysis revealed a significant increase of the co-receptors endoglin and ALK1 in whole liver tissue of allo-HSCT recipients vs. syn-HSCT recipients on day +15 after HSCT (**Figure 33C**). In contrast to those findings, there was no change in the expression level of ALK5 until day +15 post transplantation, indicating an active proangiogenic Lrg1 signalling pathway (**Figure 33D**). These findings indicate active proangiogenic signaling in allogeneic transplanted animals during aGVHD.

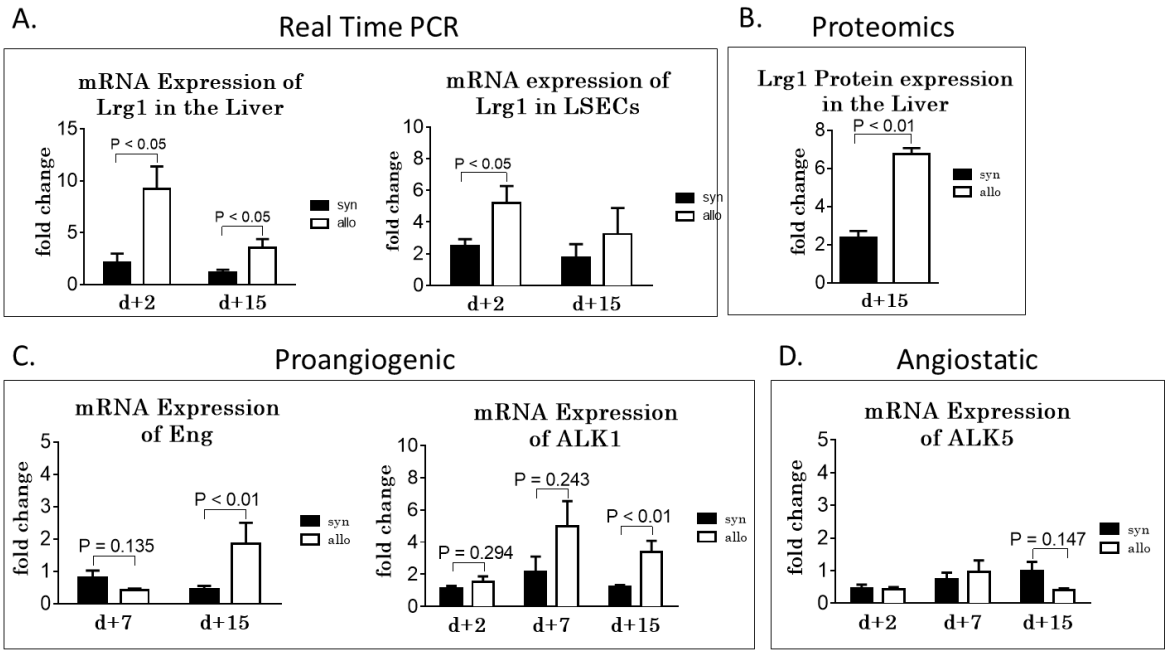

Figure 33. Expression data of liver tissue and LSECs at different time points after HSCT. (A) mRNA expression data of Lrg1 in the liver and in liver sinusoidal endothelial cells on day +2 and day +15 post HSCT. (B) Protein expression data of Lrg1 in liver tissue on day +15 after HSCT. (C) Expression data of co-receptors endoglin, ALK1 and ALK5 in the liver. For qPCR and proteomics data we used the chemotherapy-based minor mismatch model LP → C57BL/6 and harvested liver tissue from syngeneic and allogeneic transplanted animals on day +2 and day +15 post HSCT. We used liver samples from day +2 and day +15 for qPCR and liver tissue from day +15 for proteomics. Further, we isolated liver sinusoidal endothelial cells on day +2 and day +15 after HSCT for qPCR analysis. n = 4-5 per group for qPCR, n = 2-3 per group for proteomics. Error bars indicate mean ± SEM, significance tested by unpaired Student´s t-test. d: day (post bone marrow transplantation).

3.2.2 Histologic assessment of Lrg1 expression in relation to blood vessels

Besides mRNA and protein expression analyses we performed histologic staining of Lrg1 together with a blood vessels marker to verify the contribution of Lrg1 on vessel growth. Thin sections of fresh frozen liver and colon tissue were stained against a commercially available anti-Lrg1 antibody. Liver as well as colon tissue showed a significant increase in Lrg1 expression in allogeneic transplanted animals compared to syngeneic transplanted animals (**Figure 34A, B**).

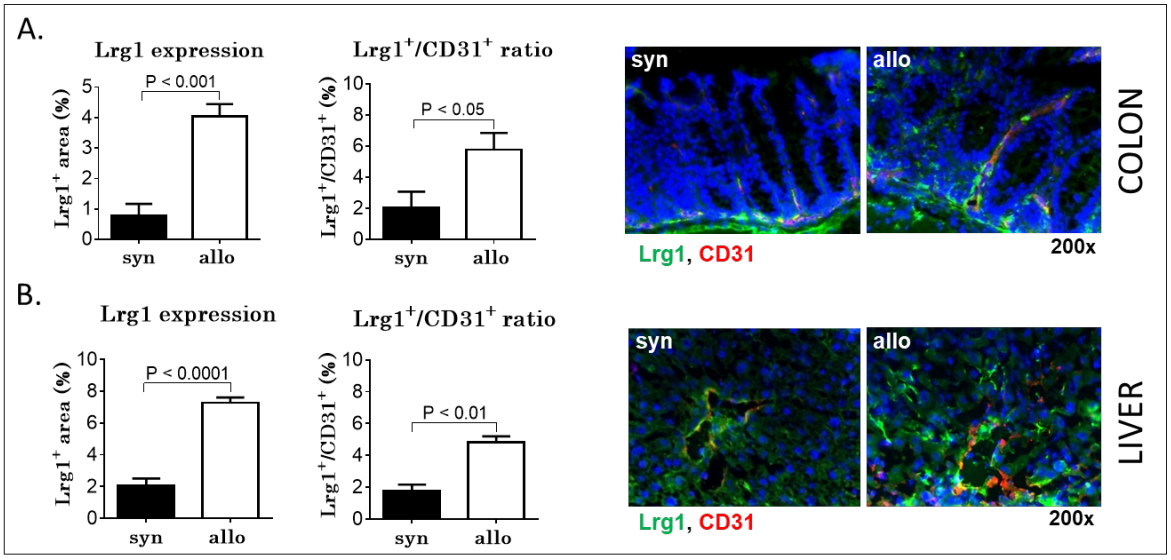

Figure 34. Immunofluorescent detection of Lrg1 in colon and liver tissue. (A) Quantification of Lrg1 positive area (left) and Lrg1/CD31 ratio (middle) in the colon on day +15 after HSCT. Right: Representative images of increased Lrg1 expression in the colon during aGVHD. (B) Quantification of Lrg1 positive area (left) and Lrg1/CD31 ratio (middle) in the liver on day +15 after HSCT. Right: Representative images of increased Lrg1 expression in the liver during aGVHD. For immunohistological staining we used the chemotherapy-based minor mismatch model 129 → C57BL/6 and harvested tissue on day +15 after HSCT. Colon and liver sections were stained against Lrg1 and CD31 and sections were counterstained with DAPI. n = 4-5 per group; error bars indicate mean ± SEM, significance tested by unpaired Student´s t-test.

The fluorescent labeling appeared specific for Lrg1 and the expression difference between syngeneic and allogeneic transplanted animals appeared reasonable. Nevertheless, we also found some positive signal in Lrg1 knockout tissue (**Figure S5**), probably due to a small residual amount of Lrg1 expression in knockout animals. To verify our results, we decided to use another detection method that is established in the lab of our collaboration partner Prof. Dr. John Greenwood. Via RNAScope (RNA in situ hybridization) it is possible to visualize single RNA molecules and quantify them microscopically (see methods section). In a preliminary experiment, the group of Prof. Greenwood analyzed colon samples of our B6 WT mice to verify the effectiveness of this method. Lrg1 RNA was found in close proximity to the blood vessels that were detected by labeling CD31 RNA (**Figure S6**), strengthening our hypothesis of Lrg1 involvement in angiogenesis.

3.2.3 The role of Lrg1 in inflammatory diseases

Knowing that the expression of Lrg1 is enhanced under inflammatory conditions, we decided to use Lrg1 knockout mice (Lrg1 KO) in different experimental disease models to determine the role of Lrg1 during inflammation.

3.2.3.1 Lrg1 in GVHD

We started with performing aGVHD experiments in different mouse models using Lrg1 KO mice either as recipients or as donors for allo-HSCTs. This approach should give insights whether the hematopoietic or the non-hematopoietic system is more influenced by Lrg1.

When using Lrg KO mice vs. B6 WT littermates as recipients of allo-HSCT, the knockout recipient mice showed significantly lower clinical GVHD scores (skin lesions, weight loss, fur ruffing, motility, posture) than B6 WT littermate recipient mice during early aGVHD (**Figure 35A**). Further, Lrg1 KO mice showed a trend towards lower clinical GVHD scores during established aGVHD. (**Figure 35B**).

In another experiment, we used Lrg1 KO mice or B6 WT littermates as allo-HSCT donors for BALB/c WT recipients. Again, clinical GVHD scores were significantly reduced when transplanting hematopoietic stem cells from Lrg1 KO donor mice vs. hematopoietic stem cells from B6 WT littermates. The clinical score difference was persistent in the course of aGVHD, during early (**Figure 35C)** and established aGVHD **(Figure 35D**).

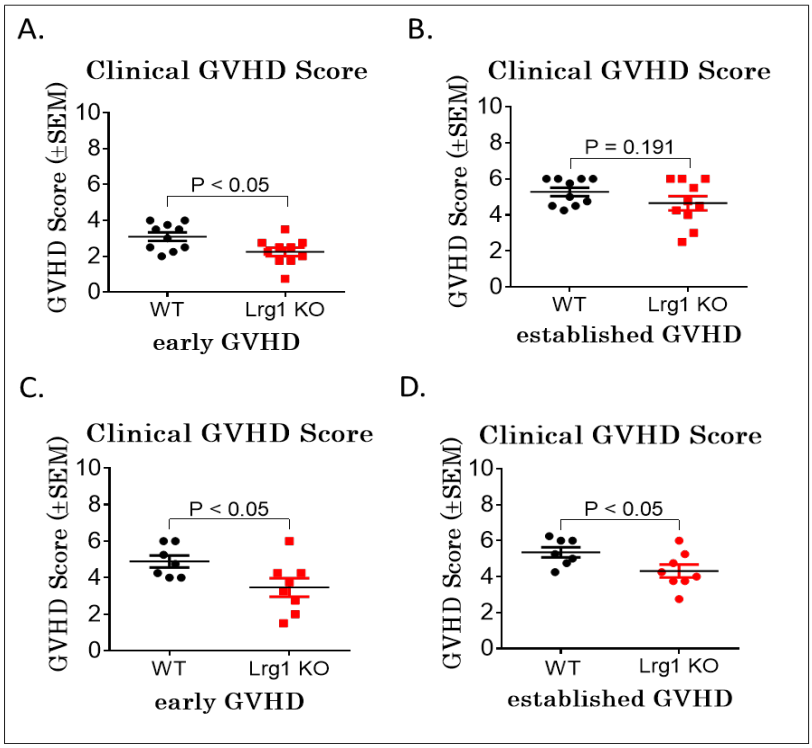

Figure 35. Clinical GVHD scores in disease models using Lrg1 KO mice as allo-HSCT recipients or donors. (A, B) GVHD scores of B6 WT and Lrg1 KO mice used as allo-HSCT recipients during early (A) and established (B) GVHD. (C, D) GVHD scores of mice receiving either B6 WT or Lrg1 KO donor cells. (C) GVHD scores during early (D) and established GVHD. n = 10 per group for A and B, mouse model: 129 → B6 (Lrg1 KO); n = 7-8 per group for C and D, mouse model: Lrg1 KO → BALB/c. Error bars indicate mean ± SEM, significance tested by unpaired Student´s t-test. WT: wildtype, KO: knockout.

Our group further defined differences in the condition of blood vessels between syngeneic and allogeneic transplanted animals. As shown in **Figure S7**, vessel leakiness is significantly increased in colon and liver tissue from allogeneic transplanted animals with aGVHD compared to syngeneic transplanted animals without GVHD. Considering the increased expression of vessel-associated Lrg1 in allo-HSCT recipients (**Figure 34**), we decided to stain colon tissue from Lrg1 KO mice and B6 WT littermates against the tight junction marker zonula occludens-1 (ZO-1). We found a trend towards a higher expression of ZO-1 in Lrg1 KO mice, probably indicating less vessel leakiness in Lrg1 KO under inflammatory conditions (**Figure 36**).

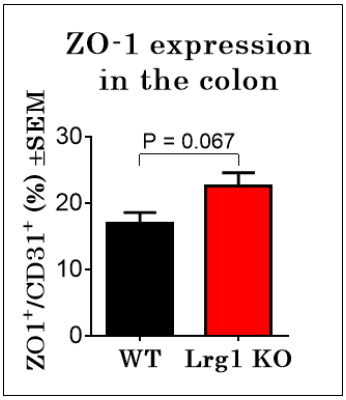

Figure 36. Endothelial ZO-1 expression in B6 WT and Lrg1 KO mice. Colon sections from B6 WT and Lrg1 KO mice were stained against the tight junction marker ZO-1 and CD31/ZO-1 double positive area was determined. n=5 per group, error bars indicate mean ± SEM, significance tested by unpaired student´s t-test. WT: wildtype, KO: knockout.

3.2.3.2 Lrg1 in experimental DSS-induced colitis

To get an overview of the influence of Lrg1 on inflammation in general, we decided to use Lrg1 KO mice in another inflammatory disease model. As an upregulation of Lrg1 was already demonstrated in the serum of inflammatory bowel disease patients[78], we performed ulcerative colitis experiments in B6 wildtype and Lrg1 KO mice. 2.5% dextran sulfate sodium (DSS) was added into the drinking water of B6 WT and Lrg1 KO mice to induce an intestinal inflammation. All mice were scored every second day for the assessment of disease activity index (DAI), defining the severity of ulcerative colitis. As shown in **Figure 37A**, DAI score was significantly lower in Lrg1 KO mice than in B6 WT littermates. Other indicators for a marked DSS-based gut inflammation are a shortened colon and enlarged spleen. Colons of B6 WT mice were clearly shortened, appeared bloody, and further showed a small and bloody caecum (**Figure 37B**). In contrast, colon lengths from Lrg1 KO mice were slightly reduced and contained considerably less blood. Furthermore, spleens of B6 WT mice suffering from experimental colitis appeared bigger than spleens of Lrg1 KO mice during DSS-colitis (**Figure 37B**). Exact measurements of colon length and spleen weight confirmed our visual assessments. Colon length reduction and spleen weight increase were significantly greater in B6 WT mice compared to Lrg1 KO during DSS-induced colitis (**Figure 37C, D**).

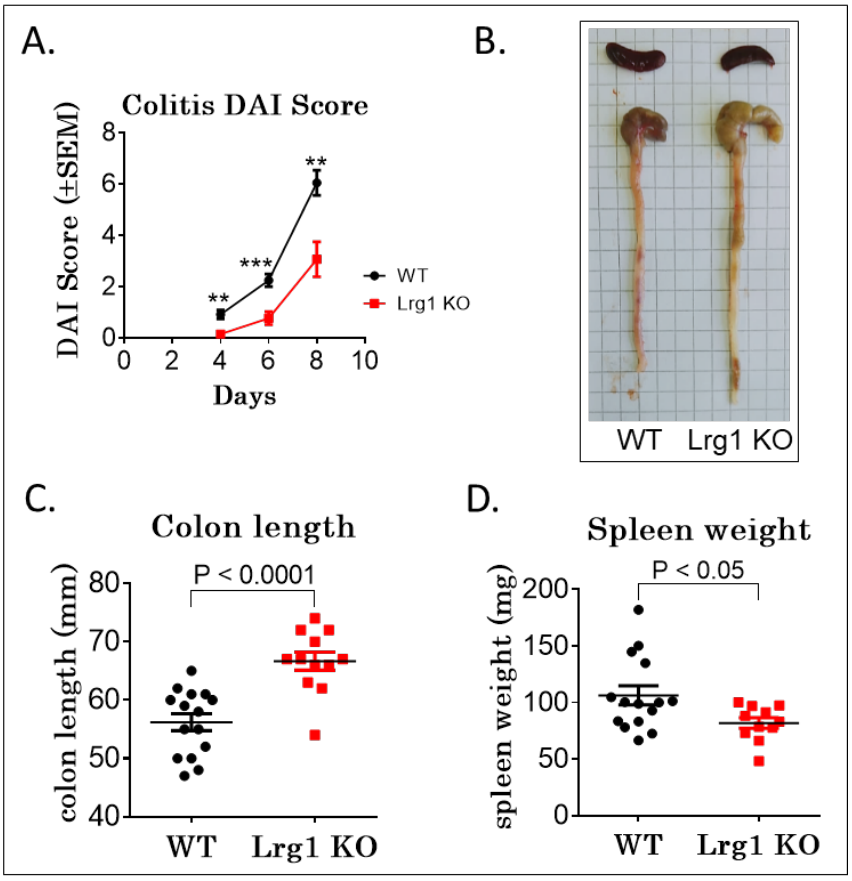

Figure 37. DSS-induced Colitis is ameliorated in Lrg1 deficient mice. Lrg1 KO mice and B6 WT littermates were challenged with 2.5% DSS in their drinking water for 7 days. Mice were monitored for DAI score every second day. On day 9 mice were sacrificed and organs were taken for histologic examinations. (A) Colitis disease activity index (DAI) of Lrg1 KO mice and wildtype littermates from day 2 to day 8. (B) Representative picture of colon and spleen from Lrg1 KO compared to B6 WT mouse. (C) Colon length was determined on day 9 after starting DSS treatment. (D) Spleen weight was determined on day 9 after starting DSS treatment. n = 12-15 per group, error bars indicate mean ± SEM, significance tested by unpaired Student´s t-test. WT: wildtype, KO: knockout.

We further embedded colon tissue of Lrg1 KO and B6 WT littermates for histologic investigation. Histopathologic colitis score comprises of the parameters inflammation and tissue damage and revealed significantly lower scores in Lrg1 KO mice than in WT littermates (**Figure 38A**). Representative images of HE stained colon sections are shown in **Figure 38B**. By immunofluorescent staining against CD3, we examined the amount of T cell infiltration in Lrg1 KO mice and B6 WT littermates. Whereas there is no difference of CD3 positive area in healthy colon tissue without inflammation, CD3 expression was significantly higher in B6 WT mice than in Lrg1 KO mice during DSS-induced colitis (**Figure 38C**).

Macrophage infiltration was determined by staining against CD11b and revealed no significant difference between Lrg1 KO mice and B6 WT littermates without colitis or during colitis. (**Figure 38D**). Nevertheless, by comparing the increase of CD11b expression in B6 WT mice and Lrg1 KO mice caused by colitis, we found a significant rise in CD11b expression in B6 WT mice upon the inflammation, whereas we found only a non-significant trend towards CD11b increase in Lrg1 KO mice. (**Figure 38D, grey shaded**).

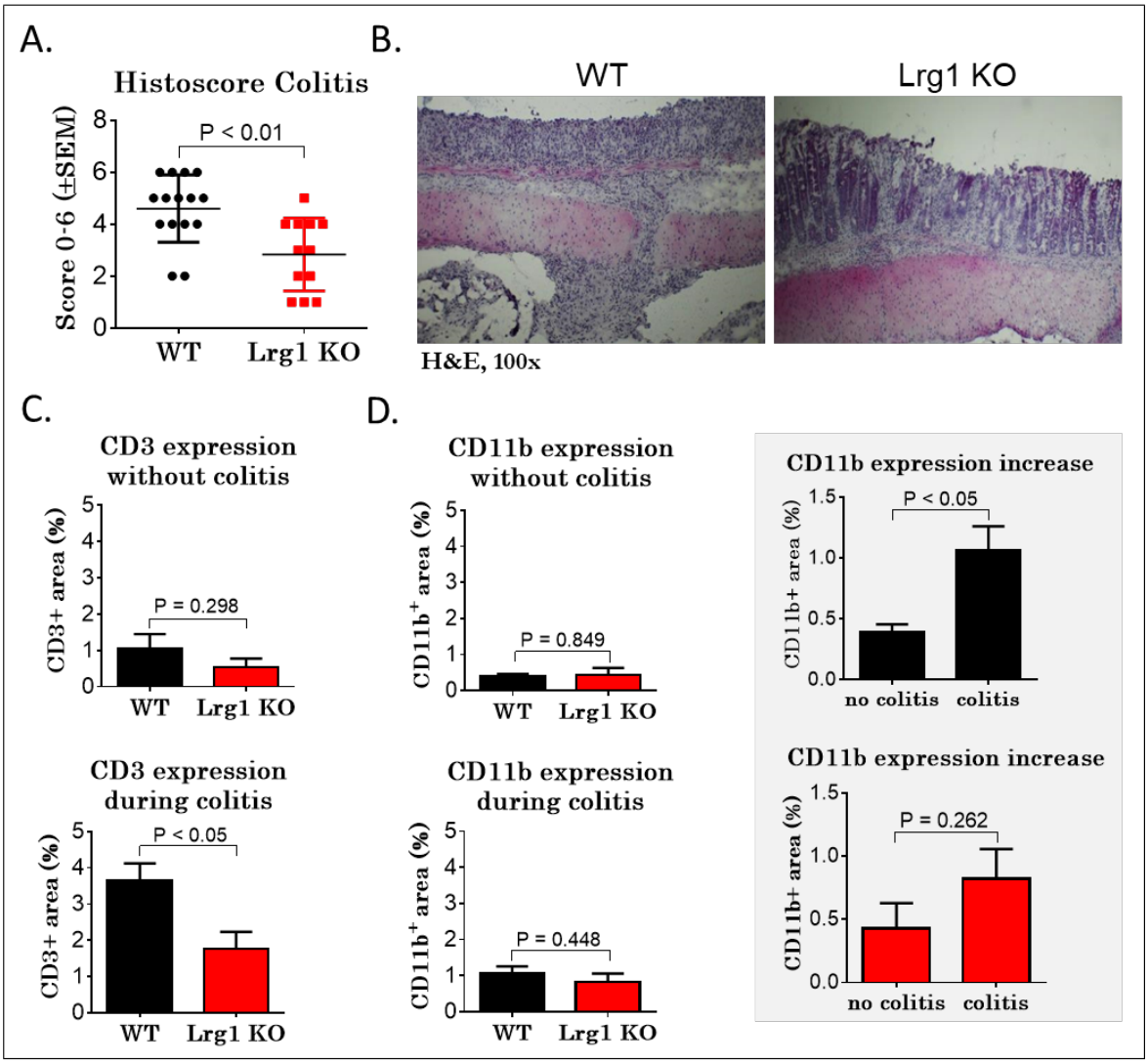

Figure 38. Histologic examination of colon tissue from Lrg1 KO mice and B6 WT littermates during inflammation. Colon sections were stained with hematoxylin and eosin (A, B) or immunostained against CD3 and CD11b (C, D). (A) Histopathologic score of Lrg1 KO and B6 WT mice on day 9 after the start of DSS treatment. (B) Representative pictures of hematoxylin and eosin staining of colon sections from B6 WT and Lrg1 KO mice. (C) $CD3^+$ area of B6 WT and Lrg1 KO mice without inflammation and during experimental colitis. (D) $CD11b^+$ area of B6 WT and Lrg1 KO mice without inflammation and during experimental colitis. n = 12-15 per group for A and B, n = 5-9 per group for C and D; error bars indicate mean ± SEM, significance tested by unpaired Student´s t-test. WT: wildtype, KO: knockout.

As shown in **Figure 36**, we found a trend towards a higher expression of the tight junction protein ZO-1 in Lrg1 KO mice under untreated conditions. Based on these findings, we checked the expression of the endothelial-specific marker CD31 and three different endothelial associated marker during DSS-induced gut inflammation in B6 WT vs. Lrg1 KO mice.

The expression difference of $CD31^+$ was not as strong as during aGVHD, but still showed a clear trend towards less $CD31^+$ cells in Lrg1 KO mice compared to B6 WT littermates (**Figure 39A, upper row**). We found that $CD31^+$ expression rises under inflammatory conditions in B6

WT mice but stays at a similar level in Lrg1 KO mice (**Figure 39A, lower row**). We found no difference in endothelial ZO-1 expression between B6 WT and Lrg1 KO mice during colitis. Again, endothelial ZO-1 expression rises in B6 WT mice upon inflammation while it nearly stays the same level in Lrg1 KO mice during inflammation (**Figure 39B**). The expression of smooth muscle cell marker αSma showed no differences between Lrg1 KO mice and B6 WT littermates with or without inflammation, though αSma expression decreases during colitis in Lrg1 KO mice and B6 WT littermates (**Figure 39C**). The pericyte marker NG2 showed no expression difference between Lrg1 KO mice and B6 WT littermates with or without the induction of experimental colitis (**Figure 39D**).

Taken together, our data suggests that Lrg1 induces blood vessel growth during DSS-induced colitis.

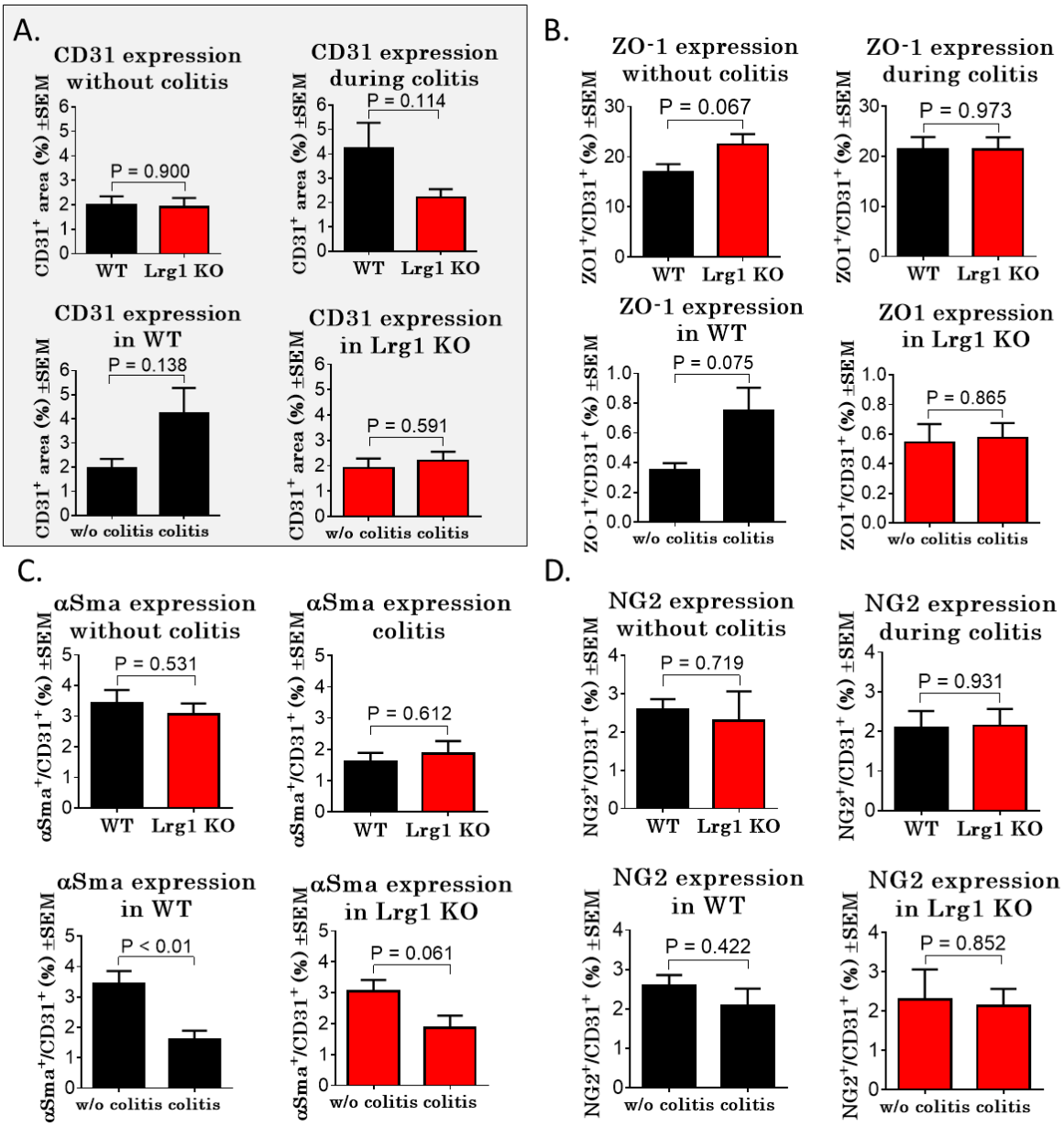

Figure 39. Histologic examination of blood vessel constitution in the colon of Lrg1 KO mice and B6 WT littermates. Sections of colon samples were double stained against CD31 together with ZO-1, αSma or NG2. (A) Determination of blood vessel density without inflammation vs. during DSS-induced colitis. (B) Evaluation of adhesion marker ZO-1 expression without and with colitis. (C, D) Histologic assessment of the expression of the complementary pericyte marker αSma (C) and NG2 (D). n= 5-8 per group; error bars indicate mean ± SEM, significance tested by unpaired Student´s t-test. WT: wildtype, w/o: without.

3.2.3.3 Lrg1 in paw edema

Another widely used model to study early acute inflammatory responses is the paw edema or footpad swelling model.[131] Inflammation is induced by the injection of the polysaccharide λ-carrageenan into the footpads of mice. The resulting footpad swelling indicates the amount of inflammation and is determined over time[117]. Carrageenan-induced footpad swelling peaks at 3-5h after the injection[132,131], for this reason we started with checking paw thickness increase during the first 6h after the carrageenan injection.

As shown in **Figure 40**, the footpad thickness increased in carrageen-treated Lrg1 WT as well as Lrg1 KO mice, whereas saline-treated footpad thicknesses did not change throughout the experiment. Footpad thickness was determined every two hours, at the 2h and 4h time point we found significantly greater paw volumes in B6 WT mice than in Lrg1 KO mice.

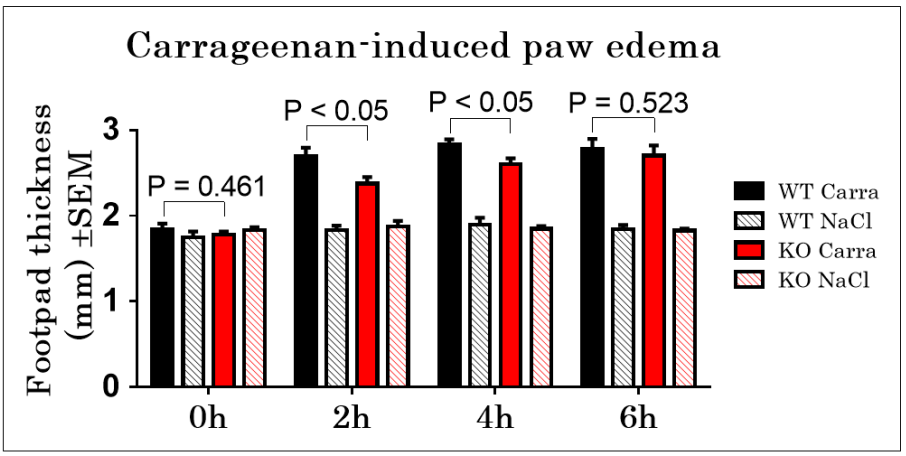

Figure 40. Development of paw edema in B6 WT and Lrg1 KO mice. Determination of footpad thickness before (0h) and after 2, 4 and 6h of carrageenan injection into one footpad. Saline injection into the other footpad served as control. n= 5 per group; error bars indicate mean ± SEM, significance tested by unpaired Student´s t-test. WT: wildtype, KO: knockout, Carra: carrageenan, NaCl: sodium chloride.

As we didn't see a significant difference after 6h and the swelling seemed to decrease again at this time point, we concentrated on earlier measurements and found the peak of footpad swelling 3h after carrageenan injection. **Figure 41** shows hourly measurements until 3h post

carrageenan injection. Again, we found a significantly greater increase of footpad swelling in B6 WT mice than in Lrg1 KO mice.

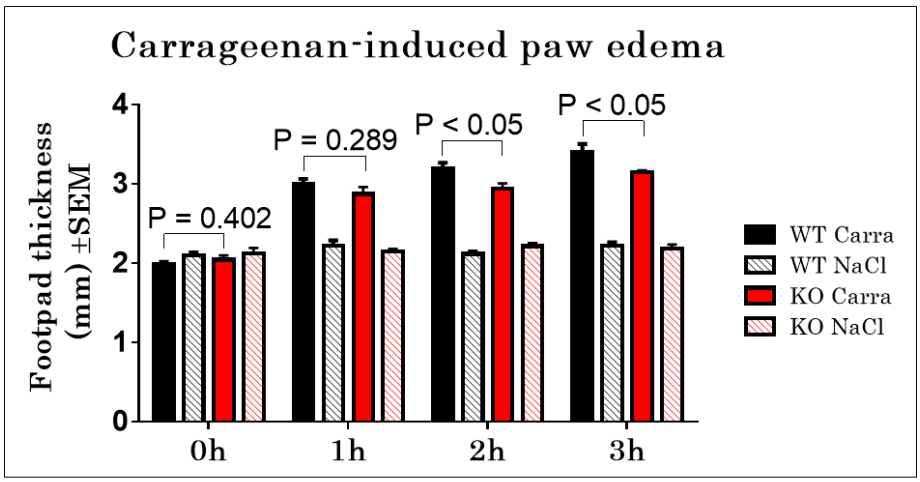

Figure 41. Development of paw edema in B6 WT and Lrg1 KO mice. Determination of footpad thickness before (0h) and after 1, 2 and 3h of carrageenan injection into one footpad. Saline injection into the other footpad served as control. n= 6-7 per group, error bars indicate mean ± SEM, significance tested by unpaired Student´s t-test. WT: wildtype, KO: knockout, Carra: carrageenan, NaCl: sodium chloride.

In order to check if the increased inflammation at 3h after induction is already due to blood vessel increase, we stained sections from footpad biopsies against CD31. As shown in **Figure 42**, we found no significant differences in vessel density in carrageenan or saline-treated footpads, demonstrating that early paw edema is not associated to angiogenesis.

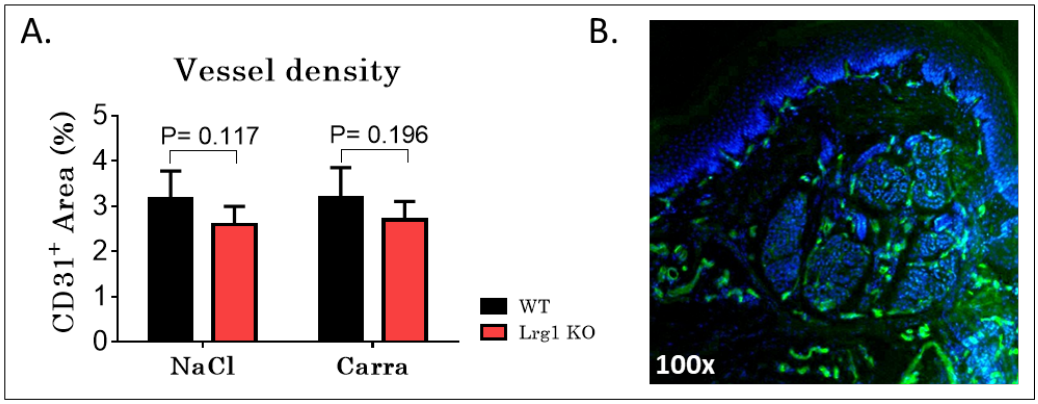

Figure 42. Vessel density of blood vessels in the footpad of carrageenan and saline-treated B6 WT and Lrg1 KO mice 3h after the injection. Sections of footpad biopsies were stained against CD31 and CD31 positive area was determined microscopically. n= 6-7 per group, error bars indicate mean ± SEM, significance tested by unpaired Student´s t-test. WT: wildtype, KO: knockout, Carra: carrageenan, NaCl: sodium chloride.

Another likely possibility of how the increased swelling may be explained is increased leakiness in blood vessels of B6 WT mice during paw edema. To check this hypothesis, we combined the paw edema model with the Evans blue (EB) assay to determine vessel leakiness. Paw edema experiments were performed as before, carrageenan and saline control solution were injected into footpads and paw thickness was determined every hour. After 3h we injected the EB solution and sacrificed the animals another 30min later. EB as an albumin-binding dye and serves as marker for extravasated blood through loosened endothelial cell contacts[133]. **Figure 43** shows the amount of extravasated EB, thus albumin, in footpad biopsies as well as spleens of B6 WT and Lrg1 KO mice that were treated with carrageenan or saline control. In both analyzed tissues we found a significantly lower EB concentration in Lrg1 KO mice than in B6 WT mice. Based on these findings we assume that Lrg1 KO mice develop significantly less blood vessel leakiness under inflammatory conditions.

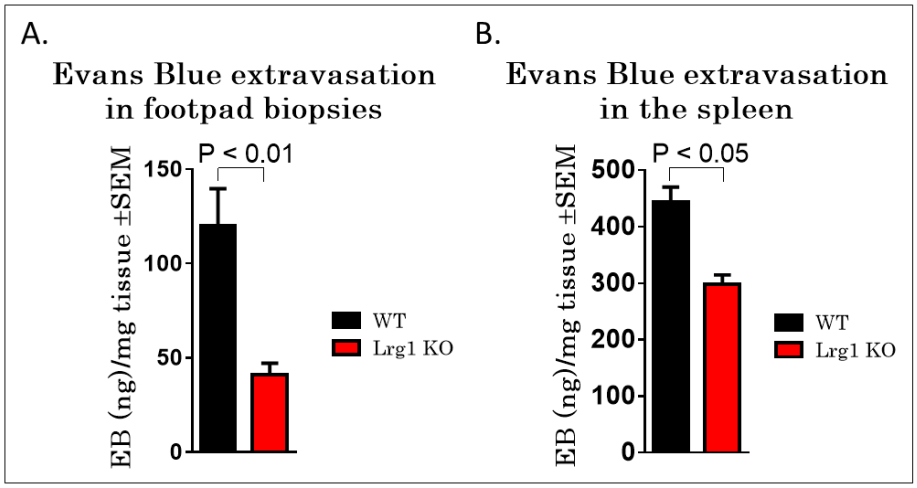

Figure 43. Evans blue extravasation in footpad biopsies and spleens of Lrg1 KO and B6 WT mice. Amount of Evans blue was determined by formamide incubation of tissues followed by optical density (OD) measurement of formamide/EB solution. n = 6-7 per group; error bars indicate mean ± SEM, significance tested by unpaired Student´s t-test. EB: Evans blue, WT: wildtype, KO: knockout.

The results from the performed paw edema experiments put further evidence to our hypothesis that Lrg1 contributes to a more pronounced inflammation and further has negative impacts on the constitution of blood vessels under inflammatory conditions.

4 Discussion

According to the results section, the discussion is divided into the parts 'Lymphangiogenesis in GVHD' and 'Leucine-rich alpha-2-glycoprotein 1 in GVHD'.

4.1 Lymphangiogenesis in GVHD

The most important signaling pathway in lymphangiogenesis is the VEGF-C/VEGFR3 pathway. The binding of VEGF-C to its receptor VEGFR3 is essential for the migration and proliferation of lymphatic endothelial cells during development. While lymphangiogenesis is essential during embryogenesis, it is rather involved in pathologic alterations like inflammation, tumor metastasis or lymphedema in adulthood.[86,90] We investigated the role of lymphangiogenesis during aGVHD and its inhibition by an anti-VEGFR3 antibody as novel treatment option in the setting of allo-HSCT.

4.1.1 Increased lymph vessel density in GVHD target organs

Our results of increased lymph vessel density in aGVHD after allo-HSCT are in accordance with observations found in Crohn´s disease[91,134], rheumatoid arthritis[91,135], psoriasis[91,136,137] and various types of cancer.[138-140] Increased lymph vessel density is a characteristic of allogeneic tissue transplants like kidney,[141] pancreatic islet,[99] skin,[142] cornea,[94,97,98] heart,[96] lung,[143] and trachea.[95]

In line with the increased lymph vessel density resulting from our experimental mouse models of aGVHD, the analysis of human biopsies revealed a higher number of lymph vessels in colon and ileum samples of patients with aGVHD than in biopsies of patients without GVHD. To our knowledge, there are currently no comparable data concerning lymph vessel density in human aGVHD available. However, clinical and pathophysiological characteristics of aGVHD exhibit strong parallels with inflammatory bowel disease.[144]

Rahier et al. showed enhanced lymph vessel density in biopsies from patients suffering from Crohn´s disease or ulcerative colitis compared to healthy control tissue.[145] Considering the similarities of inflammatory bowel disease and aGVHD, we assume that our data adds further evidence to increased lymph vessel density as a characteristic of various intestinal inflammatory diseases. Furthermore, Rahier described a similar tissue distribution of newly formed lymph vessels in the gastrointestinal tract of patients with inflammatory bowel disease than we found in patients suffering from aGVHD. In healthy control tissue, lymph vessels are restricted to the muscularis mucosa, while in patients with Crohn´s disease, lymph vessels are found throughout all layers of the intestine, preferably in inflamed areas.[145]

The blocking of VEGFR3 in our murine models of aGVHD exhibited a clear reduction of lymph vessels in the colon, whereas the reduction of lymph vessel density was less pronounced in lymph nodes and the mesentery. Besides the possibility of target organ tropism of aGVHD, the tissue heterogeneity of lymph vessels in different organs may play an important role. It is known, that lymph vessel tissues feature different properties, depending on the organ and the functional requirements.[146] Organ-specific functional and molecular properties of lymphatic endothelial cells include the dietary fat uptake and metabolism of intestinal lymphatic endothelial cells, the regulation potential of cholesterol metabolism of dermal lymphatic endothelial cells or distinct gene expression profiles of lymphatic vessels in different organs.[147]

4.1.2 Lymphangiogenesis in inflammation

Based on the literature, the formation of lymph vessels may have positive or negative effects on the development and severity of the inflammatory disease, whereby the effect seems to depend on the site of inflammation, the particular disease or the specific model used to mimic the disease. Two different possibilities of lymphangiogenesis-related mediation of inflammation are described. In both models, inflammatory cytokines trigger the expression of VEGF-C, which stimulates the formation of lymph vessels. From this point, two hypotheses regarding the impact on inflammation exist: 1) the increased number of lymph vessels causes a better drainage and clearance of proinflammatory mediators as well as immune cells and further leads to a reduction of local inflammation[91], or 2) the increased number of lymph vessels causes an increased flow of proinflammatory cytokines and immune cells to the site of inflammation and in combination with an increased leakiness, enhances the T cell response and exacerbates systemic inflammation.[88,92]

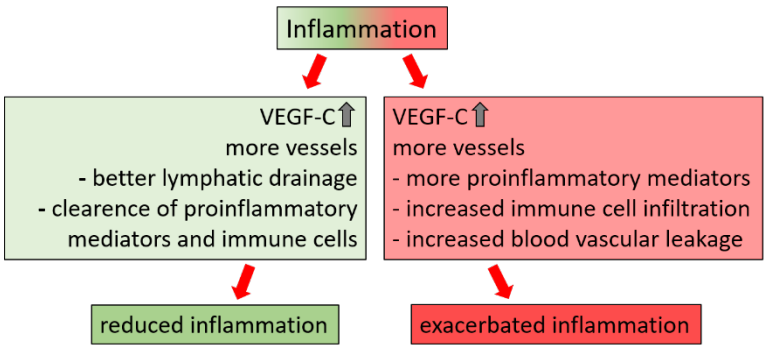

Figure 44. Model of VEGF-C-dependent inflammation development. Two hypotheses regarding the influence of VEGF-C on the development of inflammatory reactions.

We found that the inhibition of lymphangiogenesis leads to reduced inflammation and allogeneic T cell response in our experimental models of aGVHD. Hence, we assume that the

GVHD-related formation of lymph vessels leads to an increased flow of proinflammatory cytokines and thus increased immune cell infiltration in our experimental models of aGVHD. However, several studies outside the setting of transplantation, found distinct effects of lymphangiogenesis inhibition on acute and chronic inflammation in experimental disease models.

D'Alessio et al. studied the impact of lymphangiogenesis on experimental gut inflammation (Crohn's Disease and Ulcerative Colitis).[93] In contrast to our findings, D'Alessio et al. state that VEGF-C triggered an increase of lymphangiogenesis and reduced the severity of inflammatory bowel disease, attributing a protective role to the VEGFR3 ligand VEGF-C in gut inflammation.[93]

In another study, the overexpression of VEGF-C reduced the severity of skin inflammation in two experimental models of acute cutaneous inflammation, oxazolone-induced delayed-type hypersensitivity reactions and ultraviolet B irradiation.[148] Similar observations were made by Gao et al., who investigated the role of lymphangiogenesis in a mouse model of chronic inflammatory arthritis. They state that the inhibition of VEGFR3 increased the severity of arthritis and conclude that lymphatic drainage has a beneficial effect on the course of arthritis progression.[149]

Taken together, in diseases like skin or gut inflammation, increased lymph vessel density showed an ameliorative effect on inflammation. The experimental addition of VEGF-C reduced inflammatory symptoms and improved the regeneration of impaired lymph vessels, while blocking lymphangiogenesis via VEGFR3 inhibitors worsened inflammation[91,148,150].

It is unclear why the modulation of lymphangiogenesis has opposing effects on further progression of different diseases. A possible explanation by Kesler et al. is that the disease stimulus and the site of infection influence the constitution of newly formed lymph vessels and subsequently the lymphatic drainage ability.[86] In their examples, skin inflammation caused by skin-painting with oxazolone or the intraperitoneal application of LPS, showed reduced lymphatic drainage, whereas the application of complete Freund's adjuvant into footpads of mice resulted in increased lymph transport during inflammation. Based on that theory it would be necessary to examine not only the amount of lymph vessels but also their constitution to predict if the addition of VEGF-C or anti-VEGFR3 treatment may ameliorate the severity of the disease.

4.1.3 Lymphangiogenesis in transplantation

Our data on reduced aGVHD severity due to the inhibition of lymphangiogenesis is in line with results in allogeneic tissue transplantation. Several studies on allogeneic transplantation of

kidney,[141] pancreatic islet,[99] skin,[142] cornea,[94,97,98] heart,[96] lung,[143] and trachea[95] show that increased lymphangiogenesis is associated with graft rejection.

Cursiefen et al. performed transplantation experiments on the avascular cornea. They were able to demonstrate that the inhibition of lymphangiogenesis, rather than hemangiogenesis, leads to prolonged graft survival. Further, pre-existing blood vessels had no influence on graft survival upon subsequent corneal transplantation whereas pre-existing lymph vessels significantly worsened graft survival.[94]

Alitalo suggests that the mechanism behind this effect arises in the interaction between LECs and APCs. Activated LECs are able to recruit $CCR7^+$ APCs via the expression of the chemokine receptor CCL21. In turn, the increased number of APCs results in enhanced antigen presentation, increased activation of alloreactive T cells and finally graft rejection. This hypothesis is supported by Lemström et al. who detected that the inhibition of lymphangiogenesis improved graft survival after experimental allogeneic cardiac transplantation and that a decreased number of $VEGFR3^+$ lymph vessels is accompanied by reduced CCL21 expression.[96] Other preclinical studies demonstrate significant graft survival in recipients of trachea[95], pancreatic islet[99] or cardiac[96] transplantation that received anti-lymphatic treatments.

Besides the beneficial effect of the specific inhibition of lymphangiogenesis on graft survival, Cursiefen et al. see another advantage in solid organ transplantation. Cursiefen et al. state that specific inhibition of lymphangiogenesis without the affection of blood vessels may be beneficial for solid organ transplants, as the supply of nutrients via blood vessels is essential for organ survival.[94]

Taken together, our results support the hypothesis from Alitalo and we suppose that the reduced flow of APCs caused by the blocking of lymphangiogenesis, contributed to reduced alloactivation and severity of aGVHD in our experimental mouse models.

4.1.4 Inhibition of VEGFR3 – mechanisms of action

By staining fresh frozen sections of liver and colon tissue of control antibody and mF4-31c1 antibody-treated mice, we showed that the VEGFR3 antagonist works exclusively on lymph vessels and has no notable effects on blood vessel growth. These results are verified by Baluk et al. who inhibited VEGFR3 either by soluble VEGFR3-Ig, that binds the available VEGFR3 ligands VEGF-C and VEGF-D, or by the anti-VEGFR3 antibody mF4-31c1. In both cases, treatment inhibited the growth of lymph vessels while it had no effect on the growth of blood vessels.[151]

Cursiefen et al. performed lymphangiogenesis-blocking experiments in a mouse model of cornea transplantation. This model is widely used to study the impact of vessel growth on graft

rejection due to the avascularity of the cornea in healthy conditions. Their results indicate that lymph vessels, rather than blood vessels, substantially contribute to graft rejection.[94] Further, anti-lymphangiogenenic therapy ameliorated graft survival in experimental cornea transplantation.[94,152] These studies reveal a negative correlation between lymphangiogenesis and graft survival.

In compliance with that, we could demonstrate that the inhibition of lymphangiogenesis by anti-VEGFR3 therapy with the mF4-31c1 antibody ameliorated experimental aGVHD after allo-HSCT.

Alitalo published a possible mechanism of the interaction between lymph vessel growth and solid organ transplants. In his proposed model, inflammatory cells release VEGF-C, which further activates lymph vessels and triggers angiogenesis. The higher lymph vessels density enables enhanced flow of antigens and activated APCs to lymph nodes. Consequently, the higher number of antigens and APCs in lymph nodes and spleen leads to an increased allogeneic T-cell response and subsequently rejection of the graft.[88] This assumption is supported by the results of Cursiefen et al. who showed that reducing dendritic cell migration to draining lymph nodes promotes corneal graft survival.[153]

Based on our results and the pathomechanisms of aGVHD we assume that this mechanism of action applies to lymphangiogenesis during aGVHD: the higher number of lymph vessels allows an increased flow of allogeneic antigens and APCs to draining lymph nodes, subsequently leading to an enhanced T cell response that causes tissue damage in aGVHD target organs. The inhibition of lymphangiogenesis prevents antigen- and APC-flow to lymph nodes and consequently restrains allogeneic T cell response.

Though we consider that this is the main mechanism of how decreased lymphangiogenesis ameliorates aGVHD, other processes may have contributed to reduced aGVHD severity either. The group of Silvio Danese describe that VEGFR3 has an essential role on lymphatic endothelial permeability. Their results demonstrate that activation of VEGFR3 on lymphatic endothelial cells triggers loosening of cell-cell contacts leading to a reduced lymphatic endothelial barrier.[154] Anti-VEGFR3 therapy prevents activation of VEGFR3 and maintains lymphatic endothelial integrity. As a consequence, diapedesis of inflammatory leukocytes in target organs of aGVHD is attenuated.

Furthermore, VEGFR2 is also a possible binding partner of VEGF-C.[155,156] The group of Suda was able to elucidate the role of VEGFR3 signaling in vasculogenesis and hematopoiesis. Besides the observation that VEGFR3 deficient mice die by day E10.5 due to the lack of lymph vessel development, VEGFR3 seems to influence blood vessel maturation. VEGFR3 knockout mice show abnormally organized blood vessels with defective lumens. In VEGFR3 deficient

embryos, VEGF-C is able to transduce signaling via VEGFR2 and stimulate vasculogenesis. However, they assume that binding of VEGF-C to VEGFR3 regulates VEGFR2 signaling and ensures appropriate vasculogenesis and hematopoiesis.[156] According to the literature, VEGFR3 is also able to influence blood vessel angiogenesis not only in embryogenesis but also in adulthood.[157]

Nevertheless, our results depict no effect of VEGFR3 blocking on blood vessel growth and our previous data argue against a central role of VEGFR2 in aGVHD,[108] making this hypothesis unlikely.

4.1.5 Off-target effects of anti-VEGFR3 treatment

VEGFR3 has also been described to be expressed on a small subset of macrophages and dendritic cells.[158,159] Therefore, it may be possible that the anti-VEGFR3 treatment had an additional effect on macrophages and dendritic cells that contributed to the observed amelioration of aGVHD. The effect on macrophages and dendritic cells is important because of their essential role as APCs, subsequently leading to T cell activation.[160] Nevertheless, we assume that this effect is negligible due to the small number of VEGFR3 expressing macrophages and dendritic cells and because the specificity of the used anti-VEGFR3 blocking antibody to lymphatic endothelial cells was demonstrated previously.[99]

In previous work of our group we found that inhibition of VEGFR1 and VEGFR2 leads to a diminished hematopoietic engraftment,[108] which is an important factor to ensure therapeutic success after allo-HSCT. Treatment with the VEGFR3-antagonist mF4-31c1 did not have any negative effects on hematopoietic engraftment. An important difference between the mentioned VEGF receptors is that VEGFR1 and VEGFR2 are expressed on subsets of hematopoietic precursor cells whereas, in the bone marrow, the expression of VEGFR3 is restricted to sinusoidal endothelial cells.[161,162]

Additionally, VEGFR1 and VEGFR2 have been demonstrated to be involved in hematopoiesis and engraftment. As VEGFR1 is expressed on bone marrow repopulating stem cells, the inhibition of VEGFR1 leads to defective hematopoietic bone marrow recovery shown by impaired HSC cell cycling and differentiation.[163] Further, Hooper et al. describe that the blocking of VEGFR2 leads to an inhibition of hematopoietic recovery after BMT resulting in the death of treated mice due to a substantial decrease of hematopoietic precursor cells.[161]

In contrast to those findings, the inhibition of VEGFR3 in our experimental setup revealed an improved reconstitution of lymphoid and myeloid cells in the peripheral blood of allo-HSCT recipients. Nonetheless, when performing anti-VEGFR3 treatment in syn-HSCT recipients, we found no improvements in immune reconstitution. Therefore, we assume that blocking

VEGFR3 resulted in reduced bone marrow aGVHD, thus improving the hematopoietic recovery.

4.1.6 Effects of anti-VEGFR3 on tumor growth

Lymph vessels are widely described to be important for the spreading of cancer cells leading to the development of various metastases.[86,164-168] The increased lymph vessel density that is in line with increased tumor metastasis is used as a prognostic factor for patient survival.[169] Increased lymph vessel density was also found in distinct metastasis, further promoting the spreading of cancer cells to other organs.[165] VEGF-C, the main ligand triggering lymphangiogenesis, has also been found to be elevated in patients suffering from different types of cancer including breast cancer,[170] mammary cancer[171] or salivary gland cancer[172] and to promote lymph node metastasis.[173] In contrast to these profound findings, we did not see any significant difference in malignant lymphoma growth in allo-HSCT recipients that were injected with tumor cells on the day of transplantation.

The effect of the inhibition of lymph vessel density was determined by bioluminescence imaging to detect tumor load. Nevertheless, we did not isolate tumors to examine the actual lymph vessel density in treated and untreated mice. As tumor tissue is very complex and tumor cell expression differs from other cell expression patterns, more effort is needed to actually explain the outcome of mF4-31c1 treatment in tumor-bearing mice. A possible explanation for the absent effect of anti-VEGFR3 therapy could be an insufficient blocking of vessel growth. Based on rapid tumor cell proliferation, the expression of VEGFR3 by tumor cells increases and, as mentioned before, VEGF-C may use VEGFR2 as alternative binding partner. The interaction between VEGF-C and VEGFR2 would not have had an effect on lymph vessels, but on blood vessel growth, supporting nutrients and oxygen for further tumor growth.

Based on the literature, the inhibition of lymphangiogenesis in tumor settings is often achieved with factors that target VEGFR3 and VEGFR2 simultaneously, like the somatropin peptide SP5031.[174]

In contrast to mF4-31c1, the tyrosine kinase inhibitor SAR131675 serves as a ligand for VEGF-C and VEGF-D.[175] Conversed to our approach to block the receptor of VEGFR3/VEGF-C signaling axis, SAR131675 targets the ligand itself. Thus, on one hand VEGFR3 is not activated, and on the other hand, the over-activation of VEGFR2 is not possible. Nevertheless, SAR131675 is also described to be able to inhibit VEGFR2 signaling[176], making it unsuitable for our setting.

To sum up our main results and hypothesis, **Figure 30** outlines a model of the influence of lymphangiogenesis on aGVHD after allo-HSCT.

In the beginning, conditioning-induced tissue damage as well as allogeneic stem cells trigger angiogenesis. Subsequently, immune cells infiltrate target organs, finally leading to the proliferation of lymph vessels. We assume that increased lymph vessel density results in an increased infiltration of immune cells, which further triggers lymph vessel proliferation. Additionally, our results suggest that increased lymph vessel density delays immune cell reconstitution, which may be caused by increased bone marrow aGVHD. At this point it is unknown if the conditioning regimen and infiltrating T cells have any direct effects on lymphangiogenesis.

4.1.7 Outlook

We ascertained that aGVHD is associated with lymphangiogenesis in experimental models of aGVHD as well as in patients suffering from aGVHD after allo-HSCT. During the evaluation of the suitability of lymphangiogenesis as a therapeutic target, we confirmed that specific inhibition of lymphangiogenesis leads to reduced aGVHD. Clinical parameters as well as histological examinations showed less inflammation and organ damage due to the inhibition of lymphangiogenesis during aGVHD.

Based on these results and the clinical relevance, we aim at a translational development of therapeutic treatments to block pathologic lymphangiogenesis in aGVHD.

However, the conflicting data on lymphangiogenesis in inflammation and transplantation require a detailed study on the mechanisms and pathways involved in lymphangiogenesis during aGVHD. We are planning to evaluate cytokine and chemokine expression in experimental mouse models of aGVHD to identify regulating factors of lymphangiogenesis. Further, we will examine the interaction between LECs and dendritic cells. As proposed by Alitalo et al., the inhibition of lymphangiogenesis may results in decreased antigen presentation and therefore T cell activation by dendritic cells.

Further experiments should reveal more information about mechanisms of the regulation of pathologic lymphangiogenesis and may provide treatment options for additional indications.

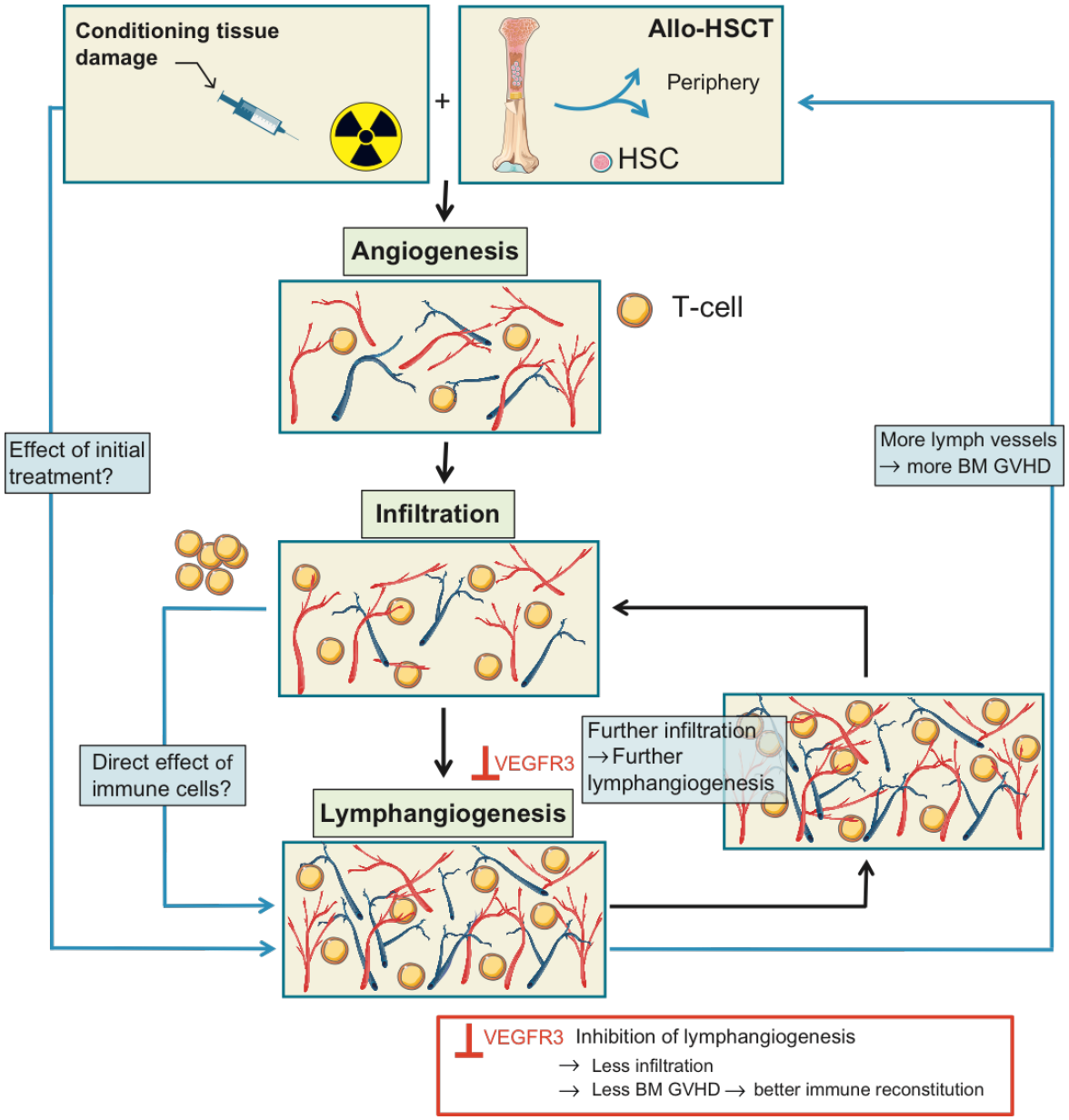

Figure 45. Model of the influence of lymphangiogenesis on aGVHD after allo-HSCT. allo-HSCT: allogeneic hematopoietic stem cell transplantation, HSC: hematopoietic stem cell, BM GVHD: bone marrow graft versus host disease, VEGFR3: vascular endothelial growth factor receptor 3 (from Penack and Holtan, 2019[107]).

4.2 Leucine-rich alpha-2-glycoprotein 1 in GVHD

The interest in Lrg1 increased following the assumption that Lrg1 is a regulator of TGF-β-controlled pathologic angiogenesis.[77] In order to determine the role of Lrg1 during inflammation, we decided to investigate Lrg1 in mouse models of different diseases with known pathologic anigogenesis. Experiments were performed in mouse models of aGVHD, ulcerative colitis and in the experimental paw edema, an acute inflammation model that is widely used to study mechanisms involved in inflammatory response.

4.2.1 Increased expression of Lrg1 under pathologic conditions

Elevated serum levels of Lrg1 were found in patients of inflammatory bowel disease,[78] rheumatoid arthritis[79] or appendicitis[80], all inflammatory diseases with known pathologic angiogenesis. Based on those findings we determined the expression of Lrg1 in target tissues of aGVHD in our experimental mouse models of aGVHD. In line with previous mentioned studies, we confirmed an increased expression of Lrg1 and its proangiogenic interaction partners during aGVHD on RNA and protein level. We detected elevated levels of Lrg1 in allogeneic transplanted mice throughout the development of acute GVHD. mRNA expression in liver and also in LSECs showed an upregulation of Lrg1 already on day +2 after BMT. In previous experiments on aGVHD we showed that pathologic angiogenesis is an early event and is found as early as day +2 after allo-HSCT.[108] Thus, the upregulation of Lrg1 on day +2 adds further evidence to the contribution of Lrg1 on the formation of pathologic blood vessels during early inflammatory processes.

The histologic assessment of Lrg1 revealed an increased expression of Lrg1 in colon and liver tissue of allogeneic transplanted mice on day +15 after allo-HSCT. Similar results were obtained for patient samples. Zhang et al. investigated tissue samples of patients suffering from colorectal cancer.[177] By immunohistochemical staining they determined elevated levels of Lrg1 in colorectal cancer biopsies compared to healthy colorectal mucosa. Further, they found a correlation between Lrg1 expression and the migration and invasion capability of cancer cells. They could show that Lrg1 promoted tumor angiogenesis by inducing the expression of VEGF-A in colorectal cancer cells.

Histologic determination of Lrg1 was also done by Gao et al., who investigated the role of Lrg1 in skin fibrosis. Their results show an enhanced expression of Lrg1 in hypertrophic scars that correlates with increased pathologic angiogenesis.[178]

To our knowledge the expression of Lrg1 has not been immunohistochemically investigated on mouse tissue so far. We used a commercially available antibody against Lrg1 that is described to work for western blot, immunohistochemistry and enzyme-linked immunosorbent assay (ELISA)

assays on murine tissue. To verify our results, we also stained Lrg1 KO tissue against the Lrg1 antibody and detected a positive background signal in KO tissue as well, seen in **Figure S5**. We assume that this signal could be caused by the polyclonal antibody binding to remaining fragments of Lrg1 or non-specifically binding to the tissue. As our cooperation partners faced similar difficulties, they established a method for staining Lrg1 mRNA on tissue sections. The RNAScope method is described to be very sensitive for the detection of low amounts of protein.[179] Together with the group of Prof. Greenwood we are currently establishing the RNAScope assay on tissue samples of mice from our aGVHD models. The method was already tested on colon tissue of aGVHD mice in a first trial (**Figure S6**). Similar to our results from immunofluorescent staining, the RNAScope assay indicates a co-expression of Lrg1 and CD31.

4.2.2 The role of Lrg1 in GVHD

In our mouse models of aGVHD, we used Lrg1 KO mice either as recipient or as donor of allo-HSCT. Both experimental setups indicated reduced clinical GVHD scores in Lrg1 KO mice compared to B6 WT littermates.

Lrg1 KO mice as allo-HSCT recipients revealed lower clinical GVHD scores during early phase of aGVHD development but no significant score difference at high grade aGVHD. Using Lrg1 KO mice and WT littermates as bone marrow donors displayed significantly lower GVHD scores in Lrg1 KO bone marrow recipients at early as well as acute phase aGVHD. Lrg1 is described to be expressed by hepatocytes, whereas studies by Druhan et al. also proved Lrg1 expression in myeloid cells.[180] A possible explanation for the slightly better outcome of Lrg1 KO bone marrow recipients could be that transplanted precursor myeloid cells lack Lrg1, which results in reduced inflammatory and angiogenic stimuli.

It is well known that the development of aGVHD is associated with pathologic angiogenesis and that the inhibition of angiogenesis offers a possible treatment option to reduce the number of tissue-infiltrating leukocytes which trigger inflammation in aGVHD and other inflammatory disorders.[66,129,181,182] We assume that the inhibition of Lrg1 led to blocking of the proangiogenic pathway of Lrg1-induced TGF-β signaling and subsequently reduced angiogenesis and the associated recruitment of leukocytes.

By investigating the condition of blood vessels of Lrg1 KO vs. Lrg1 WT mice, we found non-significant higher values of the adhesion marker ZO-1 in Lrg1 KO mice. As the involvement of Lrg1 in cell adhesion has been described earlier,[183,184] the higher values of ZO-1 in Lrg1 KO mice appeared unexpected. Summarizing, higher values of ZO-1 in Lrg1 KO mice may act protective to the pathologic leakiness of blood vessels occuring during inflammation.

4.2.3 The role of Lrg1 in DSS-induced Colitis

It is described that serum levels of Lrg1 are elevated in patients suffering from inflammatory bowel disease, including the two major types Crohn´s disease and ulcerative colitis.[78,185,186] Naka et al. correlated the serum levels of Lrg1 in inflammatory bowel disease patients to disease activity and mucosal status. In contrast to the conventionally used biomarker C-reactive protein (CRP), high levels of Lrg1 were in line with disease activity and low Lrg1 levels indicated mucosal healing.[186]

In our experiments on DSS-induced colitis in Lrg1 KO and WT mice, the clinical colitis score was significantly reduced in Lrg1 KO mice. Further parameters like colon length and spleen weight additionally revealed less pronounced colitis-associated inflammation.

As mentioned before, pathologic angiogenesis is a characteristic of colitis development and its inhibition ameliorates disease severity. Based on these findings, we assume that the inhibition of Lrg1 had a direct effect on disease development. There are several approaches described that use antiangiogenic therapy for the treatment of inflammatory bowel disease, but mostly targeting factors of the VEGF/VEGFR family.[187] Several available therapies encounter severe side effects. An example is Bevacizumab, a monoclonal antibody against VEGF-A that also inhibits wound healing, and promotes intestinal perforation and surgical anastomosis leakage. The tyrosine kinase inhibitors Sunitinib and Sorafenib inhibit VEGFR1, VEGFR2 and VEGFR3 among multiple other targets. However, the severity of inflammatory bowel disease was increased upon Sunitinib/Sorafenib treatment.[187] Knod et al. found that treatment of DSS-induced colitis with various tyrosine kinase inhibitors does not reduce microvascular density in colon tissue, despite the decrease of VEGFR2 and VEGF-A, suggesting the importance of other angiogenic pathways.[188]

The histologic examination of colon tissue confirmed reduced immune cell infiltration and tissue damage in Lrg1 KO mice during colitis. Regarding immune cell infiltration, we obtained clear results from CD3 staining, with significantly more T cell infiltration in WT mice than in Lrg1 KO mice. Expression of CD11b showed no differences in WT and Lrg1 KO mice with or without colitis. However, the expression increase of CD11b was significantly greater in WT mice than in Lrg1 KO mice. A possible explanation could be the expression of Lrg1 on subsets of myeloid cells, as described by Kumagai et al. who located Lrg1 expression on heart-infiltrating myeloid cells as well.[189]

Further, an indirect effect of the lack of Lrg1 may be considered. Endoglin is a TGF-β co-receptor that is essential for the activation of TGF-β signaling triggered by the binding of Lrg1 to both, TβRII and endoglin.[77] Besides the role in angiogenesis, endoglin is described to be important for the regulation of macrophage infiltration.[190] The lack of Lrg1 as endoglin activator may led to reduced macrophage infiltration in Lrg1 KO mice during colitis.

Similar to the development of CD11b expression, we detected an increased rise in CD31 expression under inflammatory conditions in WT mice compared to Lrg1 KO mice. This is in line with previous data about increased angiogenesis during colitis.[187] We assume that the lack of Lrg1 diminishes pathologic angiogenesis by the decreased activation of proangiogenic TGF-β signaling. Regarding further endothelial-associated marker that display vessel constitution we found no differences in the expression of adherens junctions (ZO-1), smooth muscle cells (αSma) or pericytes (NG2). As endothelial leakiness and the decrease of ZO-1 were already described in colitis[191-193], we need to verify those results by further investigation.

4.2.4 The role of Lrg1 in paw edema

In rheumatoid arthritis, pathologic angiogenesis is triggered by leukocytes at the site of hypertrophic joints for the sufficient supply of oxygen and nutrients.[194,195] To avoid the complex interplay of processes happening in the autoimmune disease rheumatoid arthritis, we decided to investigate the role of Lrg1 in a simpler model of local inflammation, namely the paw edema model. The carrageenan-induced paw edema model is widely used to assess the response to anti-inflammatory treatments like the use of nonsteroidal anti-inflammatory drugs (NSAIDs).[117,196,197]

Our data of paw edema experiments using Lrg1 KO mice and WT littermates, show a clear reduction of inflammation-associated footpad thickness in Lrg1 KO mice. These results are in line with the description of the biphasic development of carrageenan-induced inflammation. Posadas et al. describe that the first phase of inflammatory response ends 6h after carrageenan-injection with a peak of footpad swelling around 4h after injection.[131] This is in correlation to our results as we saw significantly less footpad swelling in Lrg1 KO mice after 2-4h but not after 6h. We had the impression that footpad swelling reached a plateau 3h after carrageenan-injection and further that the degree of footpad swelling in Lrg1 KO mice reached similar levels as in WT mice, but the swelling process occurred slower.

Checking the vessel density in footpads of WT and Lrg1 KO mice we saw no difference. We assume that the investigated time point of 3h post injection was too early to detect angiogenesis. In previous experiments our group could prove that angiogenesis can be detected already at day +2 post allo-HSCT, which is in advance of leukocyte infiltration into target organs.[108]

An evident explanation causing footpad swelling is an increase of extravascular fluid. To confirm that, we tested for the occurrence of vessel leakiness in Lrg1 KO mice and WT littermates after carrageenan injection. Vessel leakiness of footpads from WT mice was significantly higher than the vessel leakiness in Lrg1 KO mice, indicating a central role of Lrg1 in the formation of vascular permeability. In contrast to the histologic assessment we performed on colon samples from Lrg1 KO mice and WT littermates during colitis, the increased vascular permeability during paw edema

is in accordance with recent studies that describe an inhibitory role for Lrg1 on pericyte recruitment.[198-200]

Further, Avalos et al. found that Lrg1 is stored in secondary granules of human neutrophils. After the release of myeloperoxidase (MPO) from primary granules, Lrg1 is co-released with lactoferrin.[180] Lactoferrin levels in the serum of our allo-transplanted mice were upregulated as well,[108] suggesting a simultaneous upregulation of Lrg1. Queiroz et al. discovered a correlation between MPO protein levels in rat paws and the levels of plasma exudation.[201] As MPO and Lrg1 are both released by neutrophils, which are the first responders of the immune system, the increased exudation could be mediated by Lrg1.

Another fact that may has influenced the reduction of footpad swelling in Lrg1 KO mice in connection with neutrophils is stated by Druhan et al.. They ascertained that Lrg1 released from neutrophils binds to cytochrome c, which is involved in the initiation of arthritis via the NF-κB pathway.[180,202] The lack of Lrg1 may have diminished the activation of the NFκB pathway leading to reduced activation of leukocytes. This possibility may be less important in our paw edema model, as we did not see immune cell infiltration 3h after the induction of inflammation.

To sum up, our results indicate that Lrg1 has a negative impact on the development of experimental aGVHD, colitis and paw edema. The loss of Lrg1 resulted in specific reduction of pathologic angiogenesis under inflammatory conditions, suggesting that the inhibition of Lrg1 may inhibit pathologic angiogenesis in various inflammatory diseases and cancer. Besides the most prominent function of Lrg1 to trigger pathologic angiogenesis via TGF-β signaling, we discovered a significant impact of Lrg1 on leakiness. Considering that various diseases, including sepsis, are associated to vessel leakiness, the therapeutic blocking of Lrg1 may be useful for a wide range of indications.

4.2.5 Outlook

We identified the glycoprotein Lrg1 as new possible target for the inhibition of pathologic angiogenesis without affecting physiologic angiogenesis.

The results we gained from preclinical experiments using Lrg1 knockout mice, need to be verified in the clinical situation. Therefore, we will use blood samples collected routinely before allo-HSCT and weekly after allo-HSCT to evaluate serum levels of Lrg1 and correlate them to the occurrence and severity of aGVHD. In parallel, we will examine mechanisms and pathways that are involved in Lrg1 signaling in our murine inflammation models. We will also test serum samples of our inflammatory mouse models for levels of Lrg1 as well as their cytokine profile.

Another approach is to specifically knock out Lrg1 in endothelial cells using the CRISPR/Cas9 system. Lrg1 KO ECs will be used for *in vitro* analyses on endothelial-specific functions (tube

formation, migration, proliferation) and we will analyze the effect on cytoskeleton and metabolic changes.

The planned experiments may help us to get a more complete picture of the mechanisms involved in Lrg1-induced pathological angiogenesis and possibly reveal further functions of Lrg1.

5 References

1. Hatzimichael E, Tuthill M. Hematopoietic stem cell transplantation. *Stem Cells Cloning*. 2010;3:105-117.
2. Simpson E, Dazzi F. Bone Marrow Transplantation 1957-2019. *Front Immunol*. 2019;10:1246.
3. https://www.uptodate.com/contents/preparative-regimens-for-hematopoietic-cell-transplantation; January, 2020.
4. Gyurkocza B, Sandmaier BM. Conditioning regimens for hematopoietic cell transplantation: one size does not fit all. *Blood*. 2014;124(3):344-353.
5. Cheuk DK. Optimal stem cell source for allogeneic stem cell transplantation for hematological malignancies. *World J Transplant*. 2013;3(4):99-112.
6. Passweg JR, Baldomero H, Basak GW, et al. The EBMT activity survey report 2017: a focus on allogeneic HCT for nonmalignant indications and on the use of non-HCT cell therapies. *Bone Marrow Transplant*. 2019;54(10):1575-1585.
7. Ball LM, Egeler RM, Party EPW. Acute GvHD: pathogenesis and classification. *Bone Marrow Transplant*. 2008;41 Suppl 2:S58-64.
8. Mackall C, Fry T, Gress R, et al. Background to hematopoietic cell transplantation, including post transplant immune recovery. *Bone Marrow Transplant*. 2009;44(8):457-462.
9. Sahin U, Toprak SK, Atilla PA, Atilla E, Demirer T. An overview of infectious complications after allogeneic hematopoietic stem cell transplantation. *J Infect Chemother*. 2016;22(8):505-514.
10. Cho SY, Lee HJ, Lee DG. Infectious complications after hematopoietic stem cell transplantation: current status and future perspectives in Korea. *Korean J Intern Med*. 2018;33(2):256-276.
11. Kontoyiannis DP. Infections following allogeneic stem cell transplantation: New concepts, improved insights, and renewed hope for better outcomes. *Virulence*. 2016;7(8):898-900.
12. Ogonek J, Kralj Juric M, Ghimire S, et al. Immune Reconstitution after Allogeneic Hematopoietic Stem Cell Transplantation. *Front Immunol*. 2016;7:507.
13. Tomblyn M, Chiller T, Einsele H, et al. Guidelines for preventing infectious complications among hematopoietic cell transplantation recipients: a global perspective. *Biol Blood Marrow Transplant*. 2009;15(10):1143-1238.
14. Cheuk DK. Hepatic veno-occlusive disease after hematopoietic stem cell transplantation: Prophylaxis and treatment controversies. *World J Transplant*. 2012;2(2):27-34.
15. Trajkovska I, Georgievski B, Cevreska L, Gacovski A, Hasan T, Nedeska-Minova N. Early and Late Complications in Patients with Allogeneic Transplantation of Hematopoietic Stem Cell - Case Report. *Open Access Maced J Med Sci*. 2017;5(3):340-343.
16. Pagliuca S, Michonneau D, Sicre de Fontbrune F, et al. Allogeneic reactivity-mediated endothelial cell complications after HSCT: a plea for consensual definitions. *Blood Adv*. 2019;3(15):2424-2435.
17. Min CK. The pathophysiology of chronic graft-versus-host disease: the unveiling of an enigma. *Korean J Hematol*. 2011;46(2):80-87.
18. Espinoza JL, Wadasaki Y, Takami A. Infection Complications in Hematopoietic Stem Cells Transplant Recipients: Do Genetics Really Matter? *Front Microbiol*. 2018;9:2317.
19. Talekar MKO, Timothy. Immune Reconstitution After Hematopoietic Stem Cell Transplantation. *Hematopoietic Stem Cell Transplantation for the Pediatric Hematologist/Oncologist*. 2017:pp 371-383.
20. Danby R, Rocha V. Improving engraftment and immune reconstitution in umbilical cord blood transplantation. *Front Immunol*. 2014;5:68.
21. Jacobsohn DA, Vogelsang GB. Acute graft versus host disease. *Orphanet J Rare Dis*. 2007;2:35.
22. Ferrara JL, Levine JE, Reddy P, Holler E. Graft-versus-host disease. *Lancet*. 2009;373(9674):1550-1561.
23. Murray J, Stringer J, Hutt D. Graft-Versus-Host Disease (GvHD). In: Kenyon M, Babic A, eds. The European Blood and Marrow Transplantation Textbook for Nurses: Under the Auspices of EBMT. Cham (CH); 2018:221-251.
24. Strong Rodrigues K, Oliveira-Ribeiro C, de Abreu Fiuza Gomes S, Knobler R. Cutaneous Graft-Versus-Host Disease: Diagnosis and Treatment. *Am J Clin Dermatol*. 2018;19(1):33-50.

25. Naymagon S, Naymagon L, Wong SY, et al. Acute graft-versus-host disease of the gut: considerations for the gastroenterologist. *Nat Rev Gastroenterol Hepatol*. 2017;14(12):711-726.
26. Matsukuma KE, Wei D, Sun K, Ramsamooj R, Chen M. Diagnosis and differential diagnosis of hepatic graft versus host disease (GVHD). *J Gastrointest Oncol*. 2016;7(Suppl 1):S21-31.
27. Baron F, Labopin M, Niederwieser D, et al. Impact of graft-versus-host disease after reduced-intensity conditioning allogeneic stem cell transplantation for acute myeloid leukemia: a report from the Acute Leukemia Working Party of the European group for blood and marrow transplantation. *Leukemia*. 2012;26(12):2462-2468.
28. Janeway CA Jr TP, Walport M, et al. The major histocompatibility complex and its functions. *Immunobiology: The Immune System in Health and Disease 5th edition*. 2001.
29. Xie M, Li J, Jiang T. Accurate HLA type inference using a weighted similarity graph. *BMC Bioinformatics*. 2010;11 Suppl 11:S10.
30. Nowak J. Role of HLA in hematopoietic SCT. *Bone Marrow Transplant*. 2008;42 Suppl 2:S71-76.
31. Tiercy JM. How to select the best available related or unrelated donor of hematopoietic stem cells? *Haematologica*. 2016;101(6):680-687.
32. Tiercy JM, Nicoloso G, Passweg J, et al. The probability of identifying a 10/10 HLA allele-matched unrelated donor is highly predictable. *Bone Marrow Transplant*. 2007;40(6):515-522.
33. Shlomchik WD. Graft-versus-host disease. *Nat Rev Immunol*. 2007;7(5):340-352.
34. Cruz-Tapias P CJ, Anaya JM. Major histocompatibility complex: Antigen processing and presentation. In: Anaya JM, Shoenfeld Y, Rojas-Villarraga A, et al., editors. Autoimmunity from bench to bedside. Vol. Chapter 10. Bogota: El Rosario University Press; 2013.
35. Thorsby E. A short history of HLA. *Tissue Antigens*. 2009;74(2):101-116.
36. Nardo G, Trolese MC, Bendotti C. Major Histocompatibility Complex I Expression by Motor Neurons and Its Implication in Amyotrophic Lateral Sclerosis. *Front Neurol*. 2016;7:89.
37. Zeiser R, Socie G, Blazar BR. Pathogenesis of acute graft-versus-host disease: from intestinal microbiota alterations to donor T cell activation. *Br J Haematol*. 2016;175(2):191-207.
38. Oostvogels R, Lokhorst HM, Mutis T. Minor histocompatibility Ags: identification strategies, clinical results and translational perspectives. *Bone Marrow Transplant*. 2016;51(2):163-171.
39. Zeiser R, Blazar BR. Acute Graft-versus-Host Disease - Biologic Process, Prevention, and Therapy. *N Engl J Med*. 2017;377(22):2167-2179.
40. Choi SW, Levine JE, Ferrara JL. Pathogenesis and management of graft-versus-host disease. *Immunol Allergy Clin North Am*. 2010;30(1):75-101.
41. Pasquini MC. Impact of graft-versus-host disease on survival. *Best Pract Res Clin Haematol*. 2008;21(2):193-204.
42. Reddy P, Arora M, Guimond M, Mackall CL. GVHD: a continuing barrier to the safety of allogeneic transplantation. *Biol Blood Marrow Transplant*. 2009;15(1 Suppl):162-168.
43. Reddy P, Ferrara JLM. Mouse models of graft-versus-host disease. StemBook. Cambridge (MA); 2008.
44. Zeiser R. Advances in understanding the pathogenesis of graft-versus-host disease. *Br J Haematol*. 2019;187(5):563-572.
45. Ghimire S, Weber D, Mavin E, Wang XN, Dickinson AM, Holler E. Pathophysiology of GvHD and Other HSCT-Related Major Complications. *Front Immunol*. 2017;8:79.
46. Blazar BR, Murphy WJ, Abedi M. Advances in graft-versus-host disease biology and therapy. *Nat Rev Immunol*. 2012;12(6):443-458.
47. Jaksch M, Mattsson J. The pathophysiology of acute graft-versus-host disease. *Scand J Immunol*. 2005;61(5):398-409.
48. Ram R, Storb R. Pharmacologic prophylaxis regimens for acute graft-versus-host disease: past, present and future. *Leuk Lymphoma*. 2013;54(8):1591-1601.
49. https://www.dag-kbt.de/files/downloads/Leitlinien_Kap-09_GvHD-Prophylaxe und Therapie.pdf. *January, 2020*.
50. Ruutu T, Gratwohl A, de Witte T, et al. Prophylaxis and treatment of GVHD: EBMT-ELN working group recommendations for a standardized practice. *Bone Marrow Transplant*. 2014;49(2):168-173.

51. Penack O, Marchetti M, Ruutu T, et al. Prophylaxis and management of graft versus host disease after stem-cell transplantation for haematological malignancies: updated consensus recommendations of the European Society for Blood and Marrow Transplantation. *Lancet Haematol*. 2020;7(2):e157-e167.
52. Nassar A, Elgohary G, Elhassan T, Nurgat Z, Mohamed SY, Aljurf M. Methotrexate for the Treatment of Graft-versus-Host Disease after Allogeneic Hematopoietic Stem Cell Transplantation. *J Transplant*. 2014;2014:980301.
53. Pinana JL, Valcarcel D, Fernandez-Aviles F, et al. MTX or mycophenolate mofetil with CsA as GVHD prophylaxis after reduced-intensity conditioning PBSCT from HLA-identical siblings. *Bone Marrow Transplant*. 2010;45(9):1449-1456.
54. Bryant AR, Perales MA. Advances in Ex Vivo T Cell Depletion - Where Do We Stand? *Adv Cell Gene Ther*. 2019;2(1).
55. Saad A, Lamb LS. Ex vivo T-cell depletion in allogeneic hematopoietic stem cell transplant: past, present and future. *Bone Marrow Transplant*. 2017;52(9):1241-1248.
56. Mohty M. Mechanisms of action of antithymocyte globulin: T-cell depletion and beyond. *Leukemia*. 2007;21(7):1387-1394.
57. Kekre N, Antin JH. ATG in allogeneic stem cell transplantation: standard of care in 2017? Counterpoint. *Blood Adv*. 2017;1(9):573-576.
58. Deeg HJ. How I treat refractory acute GVHD. *Blood*. 2007;109(10):4119-4126.
59. Nassereddine S, Rafei H, Elbahesh E, Tabbara I. Acute Graft Versus Host Disease: A Comprehensive Review. *Anticancer Res*. 2017;37(4):1547-1555.
60. Cesen Mazic M, Girandon L, Knezevic M, Avcin SL, Jazbec J. Treatment of Severe Steroid-Refractory Acute-Graft-vs.-Host Disease With Mesenchymal Stem Cells-Single Center Experience. *Front Bioeng Biotechnol*. 2018;6:93.
61. Hill L, Alousi A, Kebriaei P, Mehta R, Rezvani K, Shpall E. New and emerging therapies for acute and chronic graft versus host disease. *Ther Adv Hematol*. 2018;9(1):21-46.
62. Bader P, Kuci Z, Bakhtiar S, et al. Effective treatment of steroid and therapy-refractory acute graft-versus-host disease with a novel mesenchymal stromal cell product (MSC-FFM). *Bone Marrow Transplant*. 2018;53(7):852-862.
63. Aguilar-Cazares D, Chavez-Dominguez R, Carlos-Reyes A, Lopez-Camarillo C, Hernadez de la Cruz ON, Lopez-Gonzalez JS. Contribution of Angiogenesis to Inflammation and Cancer. *Front Oncol*. 2019;9:1399.
64. Chen L, Deng H, Cui H, et al. Inflammatory responses and inflammation-associated diseases in organs. *Oncotarget*. 2018;9(6):7204-7218.
65. Szade A, Grochot-Przeczek A, Florczyk U, Jozkowicz A, Dulak J. Cellular and molecular mechanisms of inflammation-induced angiogenesis. *IUBMB Life*. 2015;67(3):145-159.
66. Tas SW, Maracle CX, Balogh E, Szekanecz Z. Targeting of proangiogenic signalling pathways in chronic inflammation. *Nat Rev Rheumatol*. 2016;12(2):111-122.
67. Adams RH, Alitalo K. Molecular regulation of angiogenesis and lymphangiogenesis. *Nat Rev Mol Cell Biol*. 2007;8(6):464-478.
68. Bautch VL, Caron KM. Blood and lymphatic vessel formation. *Cold Spring Harb Perspect Biol*. 2015;7(3):a008268.
69. Kolte DM, John Arthur; Aronow, Wilbert S. Vasculogenesis and Angiogenesis. *Translational Research in Coronary Artery Disease*. 2016:49-65.
70. Carmeliet P, Jain RK. Molecular mechanisms and clinical applications of angiogenesis. *Nature*. 2011;473(7347):298-307.
71. Carmeliet P, De Smet F, Loges S, Mazzone M. Branching morphogenesis and antiangiogenesis candidates: tip cells lead the way. *Nat Rev Clin Oncol*. 2009;6(6):315-326.
72. Jakobsson L, Franco CA, Bentley K, et al. Endothelial cells dynamically compete for the tip cell position during angiogenic sprouting. *Nat Cell Biol*. 2010;12(10):943-953.
73. Goumans MJ, Liu Z, ten Dijke P. TGF-beta signaling in vascular biology and dysfunction. *Cell Res*. 2009;19(1):116-127.

74. Aykul S, Martinez-Hackert E. Transforming Growth Factor-beta Family Ligands Can Function as Antagonists by Competing for Type II Receptor Binding. *J Biol Chem*. 2016;291(20):10792-10804.
75. van Meeteren LA, ten Dijke P. Regulation of endothelial cell plasticity by TGF-beta. *Cell Tissue Res*. 2012;347(1):177-186.
76. Goumans MJ, Valdimarsdottir G, Itoh S, Rosendahl A, Sideras P, ten Dijke P. Balancing the activation state of the endothelium via two distinct TGF-beta type I receptors. *EMBO J*. 2002;21(7):1743-1753.
77. Wang X, Abraham S, McKenzie JA, et al. LRG1 promotes angiogenesis by modulating endothelial TGF-beta signalling. *Nature*. 2013;499(7458):306-311.
78. Serada S, Fujimoto M, Terabe F, et al. Serum leucine-rich alpha-2 glycoprotein is a disease activity biomarker in ulcerative colitis. *Inflamm Bowel Dis*. 2012;18(11):2169-2179.
79. Fujimoto M, Serada S, Suzuki K, et al. Leucine-rich alpha2 -glycoprotein as a potential biomarker for joint inflammation during anti-interleukin-6 biologic therapy in rheumatoid arthritis. *Arthritis Rheumatol*. 2015;67(8):2056-2060.
80. Rainer TH, Leung LY, Chan C, et al. Circulating human leucine-rich alpha-2-glycoprotein 1 mRNA and protein levels to detect acute appendicitis in patients with acute abdominal pain. *Clin Biochem*. 2017;50(9):485-490.
81. Andersen JD, Boylan KL, Jemmerson R, et al. Leucine-rich alpha-2-glycoprotein-1 is upregulated in sera and tumors of ovarian cancer patients. *J Ovarian Res*. 2010;3:21.
82. Zhou Y, Zhang X, Zhang J, Fang J, Ge Z, Li X. LRG1 promotes proliferation and inhibits apoptosis in colorectal cancer cells via RUNX1 activation. *PLoS One*. 2017;12(4):e0175122.
83. Xie ZB, Zhang YF, Jin C, Mao YS, Fu DL. LRG-1 promotes pancreatic cancer growth and metastasis via modulation of the EGFR/p38 signaling. *J Exp Clin Cancer Res*. 2019;38(1):75.
84. Stacker SA, Williams SP, Karnezis T, Shayan R, Fox SB, Achen MG. Lymphangiogenesis and lymphatic vessel remodelling in cancer. *Nat Rev Cancer*. 2014;14(3):159-172.
85. Jiang X, Nicolls MR, Tian W, Rockson SG. Lymphatic Dysfunction, Leukotrienes, and Lymphedema. *Annu Rev Physiol*. 2018;80:49-70.
86. Kesler CT, Liao S, Munn LL, Padera TP. Lymphatic vessels in health and disease. *Wiley Interdiscip Rev Syst Biol Med*. 2013;5(1):111-124.
87. Tammela T, Alitalo K. Lymphangiogenesis: Molecular mechanisms and future promise. *Cell*. 2010;140(4):460-476.
88. Alitalo K. The lymphatic vasculature in disease. *Nat Med*. 2011;17(11):1371-1380.
89. Hsu MC, Pan MR, Hung WC. Two Birds, One Stone: Double Hits on Tumor Growth and Lymphangiogenesis by Targeting Vascular Endothelial Growth Factor Receptor 3. *Cells*. 2019;8(3).
90. Zheng W, Aspelund A, Alitalo K. Lymphangiogenic factors, mechanisms, and applications. *J Clin Invest*. 2014;124(3):878-887.
91. Schwager S, Detmar M. Inflammation and Lymphatic Function. *Front Immunol*. 2019;10:308.
92. Kim H, Kataru RP, Koh GY. Inflammation-associated lymphangiogenesis: a double-edged sword? *J Clin Invest*. 2014;124(3):936-942.
93. D'Alessio S, Correale C, Tacconi C, et al. VEGF-C-dependent stimulation of lymphatic function ameliorates experimental inflammatory bowel disease. *J Clin Invest*. 2014;124(9):3863-3878.
94. Dietrich T, Bock F, Yuen D, et al. Cutting edge: lymphatic vessels, not blood vessels, primarily mediate immune rejections after transplantation. *J Immunol*. 2010;184(2):535-539.
95. Krebs R, Tikkanen JM, Ropponen JO, et al. Critical role of VEGF-C/VEGFR-3 signaling in innate and adaptive immune responses in experimental obliterative bronchiolitis. *Am J Pathol*. 2012;181(5):1607-1620.
96. Nykanen AI, Sandelin H, Krebs R, et al. Targeting lymphatic vessel activation and CCL21 production by vascular endothelial growth factor receptor-3 inhibition has novel immunomodulatory and antiarteriosclerotic effects in cardiac allografts. *Circulation*. 2010;121(12):1413-1422.
97. Tang XL, Sun JF, Wang XY, Du LL, Liu P. Blocking neuropilin-2 enhances corneal allograft survival by selectively inhibiting lymphangiogenesis on vascularized beds. *Mol Vis*. 2010;16:2354-2361.

98. Yan H, Yuan J, Peng R, et al. The Blockade of Vascular Endothelial Growth Factor C Effectively Inhibits Corneal Lymphangiogenesis and Promotes Allograft Survival. *J Ocul Pharmacol Ther*. 2015;31(9):546-554.
99. Yin N, Zhang N, Xu J, Shi Q, Ding Y, Bromberg JS. Targeting lymphangiogenesis after islet transplantation prolongs islet allograft survival. *Transplantation*. 2011;92(1):25-30.
100. Folkman J. Tumor angiogenesis: therapeutic implications. *N Engl J Med*. 1971;285(21):1182-1186.
101. Medinger M, Tichelli A, Bucher C, et al. GVHD after allogeneic haematopoietic SCT for AML: angiogenesis, vascular endothelial growth factor and VEGF receptor expression in the BM. *Bone Marrow Transplant*. 2013;48(5):715-721.
102. Penack O. The endothelium in graft-versus-host disease and graft-versus-leukemia. *Immune Biology of Allogeneic Hematopoietic Stem Cell Transplantation - Models in Discovery and Translation*. 2013(Chaptor 20):479-492.
103. Leonhardt F, Grundmann S, Behe M, et al. Inflammatory neovascularization during graft-versus-host disease is regulated by alphav integrin and miR-100. *Blood*. 2013;121(17):3307-3318.
104. Luft T, Dietrich S, Falk C, et al. Steroid-refractory GVHD: T-cell attack within a vulnerable endothelial system. *Blood*. 2011;118(6):1685-1692.
105. Mir E, Palomo M, Rovira M, et al. Endothelial damage is aggravated in acute GvHD and could predict its development. *Bone Marrow Transplant*. 2017;52(9):1317-1325.
106. Carreras E, Diaz-Ricart M. The role of the endothelium in the short-term complications of hematopoietic SCT. *Bone Marrow Transplant*. 2011;46(12):1495-1502.
107. Penack O, Holtan S. The Endothelium During Allogeneic Stem Cell Transplantation. *Immune Biology of Allogeneic Hematopoietic Stem Cell Transplantation (Second Edition) Models in Discovery and Translation*. 2019;Chapter 21:401-414.
108. Riesner K, Shi Y, Jacobi A, et al. Initiation of acute graft-versus-host disease by angiogenesis. *Blood*. 2017;129(14):2021-2032.
109. Lazaryan A, Weisdorf DJ, DeFor T, et al. Risk Factors for Acute and Chronic Graft-versus-Host Disease after Allogeneic Hematopoietic Cell Transplantation with Umbilical Cord Blood and Matched Sibling Donors. *Biol Blood Marrow Transplant*. 2016;22(1):134-140.
110. Cooke KR, Kobzik L, Martin TR, et al. An experimental model of idiopathic pneumonia syndrome after bone marrow transplantation: I. The roles of minor H antigens and endotoxin. *Blood*. 1996;88(8):3230-3239.
111. Lerner KG, Kao GF, Storb R, Buckner CD, Clift RA, Thomas ED. Histopathology of graft-vs.-host reaction (GvHR) in human recipients of marrow from HL-A-matched sibling donors. *Transplant Proc*. 1974;6(4):367-371.
112. Batra A, Heimesaat MM, Bereswill S, et al. Mesenteric fat - control site for bacterial translocation in colitis? *Mucosal Immunol*. 2012;5(5):580-591.
113. Byrnes JJ, Gross S, Ellard C, Connolly K, Donahue S, Picarella D. Effects of the ACE2 inhibitor GL1001 on acute dextran sodium sulfate-induced colitis in mice. *Inflamm Res*. 2009;58(11):819-827.
114. Kim JJ, Shajib MS, Manocha MM, Khan WI. Investigating intestinal inflammation in DSS-induced model of IBD. *J Vis Exp*. 2012(60).
115. Park YH, Kim N, Shim YK, et al. Adequate Dextran Sodium Sulfate-induced Colitis Model in Mice and Effective Outcome Measurement Method. *J Cancer Prev*. 2015;20(4):260-267.
116. Erben U, Loddenkemper C, Doerfel K, et al. A guide to histomorphological evaluation of intestinal inflammation in mouse models. *Int J Clin Exp Pathol*. 2014;7(8):4557-4576.
117. Fehrenbacher JC, Vasko MR, Duarte DB. Models of inflammation: Carrageenan- or complete Freund's Adjuvant (CFA)-induced edema and hypersensitivity in the rat. *Curr Protoc Pharmacol*. 2012;Chapter 5:Unit5 4.
118. Rappsilber J, Mann M, Ishihama Y. Protocol for micro-purification, enrichment, pre-fractionation and storage of peptides for proteomics using StageTips. *Nat Protoc*. 2007;2(8):1896-1906.
119. Cox J, Mann M. MaxQuant enables high peptide identification rates, individualized p.p.b.-range mass accuracies and proteome-wide protein quantification. *Nat Biotechnol*. 2008;26(12):1367-1372.

120. Boersema PJ, Raijmakers R, Lemeer S, Mohammed S, Heck AJ. Multiplex peptide stable isotope dimethyl labeling for quantitative proteomics. *Nat Protoc*. 2009;4(4):484-494.
121. Mertlitz S, Shi Y, Kalupa M, et al. Lymphangiogenesis is a feature of acute GVHD, and VEGFR-3 inhibition protects against experimental GVHD. *Blood*. 2017;129(13):1865-1875.
122. Mouta Carreira C, Nasser SM, di Tomaso E, et al. LYVE-1 is not restricted to the lymph vessels: expression in normal liver blood sinusoids and down-regulation in human liver cancer and cirrhosis. *Cancer Res.* 2001;61(22):8079-8084.
123. Chung C, Iwakiri Y. The lymphatic vascular system in liver diseases: its role in ascites formation. *Clin Mol Hepatol*. 2013;19(2):99-104.
124. Kumar V, Dasoveanu DC, Chyou S, et al. A dendritic-cell-stromal axis maintains immune responses in lymph nodes. *Immunity*. 2015;42(4):719-730.
125. Rosen SD, Tsay D, Singer MS, Hemmerich S, Abraham WM. Therapeutic targeting of endothelial ligands for L-selectin (PNAd) in a sheep model of asthma. *Am J Pathol*. 2005;166(3):935-944.
126. Bock F, Onderka J, Dietrich T, Bachmann B, Pytowski B, Cursiefen C. Blockade of VEGFR3-signalling specifically inhibits lymphangiogenesis in inflammatory corneal neovascularisation. *Graefes Arch Clin Exp Ophthalmol*. 2008;246(1):115-119.
127. Pytowski B, Goldman J, Persaud K, et al. Complete and specific inhibition of adult lymphatic regeneration by a novel VEGFR-3 neutralizing antibody. *J Natl Cancer Inst*. 2005;97(1):14-21.
128. Riesner K, Kalupa M, Shi Y, Elezkurtaj S, Penack O. A preclinical acute GVHD mouse model based on chemotherapy conditioning and MHC-matched transplantation. *Bone Marrow Transplant*. 2016;51(3):410-417.
129. Penack O, Henke E, Suh D, et al. Inhibition of neovascularization to simultaneously ameliorate graft-vs-host disease and decrease tumor growth. *J Natl Cancer Inst*. 2010;102(12):894-908.
130. Szyska M, Na IK. Bone Marrow GvHD after Allogeneic Hematopoietic Stem Cell Transplantation. *Front Immunol*. 2016;7:118.
131. Posadas I, Bucci M, Roviezzo F, et al. Carrageenan-induced mouse paw oedema is biphasic, age-weight dependent and displays differential nitric oxide cyclooxygenase-2 expression. *Br J Pharmacol*. 2004;142(2):331-338.
132. Szabo C, Lim LH, Cuzzocrea S, et al. Inhibition of poly (ADP-ribose) synthetase attenuates neutrophil recruitment and exerts antiinflammatory effects. *J Exp Med*. 1997;186(7):1041-1049.
133. Radu M, Chernoff J. An in vivo assay to test blood vessel permeability. *J Vis Exp*. 2013(73):e50062.
134. Li Y, Ge Y, Gong J, et al. Mesenteric Lymphatic Vessel Density Is Associated with Disease Behavior and Postoperative Recurrence in Crohn's Disease. *J Gastrointest Surg*. 2018;22(12):2125-2132.
135. Bouta EM, Li J, Ju Y, et al. The role of the lymphatic system in inflammatory-erosive arthritis. *Semin Cell Dev Biol*. 2015;38:90-97.
136. Huggenberger R, Ullmann S, Proulx ST, Pytowski B, Alitalo K, Detmar M. Stimulation of lymphangiogenesis via VEGFR-3 inhibits chronic skin inflammation. *J Exp Med*. 2010;207(10):2255-2269.
137. Moustou AE, Alexandrou P, Stratigos AJ, et al. Expression of lymphatic markers and lymphatic growth factors in psoriasis before and after anti-TNF treatment. *An Bras Dermatol*. 2014;89(6):891-897.
138. Zhang SQ, Yu H, Zhang LL. Clinical implications of increased lymph vessel density in the lymphatic metastasis of early-stage invasive cervical carcinoma: a clinical immunohistochemical method study. *BMC Cancer*. 2009;9:64.
139. Su JL, Shih JY, Yen ML, et al. Cyclooxygenase-2 induces EP1- and HER-2/Neu-dependent vascular endothelial growth factor-C up-regulation: a novel mechanism of lymphangiogenesis in lung adenocarcinoma. *Cancer Res*. 2004;64(2):554-564.
140. Vetrano S, Borroni EM, Sarukhan A, et al. The lymphatic system controls intestinal inflammation and inflammation-associated Colon Cancer through the chemokine decoy receptor D6. *Gut*. 2010;59(2):197-206.

141. Kerjaschki D, Huttary N, Raab I, et al. Lymphatic endothelial progenitor cells contribute to de novo lymphangiogenesis in human renal transplants. *Nat Med*. 2006;12(2):230-234.
142. Hautz T, Zelger BG, Nasr IW, et al. Lymphoid neogenesis in skin of human hand, nonhuman primate, and rat vascularized composite allografts. *Transpl Int*. 2014;27(9):966-976.
143. Dashkevich A, Heilmann C, Kayser G, et al. Lymph angiogenesis after lung transplantation and relation to acute organ rejection in humans. *Ann Thorac Surg*. 2010;90(2):406-411.
144. Nalle SC, Turner JR. Intestinal barrier loss as a critical pathogenic link between inflammatory bowel disease and graft-versus-host disease. *Mucosal Immunol*. 2015;8(4):720-730.
145. Rahier JF, De Beauce S, Dubuquoy L, et al. Increased lymphatic vessel density and lymphangiogenesis in inflammatory bowel disease. *Aliment Pharmacol Ther*. 2011;34(5):533-543.
146. Ulvmar MH, Makinen T. Heterogeneity in the lymphatic vascular system and its origin. *Cardiovasc Res*. 2016;111(4):310-321.
147. Petrova TV, Koh GY. Organ-specific lymphatic vasculature: From development to pathophysiology. *J Exp Med*. 2018;215(1):35-49.
148. Huggenberger R, Siddiqui SS, Brander D, et al. An important role of lymphatic vessel activation in limiting acute inflammation. *Blood*. 2011;117(17):4667-4678.
149. Guo R, Zhou Q, Proulx ST, et al. Inhibition of lymphangiogenesis and lymphatic drainage via vascular endothelial growth factor receptor 3 blockade increases the severity of inflammation in a mouse model of chronic inflammatory arthritis. *Arthritis Rheum*. 2009;60(9):2666-2676.
150. Mahmoud Al-Kofahi JWY, Alireza Minagar, J. Steven Alexander. Anatomy and roles of lymphatics in inflammatory diseases. *Journal of Clinical and Experimental Neuroimmunology*. 2017;8:4038-4051.
151. Baluk P, Tammela T, Ator E, et al. Pathogenesis of persistent lymphatic vessel hyperplasia in chronic airway inflammation. *J Clin Invest*. 2005;115(2):247-257.
152. Hos D, Schlereth SL, Bock F, Heindl LM, Cursiefen C. Antilymphangiogenic therapy to promote transplant survival and to reduce cancer metastasis: what can we learn from the eye? *Semin Cell Dev Biol*. 2015;38:117-130.
153. Hos D, Dorrie J, Schaft N, et al. Blockade of CCR7 leads to decreased dendritic cell migration to draining lymph nodes and promotes graft survival in low-risk corneal transplantation. *Exp Eye Res*. 2016;146:1-6.
154. Tacconi C, Correale C, Gandelli A, et al. Vascular endothelial growth factor C disrupts the endothelial lymphatic barrier to promote colorectal cancer invasion. *Gastroenterology*. 2015;148(7):1438-1451 e1438.
155. Goldman J, Rutkowski JM, Shields JD, et al. Cooperative and redundant roles of VEGFR-2 and VEGFR-3 signaling in adult lymphangiogenesis. *FASEB J*. 2007;21(4):1003-1012.
156. Hamada K, Oike Y, Takakura N, et al. VEGF-C signaling pathways through VEGFR-2 and VEGFR-3 in vasculoangiogenesis and hematopoiesis. *Blood*. 2000;96(12):3793-3800.
157. Witmer AN, van Blijswijk BC, Dai J, et al. VEGFR-3 in adult angiogenesis. *J Pathol*. 2001;195(4):490-497.
158. Chung ES, Chauhan SK, Jin Y, et al. Contribution of macrophages to angiogenesis induced by vascular endothelial growth factor receptor-3-specific ligands. *Am J Pathol*. 2009;175(5):1984-1992.
159. Hamrah P, Chen L, Zhang Q, Dana MR. Novel expression of vascular endothelial growth factor receptor (VEGFR)-3 and VEGF-C on corneal dendritic cells. *Am J Pathol*. 2003;163(1):57-68.
160. Stenger EO, Turnquist HR, Mapara MY, Thomson AW. Dendritic cells and regulation of graft-versus-host disease and graft-versus-leukemia activity. *Blood*. 2012;119(22):5088-5103.
161. Hooper AT, Butler JM, Nolan DJ, et al. Engraftment and reconstitution of hematopoiesis is dependent on VEGFR2-mediated regeneration of sinusoidal endothelial cells. *Cell Stem Cell*. 2009;4(3):263-274.
162. Ivy SP, Wick JY, Kaufman BM. An overview of small-molecule inhibitors of VEGFR signaling. *Nat Rev Clin Oncol*. 2009;6(10):569-579.
163. Hattori K, Heissig B, Wu Y, et al. Placental growth factor reconstitutes hematopoiesis by recruiting VEGFR1(+) stem cells from bone-marrow microenvironment. *Nat Med*. 2002;8(8):841-849.

164. Shayan R, Achen MG, Stacker SA. Lymphatic vessels in cancer metastasis: bridging the gaps. *Carcinogenesis*. 2006;27(9):1729-1738.
165. Ma Q, Dieterich LC, Ikenberg K, et al. Unexpected contribution of lymphatic vessels to promotion of distant metastatic tumor spread. *Sci Adv*. 2018;4(8):eaat4758.
166. Zgraggen S, Ochsenbein AM, Detmar M. An important role of blood and lymphatic vessels in inflammation and allergy. *J Allergy (Cairo)*. 2013;2013:672381.
167. Alitalo A, Detmar M. Interaction of tumor cells and lymphatic vessels in cancer progression. *Oncogene*. 2012;31(42):4499-4508.
168. Christiansen A, Detmar M. Lymphangiogenesis and cancer. *Genes Cancer*. 2011;2(12):1146-1158.
169. Yoshimatsu Y, Miyazaki H, Watabe T. Roles of signaling and transcriptional networks in pathological lymphangiogenesis. *Adv Drug Deliv Rev*. 2016;99(Pt B):161-171.
170. Skobe M, Hawighorst T, Jackson DG, et al. Induction of tumor lymphangiogenesis by VEGF-C promotes breast cancer metastasis. *Nat Med*. 2001;7(2):192-198.
171. Varney ML, Singh RK. VEGF-C-VEGFR3/Flt4 axis regulates mammary tumor growth and metastasis in an autocrine manner. *Am J Cancer Res*. 2015;5(2):616-628.
172. Americo MG, Marques YM, El Abras Ankha MD, do Prado RF, Carvalho YR. Correlation of intratumoral lymphatic microvessel density, vascular endothelial growth factor C and cell proliferation in salivary gland tumors. *Med Mol Morphol*. 2016.
173. Karpanen T, Egeblad M, Karkkainen MJ, et al. Vascular endothelial growth factor C promotes tumor lymphangiogenesis and intralymphatic tumor growth. *Cancer Res*. 2001;61(5):1786-1790.
174. Lee E, Koskimaki JE, Pandey NB, Popel AS. Inhibition of lymphangiogenesis and angiogenesis in breast tumor xenografts and lymph nodes by a peptide derived from transmembrane protein 45A. *Neoplasia*. 2013;15(2):112-124.
175. Hwang SD, Song JH, Kim Y, et al. Inhibition of lymphatic proliferation by the selective VEGFR-3 inhibitor SAR131675 ameliorates diabetic nephropathy in db/db mice. *Cell Death Dis*. 2019;10(3):219.
176. Alam A, Blanc I, Gueguen-Dorbes G, et al. SAR131675, a potent and selective VEGFR-3-TK inhibitor with antilymphangiogenic, antitumoral, and antimetastatic activities. *Mol Cancer Ther*. 2012;11(8):1637-1649.
177. Zhang J, Zhu L, Fang J, Ge Z, Li X. LRG1 modulates epithelial-mesenchymal transition and angiogenesis in colorectal cancer via HIF-1alpha activation. *J Exp Clin Cancer Res*. 2016;35:29.
178. Gao Y, Zhou J, Xie Z, et al. Mechanical strain promotes skin fibrosis through LRG-1 induction mediated by ELK1 and ERK signalling. *Commun Biol*. 2019;2:359.
179. Wang F, Flanagan J, Su N, et al. RNAscope: a novel in situ RNA analysis platform for formalin-fixed, paraffin-embedded tissues. *J Mol Diagn*. 2012;14(1):22-29.
180. Druhan LJ, Lance A, Li S, et al. Leucine Rich alpha-2 Glycoprotein: A Novel Neutrophil Granule Protein and Modulator of Myelopoiesis. *PLoS One*. 2017;12(1):e0170261.
181. Danese S, Sans M, Spencer DM, et al. Angiogenesis blockade as a new therapeutic approach to experimental colitis. *Gut*. 2007;56(6):855-862.
182. Chidlow JH, Jr., Shukla D, Grisham MB, Kevil CG. Pathogenic angiogenesis in IBD and experimental colitis: new ideas and therapeutic avenues. *Am J Physiol Gastrointest Liver Physiol*. 2007;293(1):G5-G18.
183. Buchanan SG, Gay NJ. Structural and functional diversity in the leucine-rich repeat family of proteins. *Prog Biophys Mol Biol*. 1996;65(1-2):1-44.
184. O'Donnell LC, Druhan LJ, Avalos BR. Molecular characterization and expression analysis of leucine-rich alpha2-glycoprotein, a novel marker of granulocytic differentiation. *J Leukoc Biol*. 2002;72(3):478-485.
185. Shinzaki S, Matsuoka K, Iijima H, et al. Leucine-rich Alpha-2 Glycoprotein is a Serum Biomarker of Mucosal Healing in Ulcerative Colitis. *J Crohns Colitis*. 2017;11(1):84-91.
186. Naka T, Fujimoto M. LRG is a novel inflammatory marker clinically useful for the evaluation of disease activity in rheumatoid arthritis and inflammatory bowel disease. *Immunol Med*. 2018;41(2):62-67.

187. Alkim C, Alkim H, Koksal AR, Boga S, Sen I. Angiogenesis in Inflammatory Bowel Disease. *Int J Inflam*. 2015;2015:970890.
188. Knod JL, Crawford K, Dusing M, Frischer JS. Murine colitis treated with multitargeted tyrosine kinase inhibitors. *J Surg Res*. 2016;200(2):501-507.
189. Kumagai S, Nakayama H, Fujimoto M, et al. Myeloid cell-derived LRG attenuates adverse cardiac remodelling after myocardial infarction. *Cardiovasc Res*. 2016;109(2):272-282.
190. Scharpfenecker M, Floot B, Russell NS, Stewart FA. The TGF-beta co-receptor endoglin regulates macrophage infiltration and cytokine production in the irradiated mouse kidney. *Radiother Oncol*. 2012;105(3):313-320.
191. Cromer WE, Mathis JM, Granger DN, Chaitanya GV, Alexander JS. Role of the endothelium in inflammatory bowel diseases. *World J Gastroenterol*. 2011;17(5):578-593.
192. Deban L, Correale C, Vetrano S, Malesci A, Danese S. Multiple pathogenic roles of microvasculature in inflammatory bowel disease: a Jack of all trades. *Am J Pathol*. 2008;172(6):1457-1466.
193. Langer V, Vivi E, Regensburger D, et al. IFN-gamma drives inflammatory bowel disease pathogenesis through VE-cadherin-directed vascular barrier disruption. *J Clin Invest*. 2019;129(11):4691-4707.
194. Elshabrawy HA, Chen Z, Volin MV, Ravella S, Virupannavar S, Shahrara S. The pathogenic role of angiogenesis in rheumatoid arthritis. *Angiogenesis*. 2015;18(4):433-448.
195. Paleolog EM. Angiogenesis in rheumatoid arthritis. *Arthritis Res*. 2002;4 Suppl 3:S81-90.
196. Cong HH, Khaziakhmetova VN, Zigashina LE. Rat paw oedema modeling and NSAIDs: Timing of effects. *Int J Risk Saf Med*. 2015;27 Suppl 1:S76-77.
197. Amdekar S, Roy P, Singh V, Kumar A, Singh R, Sharma P. Anti-inflammatory activity of lactobacillus on carrageenan-induced paw edema in male wistar rats. *Int J Inflam*. 2012;2012:752015.
198. Sepetis A, O'Connor M, Hoeh A, Gourlaouen M, Moss SE, Greenwood J. LRG1 as a modulator of pericyte-coverage in oxygen-induced retinopathy. *Investigative Ophthalmology & Visual Science*. 2016;57(12).
199. Greenwood J. The pathogenic role of LRG1 in ocular neovascularisation: From discovery to targeted therapy; 2016.
200. John Greenwood MNOC, David Kallenberg et al. Inhibition of LRG1 normalizes tumor vessels and improves efficacy of cancer therapeutics; 2018.
201. Queiroz RF, Jordao AK, Cunha AC, et al. Nitroxides attenuate carrageenan-induced inflammation in rat paws by reducing neutrophil infiltration and the resulting myeloperoxidase-mediated damage. *Free Radic Biol Med*. 2012;53(10):1942-1953.
202. Makarov SS. NF-kappa B in rheumatoid arthritis: a pivotal regulator of inflammation, hyperplasia, and tissue destruction. *Arthritis Res*. 2001;3(4):200-206.

6 Appendix

6.1 Supplementary figures

The following section displays supplementary data for a better understanding and traceability of the described results.

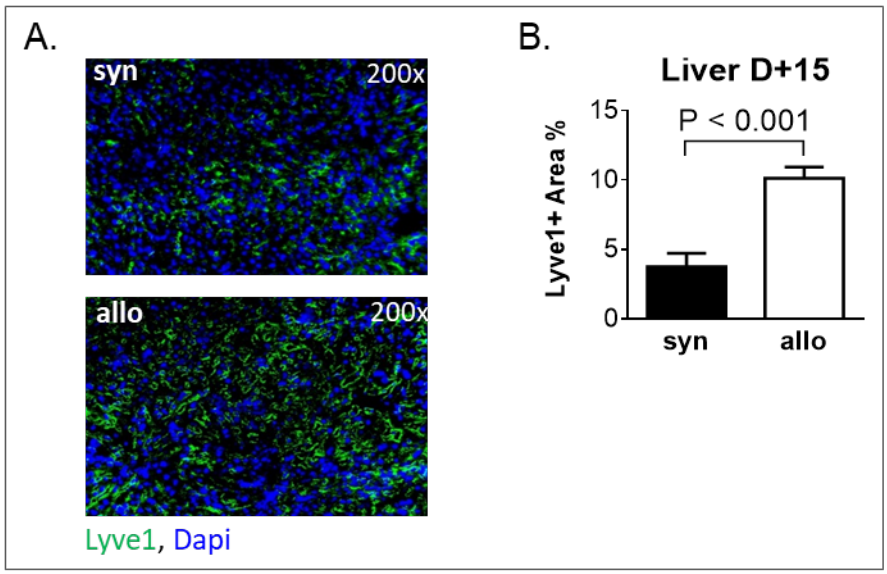

Figure S1. Lyve-1 staining in the liver. (A) Representative images of Lyve-1 staining on liver sections from syngeneic and allogeneic transplanted animals on day 15 post HSCT. Liver sections were stained against Lyve-1, counterstained with the nuclear stain DAPI. (B) Quantification of vessel density in liver sections from syn and allo transplanted animals on day 15 post HSCT. (n=6 per group); error bars indicate mean ± SEM, significance tested by unpaired Student´s t-test, $p<0.05$ *, $p<0.01$ **, $p<0.001$ ***.

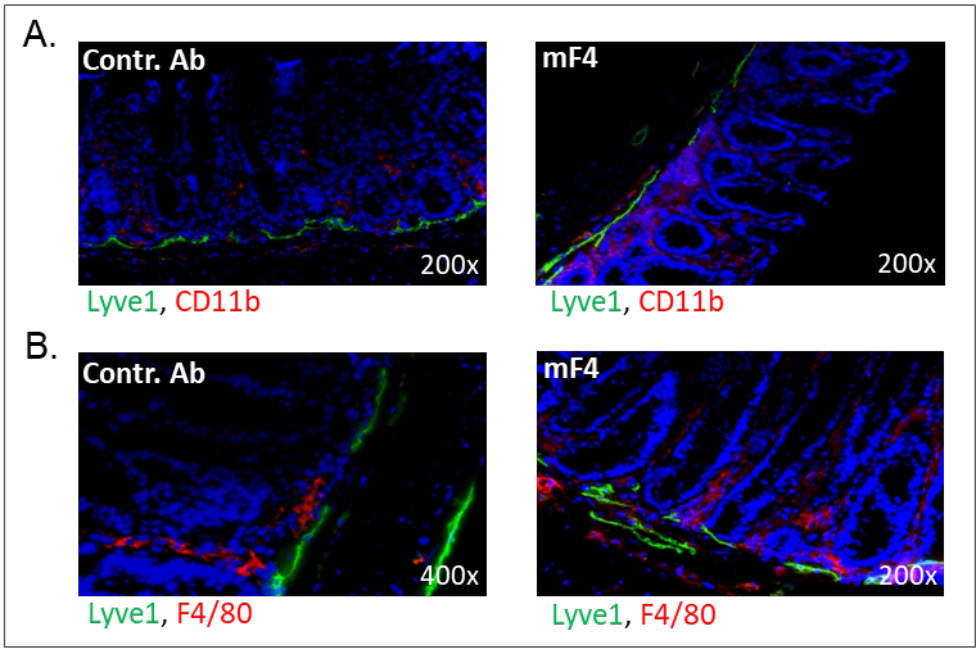

Figure S2. Double staining of lymph vessels and macrophages. Representative images of colon sections stained against the lymph vessel marker Lyve-1 (green) and two different macrophage marker: CD11b (A, red) and F4/80 (B, red). Counterstained with the nuclear stain DAPI.

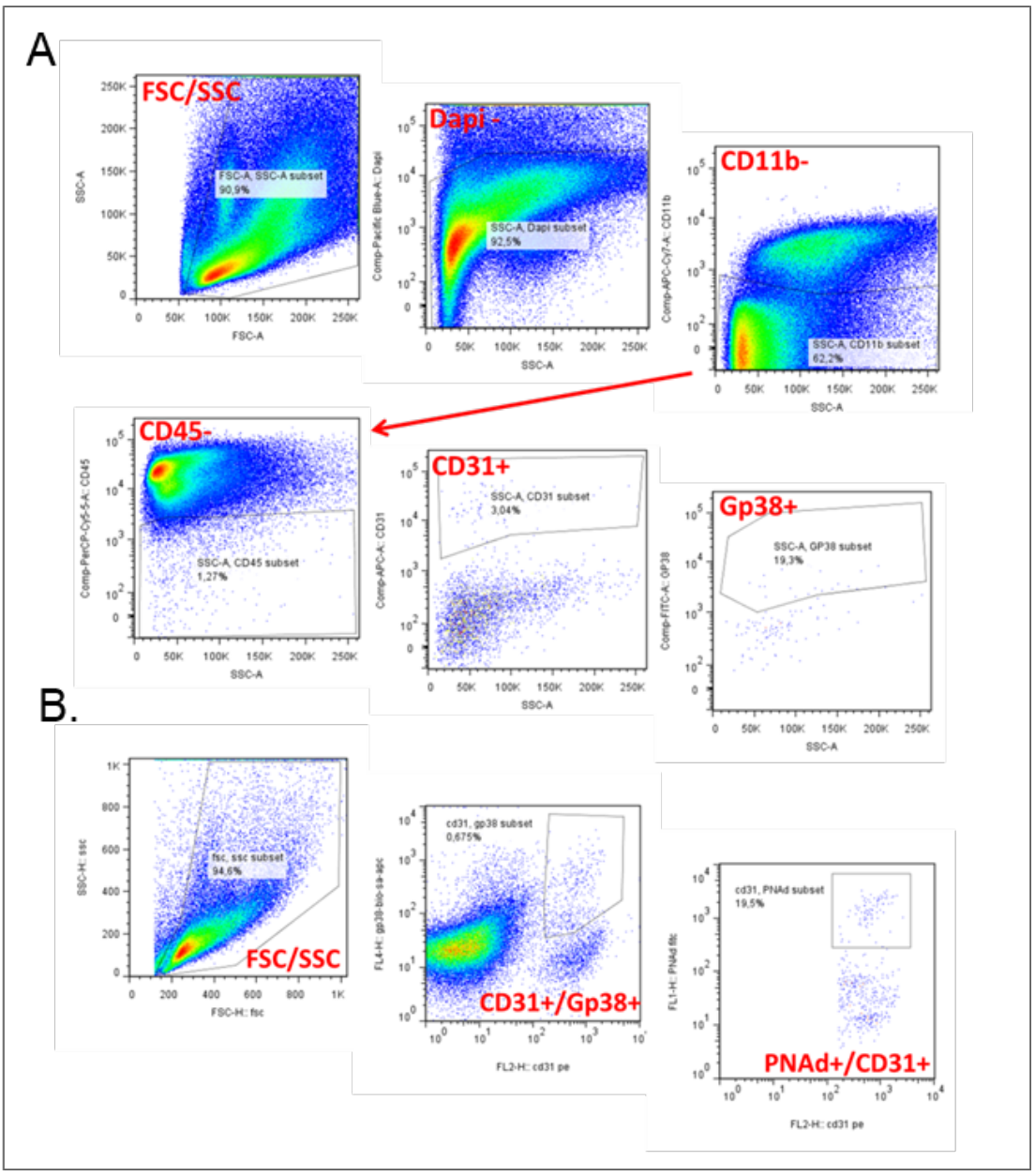

Figure S3. Representative FACS plots for gp38+ and PNAd+ cells. (A) Gating strategy for gp38+ lymphatic endothelial cells. (B) Gating strategy for PNAd+ lymphatic endothelial cells.

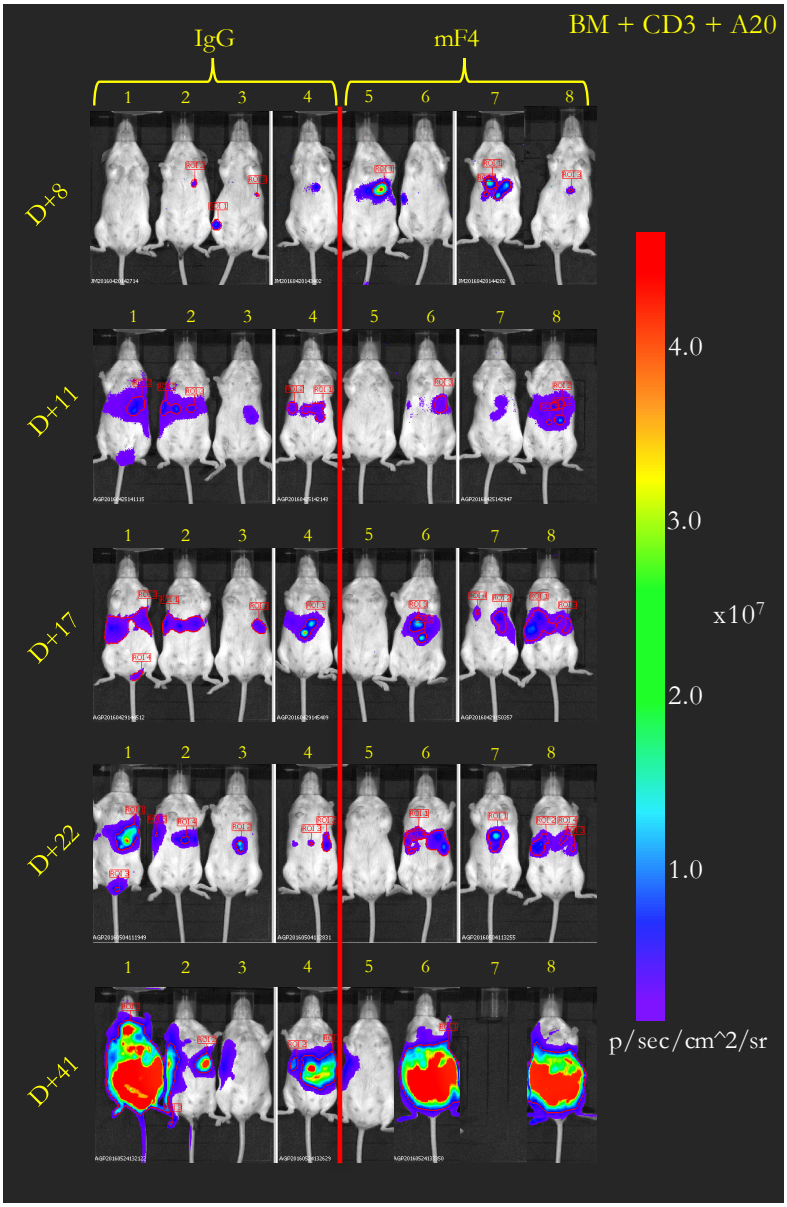

Figure S4. Representative images of in vivo bioluminescence imaging. Allo-HSCT recipients were injected with luciferase-transfected A20 tumor cells. Before imaging, anesthetized mice were injected with luciferase to visualize tumor cells. Tumor load was measured as average radiance (photons/second/cm²/ste

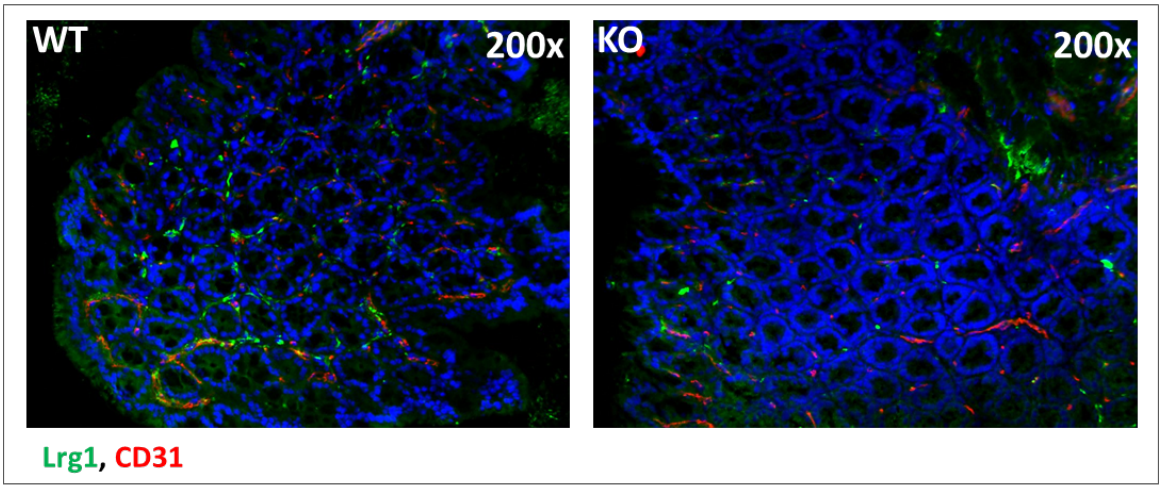

Figure S5. Representative images of staining of colon samples from Lrg1 WT mice and Lrg1 KO mice against Lrg1 and CD31. WT tissue shows co-localization of Lrg1 and CD31, indicating the expression of Lrg1 on blood vessels. Diffuse staining of the Lrg1 antibody is also found on KO tissue, probably due to binding to remaining Lrg1 fragments.

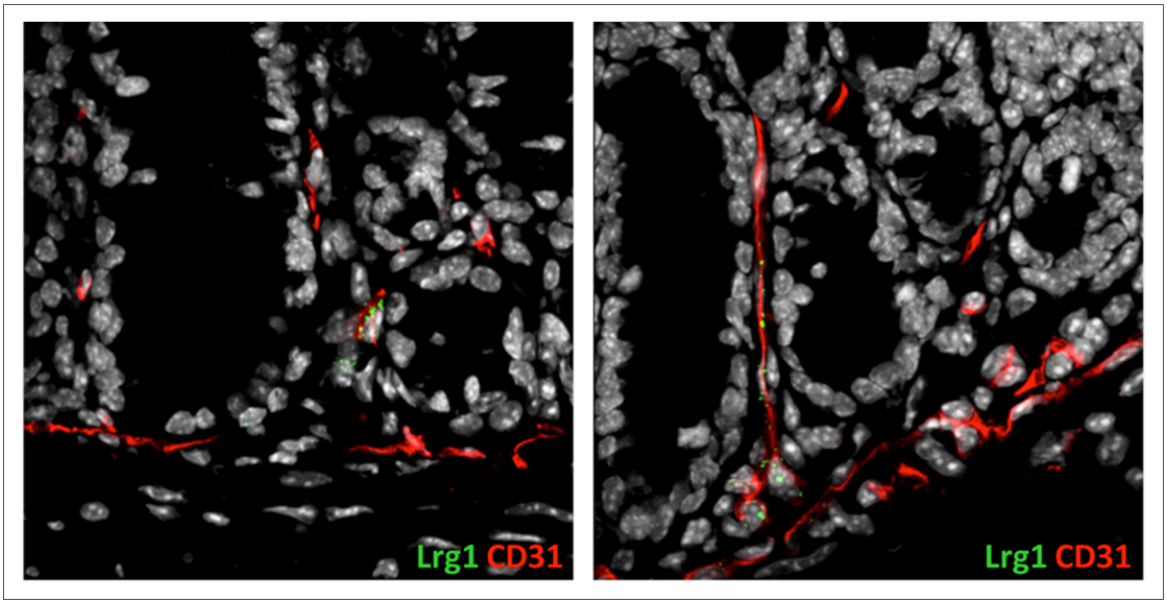

Figure S6. Detection of RNA using the RNAscope technology. Colon samples of wildtype mice were used to detect and label RNA on the section. Positively stained vessels (CD31, red) could be detected throughout the section. Lrg1 expression (green punctae) was rare and was found both at the base and the tip of the villi. No Lrg1 expression could be detected on Lrg1 KO tissue, concluding specific staining in wildtype samples. Experiment was performed on samples of the 129/SV → C57BL/6 model.

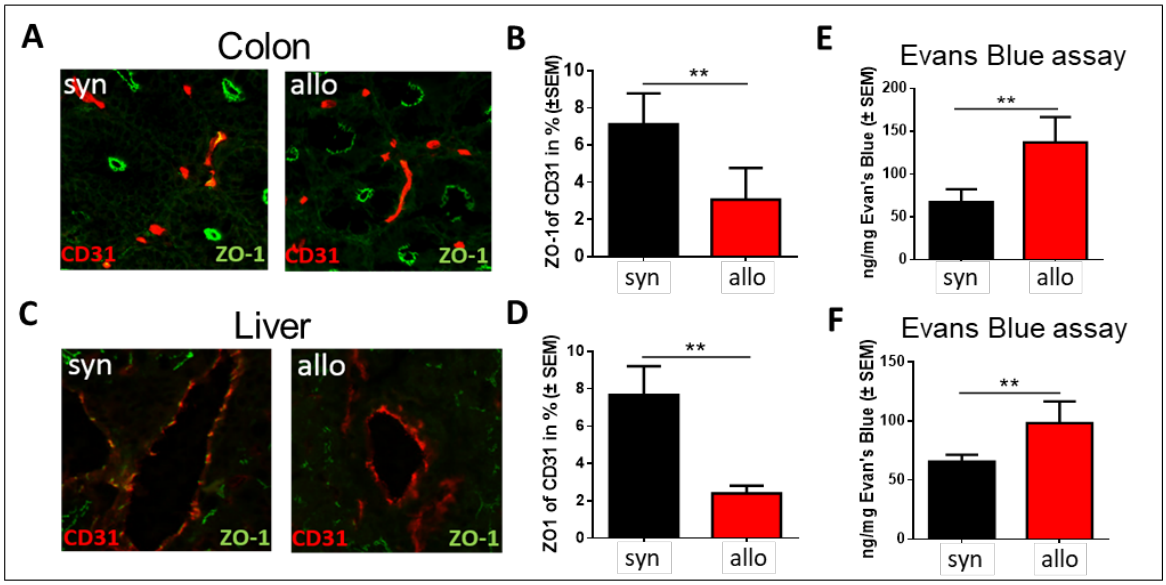

Figure S7. Assessment of endothelial leakiness by in vivo Evan´s blue assay and histological staining of ZO-1 in colon and liver during GVHD. (A) Representative pictures endothelial ZO-1 expression on colon tissue from syn- and allo transplanted mice. (B) Quantification of ZO-1 expression in the endothelium of colon mucosa. (C) Representative pictures of livers from syn- and allo-HSCT recipients showing CD31 in red and ZO-1 in green. (D) Quantification of ZO-1 expression in liver sinusoidal endothelium. (E) Amount of extravasated Evan's blue per mg colon tissue. (F) Amount of extravasated Evan's blue per mg liver tissue. Experiments were performed in the LP/J→B6 chemotherapy based GVHD model. N=5 per group, error bars indicate mean ± SEM, significance tested by unpaired student´s t-test, $p<0.05$ *, $p<0.01$ **, $p<0.001$ ***. Experiment was performed by Dr. Steffen Cordes.

6.2 List of abrreviations

AAT	alpha-1 antitrypsin
ActRIIA	activin receptor IIA
ActRIIB	activin receptor IIB
ADMA	asymmetric dimethylarginine
aGVHD	acute graft-versus-host disease
AKT (PKB)	serine-threonine-protein kinase (also known as protein kinase B)
ALK	activin receptor-like kinase
allo-HSCT	allogeneic hematopoietic stem cell transplantation
AMHRII	anti-Mullerian hormone receptor type 2
ANG1/2	angiopoietin 1/2
APC	antigen presenting cell
ATG	antithymocyte globulin
ATP	adenosine triphosphate
auto-HSCT	autologous hematopoietic stem cell transplantation
BM	bone marrow
BMP	bone morphogenic protein
BMPRII	bone morphogenetic protein receptor type II
C-ets-1	known as transforming protein p54, AP-1: transcriptional activator protein 1
CB	cord blood
CCBE1	collagen- and calcium-binding EGF domains 1
CCL	CC-motif ligand (C: cysteine residue)
CCR7/10	C-C chemokine receptor 7/10
CD	cluster of differentiation
CRP	C-reactive protein
CTL	cytotoxic T lymphocyte
CTLA-4	cytotoxic T-lymphocyte-associated protein **4**
CXCL	CXC-motif ligand (C: cysteine residue)
DAMP	damage-associated molecular patterns
DLI	donor lymphocyte infusion
Dll4	delta-like 4
DNA	deoxyribonucleic acid
E-selectin	Endothelial-selectin
EASIX	Endothelial Activation and Stress Index
EBV	Epstein-Barr virus
EC	endothelial cell
ECM	extracellular matrix
EFNB2	ephrin-B2
ENG	endoglin
EPC	endothelial progenitor cell
ERK1/2	extracellular signal-regulated kinase 1/2
FAK	focal adhesion kinase
Fas	APO-1: apoptosis antigen 1
FasL	Fas ligand

FGF	fibroblast growth factor
FGFR	fibroblast growth factor receptor
FIAF	fasting-induced adipose factor
FOXC2	forkhead box protein C2
FOXO	forkhead box protein O
G-CSF	granulocyte colony stimulating factor
GVHD	graft-versus-host disease
GVT	graft-versus-tumor
HHV	human herpesvirus
HIF	hypoxia-inducible factor
HLA	human leukocyte antigen
HMGB-1	high-mobility group box 1
HSC	hematopoietic stem cell
HSCT	hematopoietic stem cell transplantation
I-Smads	inhibitory small mothers against decapentaplegic
ICAM-1	intercellular adhesion molecule 1
IKK	IκB kinase
IL	interleukin
INF-γ	Inerferon-gamma
IκB	inhibitor of kappa B
JAK	Janus kinase
JNK1/2	c-Jun N-terminal kinase 1/2
L-selectin	leukocyte-selectin
LDH	lactate dehydrogenase
LEC	lymphatic endothelial cell
LPS	lipopolysaccharide
Lrg1	leucine-rich alpha-2-glycoprotein 1
LSEC	Liver sinusoidal endothelial cell
LYVE-1	lymphatic vessel endothelial hyaluronan receptor 1
MAP2K	mitogen-activated protein kinase kinase
MAPK	mitogen activated protein kinase
MHC	major histocompatibility complex
miHA	minor histocompatibility antigen
MMF	mycophenolate mofetil
MMP	matrix metalloprotease
MPO	myeloperoxidase
MSC	mesenchymal stem cell
mTOR	mammalian target of rapamycin
MTX	methotrexat
NFATc-1	nuclear factor of activated T cells-1
NFkB	nuclear factor kappa B
NIH	National Institutes of Health
NIK	NFκB-inducing kinase
NK cell	natural killer cell

NLRP3	nucleotide-binding domain leucine-rich repeats family protein 3
NOD-R	nucleotide-binding oligomerization domain-like receptor
NRARP	Notch-regulated ankyrin repeat protein
NRP-1/2	neuropilin-1/2
NSAIDs	nonsteroidal anti-inflammatory drugs
P2X7	P2X purinoceptor 7
P2Y2	P2Y2 purinoceptor 2
PAMP	pathogen-associated molecular patterns
PBSC	peripheral blood stem cell
PDGFB	platelet-derived growth factor B
PDPN	podoplanin
PI3K	phosphoinositide 3-kinase
PLC	phospholipase C
PlGF	placental growth factor
PROX-1	prospero-related homeobox-1
PTEN	phosphatase and tensin homologue
PTLD	post-transplant lymphoproliferative disease
RelB	Rel-like domain-containing protein
RIC	reduced intensity conditioning
ROS	reactive oxygen species
S1P	sphingosine-1-phosphate
S1PR1	sphingosine-1-phosphate receptor 1
SK	sphingosine kinase
SLP76	SH2 domain-containing leukocyte protein of 76 kD
Smads	small mothers against decapentaplegic
SMC	smooth muscle cell
SNP	single nucleotid polymorphism
SOCS	suppressor of cytokine signalling
Sph	sphingosine
SR-aGVHD	steroid refractory acute GVHD
Src	acronym from cellular and sarcoma
ST2	suppression of tumorigenicity
STAT	signal transducers and activators of transcription
SYK	spleen tyrosine kinase
syn-HSCT	syngeneic hematopoietic stem cell transplantation
TGF-β	transforming growth factor-beta
TβRII	transforming growth factor beta receptor II
Th cell	T helper cell
Tie1/2	tyrosine kinase with immunoglobulin-like and EGF-like domains 1/2
TIMP	tissue inhibitor of metalloproteinases
TLR	toll-like receptor
TNF-a	tumor necrosis factor-alpha
TNFR1	TNF receptor 1
Treg	regulatory T cell

UA	uric acid
VCAM-1	vascular cell adhesion protein 1
VE-cadherin	vascular endothelial cadherin
VEGF	vascular endothelial growth factor
VEGFR	vascular endothelial growth factor receptor
vSMC	vascular smooth muscle cell
vWF	von Willebrand factor
WNT	wingless-related integration site

6.3 List of figures

6.4 List of tables

6.5 Curriculum vitae

The CV is not included in the online version for reasons of data protection.

The CV is not included in the online version for reasons of data protection.

The CV is not included in the online version for reasons of data protection.

Selbstständigkeitserklärung

Hiermit erkläre ich, dass ich diese Arbeit selbständig verfasst habe und keine anderen als die angegebenen Quellen und Hilfsmittel in Anspruch genommen habe. Ich versichere, dass diese Arbeit in dieser oder anderer Form keiner anderen Prüfungsbehörde vorgelegt wurde.

Berlin, den 25.02.2020 Sarah Mertlitz